

Exploring Bone Dynamics By In-Vivo Micro-CT Imaging

Erwin Waarsing

Printed by Ponsen & Looijen bv, Wageningen, The Netherlands

ISBN-10: 90-6464-039-4

ISBN-13: 978-90-6464-039-1

© J.H. Waarsing

Dept. of orthopaedics, Erasmus Medical Center, Rotterdam, The Netherlands.

This work was funded by EU grant QLRT-1999-02024 (MIAB), NWO Netherlands Organization for Scientific Research and stichting Anna Fonds

Printing of this thesis was financially supported by N.V. Organon, Oss, The Netherlands; Skyscan, Belgium; stichting Anna Fonds, Leiden, The Netherlands.



Exploring Bone Dynamics by In-Vivo Micro-CT Imaging

Het verkennen van botdynamiek door middel van
in-vivo micro-CT beeldanalyse.

Proefschrift

ter verkrijging van de graad van doctor aan de
Erasmus Universiteit Rotterdam
op gezag van de
rector magnificus

Prof.dr. S.W.J. Lamberts

en volgens besluit van het College voor Promoties.

De openbare verdediging zal plaatsvinden op
donderdag 16 november 2006 om 16.00 uur

door

Jan Hendrik Waarsing
geboren te Stadskanaal

Promotie commissie

Promotoren: Prof.dr.ir. H. Weinans
 Prof.dr. J.A.N. Verhaar

Overige leden: Dr. J.P.T.M. van Leeuwen
 Prof.dr. W.J. Niessen
 Prof.dr. P. Lips

Voor Arelly

Contents

1	General introduction	9
1.1	Introduction	10
1.2	Bone remodelling	11
1.3	Mechanical loading and bone adaptation	13
1.4	The aging skeleton and osteoporosis	15
1.5	Measuring the result of remodelling: Bone morphometry	16
1.6	In-vivo micro-CT	17
1.7	Structure of this thesis	18
2	An improved segmentation method for in-vivo micro-CT imaging	21
2.1	Introduction	23
2.2	Material and Methods	25
2.3	Results	32
2.4	Discussion	37
3	Detecting and tracking local changes in the tibiae of individual rats: A novel method to analyse longitudinal in vivo micro-CT data	41
3.1	Introduction	43
3.2	Method	43
3.3	Results	44
3.4	Discussion	48
4	Bone loss dynamics result in trabecular alignment in aging and ovariectomised rats	51
4.1	Introduction	53
4.2	Methods	53
4.3	Results	55
4.4	Discussion	61
5	Effects of tibolone treatment on trabecular architecture in the tibia of mature rats: an in-vivo micro-CT study	65
5.1	Introduction	67
5.2	Methods	68
5.3	Results	71
5.4	Discussion	78
6	In the rat, bone adaptation is regulated by local mechanical stimuli, while ovx-induced bone loss is regulated by local bone density	83
6.1	Introduction	85

6.2	Methods	86
6.3	Results	91
6.4	Discussion	98
7	General discussion	103
7.1	Introduction	104
7.2	Thoughts on the methods	104
7.3	Radiation and in-vivo scanning	105
7.4	Thoughts on the role of imaging in bone research	109
7.5	Thoughts on the interaction between estrogen levels and mechanical driven bone adaptation.	110
7.6	Thoughts about possible experiments.	113
7.7	Concluding remarks	114
	Summary	117
	Samenvatting	121
	References	125
	Dankwoord	137
	Curriculum Vitae	141
	Lijst met publicaties	143

1

General introduction

*Part of this chapter has been published: Waarsing et al., J Musculoskelet
Neuronal Interact. 2005 Oct-Dec;5(4):310-2.*

1.1 Introduction

In prehistoric times, when our ancestors were sitting comfortably in their caves around a cosy fire, stomachs filled with roots and mammoth meat, it is likely that their minds started to roam. One of the biggest preoccupations on their minds and on the mind for all following generations, must have been the question ‘who am I?’ and related to this ‘what is the location of this I?’ Undoubtedly inspired by the effect of emotion on our body, one of the first hypothesis probably was that the ‘I’, the ‘soul’, the ‘atman’, our ‘ego’ or what other terminology people might have used over the ages, was located in the heart. Later on, less romantic and more intellectual philosophers formulated the alternative hypothesis that the ‘I’ must be located in our brains, the organ of thought. It wouldn’t be surprising if other hypotheses might have existed about the centre of the ‘I’, for example the stomach or the sexual organs could be good candidates.

But wouldn’t the skeleton have been another good option for the seat of our soul? Isn’t the skeleton the fundamental part of our body? It is the frame that has equipped itself with muscles as a motor to move itself around that has developed guts so it could generate energy and could supply itself with building material. The brain was needed to coordinate all this equipment and could nicely function as a toy to play with at times when nothing else was at hand. After our life has ended, and our bodies return to dust, it is the skeleton that remains for ages to come...

Rephrased more scientifically, our skeleton fulfils an important role in our



figure 1.1 The skeleton as seat of the soul... (“La Catrina” by José Guadalupe Posada)

physical system. It forms the frame on which the muscles are attached; it offers protection for vulnerable organs like our heart, lungs and brain. Further, it is a big reservoir for calcium. And most of all, it is a complex living organ about which much knowledge has been gathered, and about which maybe even more questions still remain open.

1.2 Bone remodelling

The main components of bone as an organ are the bone tissue itself and the bone cells. The tissue consists of a mineral and an organic phase and gives the bone its mechanical strength. The bone cells replace old bone tissue with new in a process called remodelling.

The organic phase of the bone tissue consists of a matrix of long collagen proteins, intertwined with smaller proteins. This matrix is mineralized with calcium phosphate crystals. Within the bone tissue lays an extensive network of osteocytes that connect to each other via small canaliculi through the bone tissue. Architecturally this network has strong similarities with neuronal networks, which is one of the reasons why these cells are speculated to be the sensors of the bone organ. Knowledge about these cells is still relatively limited.

The bone surface is covered with a layer of flat bone lining cells that are in contact with the osteocyte network inside the bone tissue. The function of these cells is not completely clear, but one of their functions might be related to initiate local remodelling.

Osteoclasts and osteoblasts work together in structural units called BMUs to renew the bone tissue. Osteoclasts are big bone specific multi-nucleated macrophages that resorb old bone tissue. They are followed by the osteoblasts that deposit the new bone matrix (osteoid) to fill up the resorption pits made by the osteoclasts. Some osteoblasts are built into the bone matrix and differentiate into osteocytes (figure 1.2).

The role of bone remodelling is three-fold. First of all, it forms part of the regulating mechanism that keeps the serum level of calcium constant. Further, remodelling repairs micro-damage in the bone tissue that originates from mechanical deformation. In this, bone is a self-repairing mechanical structure. The third role of the remodelling process is to alter the shape of the bone as is needed during growth, which is referred to as modelling, and to adapt its structure to changing mechanical loading. No consensus exists on how these tasks are regulated. Some hypotheses suggest that remodelling can be purely random, others suppose that micro-damage kills osteocytes and thus attracts remodelling activity. A third option suggests that mechanical deformation of the bone tissue is sensed by the bone cells and thus regulates bone cell action.

The regulation of bone cells is very complex to say the least. The most important systemic regulators of bone remodelling are hormones like

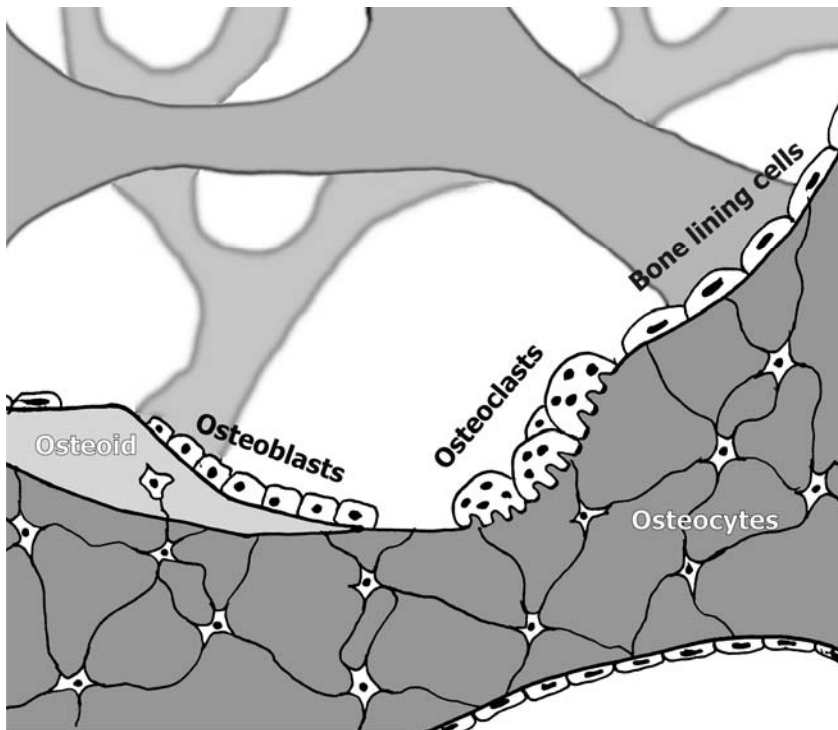


figure 1.2: Schematic depiction of a BMU. Osteoclasts create a resorption pit by eating away bone tissue. Osteoblasts enter the pit and position new lowly mineralised bone tissue called osteoid.

parathyroid hormone (PTH), vitamin D and calcitonin, and steroids like estrogen and to a lesser extent testosterone. PTH is part of a classic negative feedback regulatory mechanism that maintains serum calcium levels constant. Low levels of serum calcium result in an increase in PTH, which stimulates osteoclasts to resorb bone what re-establishes calcium levels, and decreases PTH levels. This feedback loop is further influenced by vitamin D. PTH increases active vitamin D levels by stimulating the activation of vitamin D in the kidney, while vitamin D decreases PTH levels both directly through the parathyroid gland and indirectly by stimulating absorption of calcium in the intestinal tract and stimulating bone resorption. A shortage of calcium, whether due to insufficient intake or due to lack of vitamin D, is thus an important cause for bone loss.

Estrogen might very well be the main regulator of bone metabolism. It influences activity of both osteoclasts and osteoblasts and is a regulator of growth-plate activity. The main cause of post-menopausal bone loss is the decrease in circulating levels of estrogen after onset of menopause.

A large number of small signalling molecules like cytokines and growth-factors (e.g. IL-4, BMPs, TGF- β , VEGF etc.) further influences bone cell

activity. These factors are produced by bone cells themselves and thus are part of mechanisms by which bone cells can influence each other's behaviour. Some are incorporated into the bone matrix and are released again when bone matrix is resorbed. This can locally alter behaviour of bone cells. An important regulatory mechanism is the RANK-RANKL pathway. Osteoblasts produce RANKL that attaches to receptors on the surface of pre-osteoclasts and signals these cells to differentiate into mature osteoclasts. Osteoblasts also produce OPG, which is released into the interstitial fluid. OPG binds to RANKL thus preventing the differentiation of pre-osteoclasts into active osteoclasts (5). An interesting recent finding involves the SOST gene, which is expressed by osteocytes. Osteocytes can regulate osteoblast activity by the inhibitory action of the SOST gene product sclerostin on osteoblasts (185). Sclerostosis and Van Buchems disease are characterized by high bone mass that continually increases. All patients suffering from these diseases have genetic mutation that hinder the production of fully functional sclerostin by osteocytes (10).

Recent research looking for how the hormone leptin regulates bone mass, has revealed yet another regulatory mechanism of bone remodelling: The central nervous system directly influences bone metabolism (177). This finding is corroborated by discovery of serotonin receptors in bone cells (206) and the fact that serotonin and serotonin re-uptake inhibitors like Prozac influence bone architecture in rats (67, 201). The fact that bone is highly innervated with both sympathetic and sensory nerves (78, 121) promises interesting research results on this topic in the future.

Bone remodelling is regulated through many positive and negative feedback strategies, each influencing each other. This makes that the regulation of bone mass and architecture is a highly complex non-linear system and it's not surprising that no general model exists that gives us a firm understanding of this process. The importance of this issue is reflected in that the major cause for many skeletal disorders, among which major disorders in the elderly like osteoporosis and osteoarthritis, are related to changes in bone remodelling.

1.3 Mechanical loading and bone adaptation

The idea that bone can adapt itself to its mechanical environment was formulated long ago, at the end of the 19th century by Roux and Wolff (163, 208). Wolff noted that the trabecular bone structure was aligned along the principle loading directions. He supposed that bone must be able to sense mechanical deformation of its tissue and adapt its form in reaction to these deformations. Being a contemporary of Darwin, Roux described bone as a self-organizing tissue, in which bone cells compete for a limited resource, the mechanical stimulus. Many theories and variations of the same theme were to follow. One of the most influential theories on current

thinking of bone adaptation is known as the mechanostat theory, formulated by Frost (59). He posed that a general threshold exists below which a mechanical stimulus results in loss of bone. Mechanical stimulation above another threshold results in apposition of more bone. When the stimulus is in between these thresholds, no bone is lost or formed. This is referred to as the 'lazy zone' (29).

These theories have inspired an area in bone research in which computer simulations are performed to study the relation between mechanical loading and the remodelling process. In general, these simulations determine the local mechanical environment via finite element (FE) calculations and bone is added or removed iteratively based on the value of a mechanical signal derived from the FE calculations. Simple 2D models of homogenized whole bones or pieces of trabecular architecture, have shown the feasibility of the idea that the mechanical environment can influence bone architecture (38, 61, 84, 204). Sophisticated 3D models using micro-CT scans of real bone biopsies as inputs that mimicked the activity of single bone cells have tried to come as close as possible to real bone physiology (134, 165, 178, 187). They showed that many observations on cell behaviour in the 'real world' could be explained by mechanical adaptation. However stunning the similarities between the real world and these computer simulations, they only show a possibility and do not deliver evidence that cell behaviour is truly directed by mechanical stimuli.

In humans the influence of the mechanical environment has been confirmed by the finding that exercise can increase bone mass while unloading reduces bone mass. For instance, the dominant arm of a professional tennis player has a much higher bone mass than the contra lateral arm (11, 68, 83), while space-flight and long-term bed rest strongly reduce bone mass (15, 116). A variety of animal experiments ranging from rats wearing backpacks, ulna loading devices for turkeys and mice and loading devices for tail vertebrae of rodents to tail-suspension of rodents as unloading experiments have shown the same: mechanical loading increases bone mass and lack of mechanical stimuli reduces bone mass (19, 22, 40, 86, 125, 160, 164). All this has shown that mechanical loading undeniably influences bone mass, though it is still unclear in which way changes in mechanical loading influence bone architecture.

If bone has the ability to adapt its shape to changes in the mechanical environment, then it needs to have sensors with which to sense mechanical stimuli. Cells of the osteoblast lineage have been shown to respond to mechanical stimuli in many cell culture experiments (12, 91, 133). Though all osteoblasts-like cells respond to mechanical stimuli, it are the osteocytes and to a lesser extent the bone lining cells that are thought to be the major mechanical sensors of bone. This is mainly because of the perfect location of osteocytes inside the bone matrix and the fact that they form an

interconnected network (24, 135). No consensus exists as to how these cells sense mechanical stimuli. Some theories suggest that osteocytes react to fluid flows through the canaliculi that are associated with deformations of the bone tissue (23, 175). Other theories assume that bone cells sense mechanical stimuli through deformations of the cell membrane and the cytoskeleton that is attached to the membrane and the nucleus (99, 128). It is of course not unlikely that bone cells sense mechanical stimuli through both mechanisms (54).

1.4 The aging skeleton and osteoporosis

Despite the intricate mechanisms that regulate bone remodelling, bone mass is not constant but declines in the elderly. In young adults, after cessation of longitudinal growth, bone mass still increases until peak bone mass is reached at an age between 25 and 30. From then on, bone mass slowly decreases which is caused by a small negative balance of each remodelling cycle, as is the accepted opinion. In women bone loss is temporarily accelerated at the onset of menopause. In many elderly, bone loss worsens because of a decreased calcium intake and low levels of vitamin D, which is called secondary hyperparathyroidism (158). Bone mass can be reduced to pathological levels, a condition called osteoporosis which is associated with high fracture risk. Due to the phase of accelerated bone loss in post-menopausal women, osteoporosis is more frequent in the female population.

The principle cause for the accelerated phase of bone loss in post-menopausal women is the decreased level of estrogens. Estrogen deficiency leads to an increase in bone remodelling, which leads to the resorption of cancellous bone. It has been shown that estrogen directly affects both osteoblast and osteoclast activity, since both cell types express estrogen receptors. Some other effects of estrogen deficiency on bone metabolism have been observed: Lack of estrogen stimulates apoptosis of osteocytes in human bone (182); estrogen influences the generation of blood vessels (129) and nerve innervation of bone tissue (25). Still, it is not clear in what way these effects lead to such drastic bone resorption.

Since the first trabeculae to disappear are assumed to be the lesser-loaded ones, it has been proposed that estrogen interacts with bone's ability to adapt to mechanical stimulation. The finding that mechanical stimulation can activate the estrogen receptors (95, 117) further supports this idea. Frost suggested, using his mechanostat theory, that estrogen influences the mechanical set points that determine whether mechanical stimuli result in bone loss or bone apposition (59). When estrogen levels are low, the threshold that regulates bone resorption is raised. The consequence is that more bone is stimulated below this threshold and will be resorbed accordingly (figure 1.3). Rephrased differently, estrogen sensitizes bone for

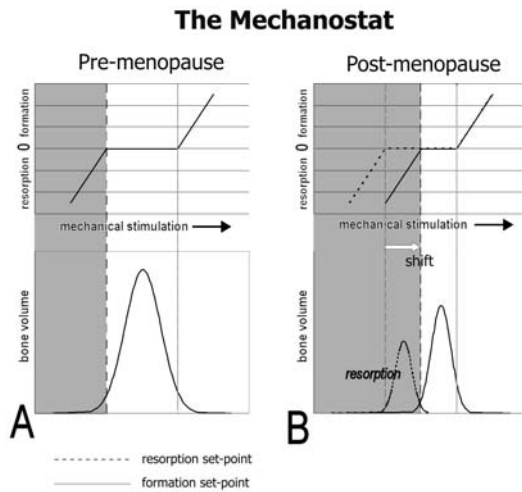


figure 1.3 The influence of estrogen on bone metabolism according to the mechanostat theory. (A) Before menopause, when estrogen levels are high, bone is in a stable situation. All bone cells sense stimuli that fall inside the lazy zone, thus no bone is resorbed or formed. (B) After menopause, when estrogen levels drop, the resorption set-point shifts upward and bone tissue that is now stimulated below this set-point will be resorbed until a new stable situation is reached. When estrogen levels are low, bone is less sensitive to mechanical stimuli.

mechanical stimulation (115). Although this idea is widely accepted, a few publications exist that raise a few questions on this issue, and even suggest that bone might be more sensitive to mechanical stimuli in the absence of estrogen (92, 93).

1.5 Measuring the result of remodelling: Bone morphometry

For a long time bone mass or bone mineral density (BMD) is considered as the main predictor for fracture risk in the clinic. In laboratory experiments bone mass or bone volume fraction is a reasonably good predictor of cancellous bone mechanical properties i.e. stiffness and strength. Obviously, since bone volume fraction is a scalar property it cannot predict all cancellous bone mechanical properties in highly anisotropic regions. It has become clear that bone mass or BMD has strong shortcomings for the prediction of fracture risk (169, 198). The new paradigm is to measure bone quality as a surrogate for fracture risk. However there is no clear definition of bone quality. Many architectural parameters have been measured in cancellous bone and tested for their ability to predict fracture risk independent of bone mass. For most of those measures of bone architecture, it is not clear what the relation is with the mechanical properties or fracture risk. Trabecular anisotropy seems to be the most promising parameter, so far, that might be useful as an independent contributor to fracture risk (35, 79). This is likely due to the fact that high anisotropy relates to a relatively weak structure in the off-axis loading direction (80).

The measurement of bone architecture has a long history. Histomorphometry, still considered the gold standard, is an early technique

based on histology. Stereological methods were applied to estimate the three-dimensional architecture from two-dimensional histological slices. In addition to the morphological descriptions and estimates of the three-dimensional architecture, histomorphometry offers a number of other important measures such as the unmineralised osteoid surface, cell counts of osteoblasts, osteocytes and osteoclasts and most important a measure of bone formation rates through use of fluorescent labels incorporated in the mineralizing front. Because of these latter advantages these techniques are still in widespread use, even though there are big disadvantages such as the reliance on biased two-dimensional (indirect) bone morphometric parameters and the labour intensiveness.

Around 1990 a high-resolution version of the clinical CT scanner was introduced in the research laboratory (107), and has become an important modality for bone morphometry measurements. The apparatus yields true 3 dimensional datasets of bone biopsies and whole bones of small animals like mice and rats. Voxel sizes can be smaller than 5 microns. Advantages of this modality above histological sections are the unbiased 3-D morphometric measures of bone architecture, and that the samples can be imaged non-destructively so the bones are available for other measuring techniques such as e.g. failure tests.

The popularity of these devices have led to an explosion of new parameters that claim to measure important aspects of bone architecture, ranging from accepted measures like volume fraction and trabecular thickness to more exotic measures like Gaussian curvature of the bone surface (96). It is not clear which of these parameters are useful and what they tell us about bone structure or quality. A standardization of these measures would be useful, just like the standardization of parameters led by Parfitt et al (151) following a similar explosion of 2D measures in bone histomorphometry.

1.6 In-vivo micro-CT

A common factor for both micro-CT and histology is that all studies using these techniques have a cross-sectional nature, due to the invasiveness or destructiveness. Although very interesting results have been obtained that have increased our knowledge about bone and bone remodelling to a great extent, many questions remain open, particularly where it concerns the influence of ageing, drug treatment or mechanical loading regimens on structural changes of the trabecular architecture. To answer these questions, more subtle measurements would be needed, a subtlety that can probably only be reached by imaging studies using a longitudinal study set-up. High-resolution in vivo micro-CT, similar to clinical CT, would be the most obvious option. However, the high radiation dose that is necessary to obtain useable images has hampered this development. An alternative option

would be to use high resolution MRI which does not involve radiation. At present, the obtained results using this technique are only moderate and involve long scanning times and costly high field (>7 T) machines.(202). Currently, innovations that improved the sensitivity of CCD cameras have reduced the necessary dose to obtain good quality micro-CT images and the first generation of in vivo scanners has now reached the laboratories.

Even though the necessary radiation has been reduced to a great extent, the dose needed to obtain useable images at high resolutions of 20 microns or less are still 10 to 100 fold higher than in clinical CT scanners. Long-term stochastic effects of radiation are not an issue as it is in human CT scanners, but radiation between 100 and 1000 mGy can be harmful. Even though it's not lethal to the animal, it might affect bone metabolism and therefore interact with and confound the experimental findings. The only option is to scan at lower resolutions, or work with poor image qualities.

1.7 Structure of this thesis

The work in this thesis has evolved around the development of one of the first in vivo micro-CT scanners. The first part of the work is of a methodological nature. In here we have tried to improve and use techniques to optimize the potential of the in vivo micro-CT methodology. In the second part of the work, this methodology has been applied to study the structural changes related to loss of bone mass due to aging and ovariectomy in individual female rats.

In the first study (**chapter 2**) we introduce a novel algorithm to segment micro-CT images, which is a very important and unfortunately often ignored topic in micro-CT scanning. Segmentation refers to the conversion of the raw reconstructed images in which the grey value of each voxel represents an attenuation coefficient in Hounsfield units, into binary images that only represent bone and non-bone. In other words, for each voxel in the data set a decision needs to be made whether it represents bone or not. This issue becomes even more important when the quality or the resolution of the images is limited, as with in vivo micro-CT. Simple segmentation methods using a single global threshold value are far from optimal in this case. We have therefore developed an algorithm using local thresholds that tries to segment the non-optimal in vivo images in an optimal way.

Perhaps the most exciting possibility of in vivo micro-CT is that changes in bone architecture can be followed over time as it occurs in individual animals. Due to the high resolution it is, in theory, possible to follow changes at the level of single trabeculae. This is however not trivial. The shape of bones changes over time, trabeculae are resorbed, new trabeculae are formed, and longitudinal growth increases the size of the bones. In **chapter 3** we have investigated the possibility to use image registration algorithms to position scans made at different time points on top of each

other. Especially, we investigated how to apply these algorithms in such a way that the optimal mathematical match that results from the registration algorithms coincides with the optimal biological match.

In **chapter 4** we have applied the in-vivo micro-CT technology and methodology in an animal study. During 54 weeks, we followed the changes in trabecular architecture due to aging and ovariectomy in the tibia of mature rats. The aging rat and especially the ovariectomised rat are much-studied models of age related and postmenopausal bone loss in humans and thus much is already known on the effects of aging and ovariectomy on bone architecture. In this study we were especially interested in the dynamics of bone loss, how changes in individual trabeculae result in the known architectural changes.

Hormone Replacement Therapy (HRT) is widely used to prevent and treat bone loss in post-menopausal women. The increase in risk on breast cancer that accompanies HRT has increased feelings of unease among users and thus has stimulated interest in alternative options. One option is the drug Tibolone that is used to prevent menopausal symptoms. The drug has convincingly been shown to prevent bone loss, while reducing the side effects caused by conventional HRT. **Chapter 5** describes our attempts to gain more insight in the effects of Tibolone on bone quality more than bone mass alone. We have studied the preventive effects of Tibolone use on the ovariectomy-induced changes in trabecular architecture using our in-vivo micro-CT methodology and examined the effects on the mineralization of bone tissue using backscatter Scanning Electron Microscopy.

As mentioned above, a number of theories exist that try to explain the regulation of bone adaptation. Many studies have tried to proof these theories by using cleverly designed animal experiments or computer simulations of the remodelling process. A drawback in all these studies is that it has never been possible to relate ‘real’ changes in bone with the ‘real’ mechanical situation. In **chapter 6** we try to do just that. By combining the unique possibility of in-vivo micro-CT to identify resorbed and newly formed bone –as described in previous chapters- with FE models and simulations of the remodelling process, we explored the relation between resorption/formation of bone and various possible mechanical signals derived from strain distributions.

Findings in bone cell biology, biochemistry and genetics result in more and more detailed information about regulation of bone remodelling. These results stress how complicated the interaction and regulation of bone cells is. All the pieces of this jigsaw puzzle can only be put together when the image of the puzzle is known. In this body of work we have shown that in-vivo micro-CT, especially when combined with image registration and computer simulation can be a very powerful tool that helps to understand what the image of the jigsaw puzzle of bone remodelling should look like.

Together with other techniques in bone research in vivo micro-CT might bring us closer to unravelling the bone remodelling process and thus give us better understanding of bone diseases that affect the elderly, which are principally a failure of the bone remodelling process.

2

An improved segmentation method for in-vivo micro-CT imaging

J.H.Waarsing, J.S.Day, H.Weinans

Reprinted from: Waarsing et al., JBMR, 2004 Oct;19(10):1640-50

Abstract

- **Introduction:** An important topic for micro-CT analysis of bone samples is the segmentation of the original reconstructed grey-scale data sets to separate bone from non-bone. Problems like noise, resolution limitations and beam-hardening make this a non-trivial issue. Inappropriate segmentation methods will reduce the potential power of micro-CT and may introduce bias in the architectural measurements, in particular when new in-vivo micro-CT with its inherent limitations in scan quality is used. Here we introduce a new segmentation method using local thresholds and compare its performance to standard global segmentation methods.
- **Methods:** The local threshold method was validated by comparing the result of the segmentation with histology. Further, the effect of choosing this new method versus standard segmentation methods using global threshold values was investigated by studying the sensitivity of these methods to signal to noise ratio and resolution.
- **Results:** Using the new method on high quality scans yielded accurate results and virtually no differences between histology and the segmented data sets could be observed. When prior knowledge about the volume fraction of the bone was available the global threshold also resulted in appropriate results. Degrading the scan quality had only minor effects on the performance of the new segmentation method. Although global segmentation methods were not sensitive to noise, it was not possible to segment both lower mineralised thin trabeculae and the higher mineralised cortex correctly with the same threshold value.
- **Conclusion:** At high resolutions both the new local and conventional global segmentation methods gave near exact representations of the bone structure. When scanned samples are not homogenous (e.g. thick cortices and thin trabeculae) and when resolution is relatively low, the local segmentation method outperforms global methods. It maximises the potential of in-vivo micro-CT by giving good structural representation without the need to use longer scanning times that would increase absorption of harmful x-ray radiation by the living tissue.

2.1 Introduction

Diseases like osteoporosis can seriously affect the mechanical integrity of bone. Measuring the bone mineral density (BMD) alone is not sufficient to understand how bone loss affects fracture risk. It is also important to study the actual structure of the trabecular network, for instance by micro-CT (142). Since its introduction by Feldkamp et al. (57) micro-CT has become an important tool to quantify the morphometry of the trabecular structure of bone biopsies of, e.g., humans and of whole bones of small animals like rats or mice. In addition, micro-CT provides the possibility to set up finite element (FE) models to determine the strength and stiffness of the bone sample based solely on the trabecular architecture (100, 191). Further, the 3D representations of bone can be used as the input for computer simulations of bone remodelling (189). Recent advances in technology have made in-vivo micro-CT possible; increasing the value of micro-CT as a research tool by enabling the design of longitudinal studies to follow changes in trabecular structure (41, 194).

A number of studies have validated the accuracy of micro-CT. Comparison with histology showed relative small to rather high deviations in 2D morphometric parameters depending on scan resolution and especially on which segmentation method was used (56, 87, 131, 140). Other studies on the effects of scanning resolution and segmentation methods on morphometric parameters support and stress the importance of choosing an appropriate segmentation technique to separate bone from non-bone (31, 50, 71, 139). The demands on segmentation techniques become even more stringent when the quality of the scans is limited, as is the case for in-vivo scanning, where scanning time should be as short as possible to limit radiation dose absorbed by the living tissue.

The most widely used segmentation techniques use global thresholds; a single CT-number is chosen above which all voxels (3D pixels) are marked as bone and below which all remaining voxels are marked as non-bone. The value that is used as a threshold is selected either visually, by analysing the histogram of CT-numbers, or by forcing the resulting binary data set to have the same volume as the original bone sample as determined by doing an Archimedes test (50).

Despite the ease and speed of using a global threshold, serious problems such as beam hardening, noise and partial volume effects can considerably reduce the quality of the segmentation. The effect of beam hardening can be reduced by using a physical filter during scanning and by using corrective algorithms during reconstruction. Partial volume effects (a voxel that contains both bone and non-bone has a lower CT number than a bone voxel, but a higher CT number than a non-bone pixel) will limit the frequency content of the reconstructed images. This will 'smear out' the

bone around its real edge in a reconstructed data set. Trabeculae that are thin relative to the resolution can even be smeared out such that the CT number of the trabeculae does not reach the CT number that would represent the true density of the material (107). The combination of these effects causes the optimal threshold value for a certain part of the reconstruction to be different from the optimal value in other parts. In general, using a single global threshold value will result in the loss of thin trabeculae and oversizing of thicker trabeculae.

Segmentation can be improved by using local threshold values rather than a single global threshold value such that each voxel can be thresholded optimally within its neighbourhood. Dufresne (51) has developed a local threshold algorithm for CT-scans to compensate for beam-hardening effects based on the analysis of the histogram of the local neighbourhood of a voxel. The efficiency of this method will decrease when the resolution is limited and tissues are not homogenous. Kuhn et al. (107) and Elmoutaouakkil et al (55) proposed more general local segmentation methods, both based on the so called Half-Maximum Height (HMH) protocol. Summarized, voxels are considered bone if their CT number is higher than half the difference between local minima (background) and local maxima (bone). The more rigorously validated method of Kuhn et al. gives very accurate results for structures much thicker than the resolution of the micro-CT system, however, structures that are thin relative to the resolution are still oversized.

Segmentation techniques have been studied more extensively for in-vivo imaging of human bone by micro-MRI (63, 65, 110, 123, 141) and PQCT (64, 108, 111, 137, 138). Because of their relatively low resolutions (approximately 150 μm), these systems lack the ability to accurately resolve individual trabeculae. Hence, most studies have focused on parameter extraction techniques that indirectly estimate properties of the trabecular bone. These methods have only been validated by assessing the reproducibility and by demonstrating that they could discriminate between populations.

In this paper we introduce an automated segmentation method using local threshold values obtained by applying standard edge detection algorithms, while compensating for smeared out thin trabeculae. The method was validated by comparing segmented data sets with traditional histological sections. Further, the consequences of choosing a local versus a global threshold method were investigated by studying the behaviour of these methods at different scan qualities and resolutions.

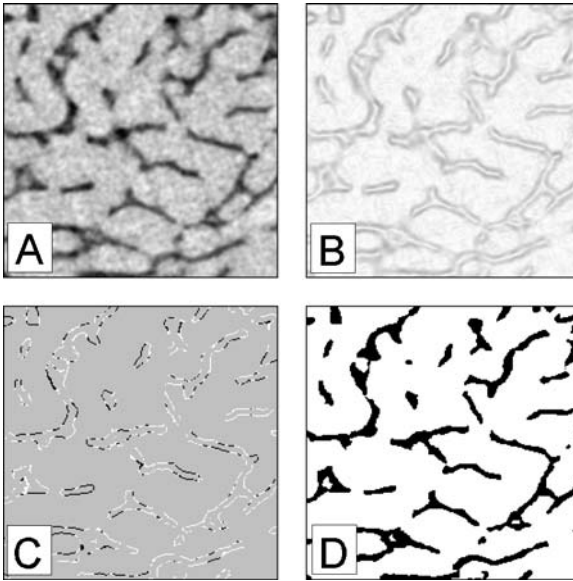


figure 2.1 The different steps of the local segmentation method illustrated. From the original greyscale images (A) the 3D spatial gradient is calculated (the highest gradients have the darkest colour) (B). The local maxima in the gradient field are the edges of the bone (strong edges are black, weak edges are white) (C). From these edges a set of local thresholds is derived that is used to obtain the binary image (D).

2.2 Material and Methods

The algorithm

Before applying the segmentation algorithm, noise was reduced by filtering the data sets with a 3D Gaussian smoothing function. Each voxel in the data set was replaced by the weighted average of the voxels in its $5 \times 5 \times 5$ neighbourhood. The weights were functions of the distance of each voxel to the central voxel in the $5 \times 5 \times 5$ neighbourhood, according to the Gaussian function of which the standard deviation or radius was a parameter (*GaussRadius*) that was set by the user.

A standard edge detection algorithm, extended to 3D, was used to find the surface of the bone in the smoothed data set (figure 2.1a). The edges were detected by calculating the 3D spatial gradient of the reconstructed data using three orthogonal 3×3 Sobel operators (166) that favour localisation of edges above (noise sensitive) detection of edges (28) (figure 2.1b, figure 2.2b). The ridges in the gradient field are the edges, indicating the transition from bone to non-bone and correspond to the Half Maximum Height points. The ridges were detected by finding local maxima in the direction of the gradient. To prevent detection of false (noisy) edges and streaking (breaking up of an edge contour because of noise), only local maxima that were above a high threshold were kept (strong edges), together with smaller maxima that were connected to these high maxima but were still above a low threshold (weak edges) (28) (figure 2.1c, figure 2.2c). The

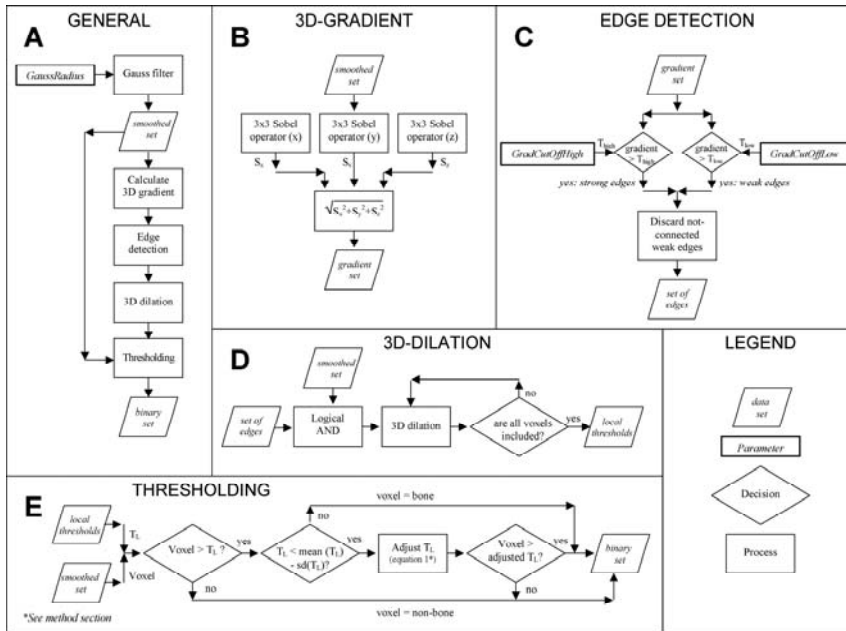


figure 2.2 Flow-chart diagram that gives a schematic representation of the local segmentation algorithm. (A) General outline of the entire algorithm. Detailed flow-charts of each sub-process in the general outline are presented for (B) the calculation of the 3D-gradient, (C) the edge detection step, (D) the dilation of the original set of local thresholds and (E) the final thresholding step including adjustment for thin trabeculae.

values of the high and low threshold values that define the strong and weak edges were set by the user (*GradientCutOffHigh*, *GradientCutOffLow*). The possible values for these parameters ranged between 1 (strongest edges) and 0 (no edge). These values are obtained by normalizing the cumulative histogram of the gradient values in a data set. A parameter value of 0.9 would refer to that gradient value where the cumulative histogram is at 90% of its maximum value.

The set of edges that resulted from the edge detection step was used to obtain local threshold values spanning the surface of the bone. The CT-number of a voxel that is part of the set of edges, served as a local threshold value for its neighbourhood. The total set of local thresholds was obtained by dilating the local-threshold surface in 3D iteratively until it filled a matrix of local threshold values, giving each voxel its own local threshold. During a dilation step, a voxel was included into the set of local thresholds if it had neighbouring voxels in a 3x3x3 neighbourhood that were included in previous steps. The local threshold value for the to-be-included voxel was calculated by taking the Gaussian weighted average of the threshold values of the voxels in the 3x3x3 neighbourhood. The dilation process was

continued until all voxels in the data set had been appointed a local threshold value (figure 2.2d).

The last step of the algorithm consisted of comparing the grey value of each voxel with its local threshold value and marking it as bone when it was higher than this value and marking it as non-bone otherwise, resulting in a binary data set (figure 2.1d, figure 2.2e). An extra condition was included here to decrease the effect of smearing out trabeculae that were thin relative to the resolution. The maximal CT numbers of such a thin trabecula will be lower than the CT number corresponding to the average density of the material. For a rod-shaped trabeculae, this decrease in CT number is proportional to the decrease in radius (4). By assuming all trabeculae have approximately the same mineral density, thin trabeculae could be identified by comparing a local threshold value to the average threshold value; when it was lower, a thin trabecula was identified. To reduce the risk of false positives, that is, classifying a thick trabecula as being thin, a minimal difference of one standard deviation between the local and the average threshold value was required before a trabecula was identified as being thin. The local threshold value was then adjusted upwards proportional to the difference between the original local threshold value (T_L) and the average threshold value ($T_{L,mean}$), scaled by the difference between the average threshold value and the average CT-number of the background ($CT_{background}$).

$$T_{L,adjusted} = T_L \left(1 + \frac{(T_{L,mean} - T_L)}{(T_{L,mean} - CT_{background})} \right) \quad (1)$$

The average CT-number of the background was a parameter that was set by the user (*BackgroundValue*). As a consequence of the adjustment, the resulting trabecula was slightly thinner than when the local threshold would not have been adjusted.

If not stated differently, the value for the radius of the Gauss filter (*GaussRadius*) was determined by trial and error, as was the *GradientCutOffLow* parameter. The *GaussRadius* had values ranging from 0.4 for scans with low noise content to 1.0 for scans with high noise content. *GradientCutOffHigh* was held constant for all segmentations and was set to 0.99. The value of *BackGroundValue*, needed for the compensation of smeared out thin trabeculae was set equal to the average CT-value of the background material, which is air in clean and dry samples and marrow or soft-tissue in whole bones and in-vivo scanning.

Decreasing the value of *GradientCutOffLow* resulted in the inclusion of thinner trabeculae and eventually in the inclusion of noise, but did not influence the thickness of the trabeculae. The value for this parameter was chosen just above the level where noisy structures started to appear in the

data sets. Increasing *GaussRadius* decreased the noise in the data sets, but also smeared out trabeculae, what could result in thickening of trabeculae. This value was adjusted in conjunction with *GradientCutOffLow* such that the lowest values possible for both parameters could be used.

Validation: Comparison with histological sections

Two rat tibias were scanned in a Skyscan-1072 Micro-CT scanner (Skyscan, Antwerp, Belgium), yielding reconstructed data sets with a voxel size of 11 μm . The system had an actual resolution of 8 μm specified by the manufacturer (10%MTF). The data sets were segmented both by using the local threshold method, and by applying a global threshold such that the resulting data sets had the same volume fraction as the data sets obtained from the local threshold method.

After scanning, the bones were embedded in MMA (Methyl Metacrylate). Serial sections were obtained by repeatedly slicing 30 μm thick sections off the MMA block. After each cut the bone at the surface of the block was stained with alyzarine-red, colouring the calcium red, and a microphotograph with a pixel size of 2 μm was taken of the block surface. Processing the sample en-block prevented geometrical distortion that occurs when processing thin sections.

Registration software from the university of Leuven (122) was used to automatically reposition the segmented data sets such that they optimally matched the set of histological microphotographs.

The cross-sections of the scan data were then compared to the histological data by overlaying the segmented serial microphotographs with the registered scan data and calculating the difference in bone area.

Comparing segmentation methods at different resolutions

To obtain data sets with different scan resolutions, but with equal noise content, scanning was simulated using a real scan as input. To serve as input data sets, six pieces of trabecular bone from core biopsies of canine distal femora, embedded in MMA were scanned in a Skyscan-1076 Micro-CT scanner. The system resolution, as specified by the manufacturer, was 15 μm (10% MTF). The resulting data sets had a voxel-size of 18 μm . Prior to embedding, the volumes of the core biopsies were measured using Archimedes' principle (50).

To simulate scanning at different resolutions, the radon transform of the original scan was calculated resulting in virtual shadow projections. These shadow projections were resampled to pixel sizes of 35 and 53 μm by selecting a random voxel in a 2x2x2 neighbourhood in case of the 35 μm samples and in a 3x3x3 neighbourhood in case of the 53 μm samples. By resampling, the noise levels remained constant. The inverse radon transform was calculated for the original sets of virtual shadow projections and the two

table 2.1: Overview of the study set-up to compare segmentation methods at different resolutions and noise levels

Noise levels	Resolutions		
	18 μm	35 μm	53 μm
Reconstruction types			
Low	X	X	X
Medium		X	
High		X	
Segmentation methods			
<i>GlobalArch</i>	One global threshold value determined by volume measurements		
<i>GlobalHist</i>	One global threshold value determined by histogram analysis		
<i>LocalAuto</i>	Local thresholds obtained through automated segmentation algorithm		

N=6. Each sample was reconstructed at three different resolutions with low noise levels, and at 35 μm also with medium and high noise levels. Each reconstructed data set was segmented with all three segmentation methods.

sets of resampled shadow projections, giving reconstructed data sets with voxel sizes of 18, 35, and 53 μm . The calculations were performed using Matlab (The Mathworks, Inc.).

All reconstructed data sets were segmented in three different ways. One set of data was obtained by applying the automatic local threshold algorithm with adjustment for smeared out trabeculae (*LocalAuto*). A second data set was obtained by applying a global threshold value that was chosen such that the volume of the resulting data set was equal to the volume of the original sample as determined using Archimedes' principle (*GlobalArch*). The third set was obtained by setting the global threshold at a value where the sensitivity of the volume to changes in threshold value was smallest, as determined after analysis of the density histogram (50) (*GlobalHist*). The study set-up is summarized in table 2.1.

For the *LocalAuto* method, the parameters *GaussRadius* and *GradientCutOffLow* were determined by trial and error for the data sets with 18 μm voxel size. The *GaussRadius* for the data sets with voxel sizes of 35 and 53 μm were respectively scaled to one half and one third of the *GaussRadius* of the data sets with the highest resolution. *GradientCutOffLow* was then adjusted to get the lowest acceptable value.

All samples in the same group were segmented with the same parameter values. To ascertain that only the segmentation methods themselves were compared, the Gaussian smoothing was also applied to all data sets before global segmentation. The same value for *GaussRadius* was used as for the local threshold algorithm.

For all resulting data sets, volume fraction and 3D-direct thickness (75) were calculated, as well as connectivity (149) and structure model index (SMI) (76). The first two parameters are representations of the bone mass

and its distribution and the last two parameters characterise geometry and topology of the bone sample. The parameters were calculated using the freely available software of the 3D-Calculator project¹. The effects of scanning resolution and the addition of noise on each segmentation method were assessed by analysing the relative change of the morphometric parameters.

A reliable segmentation method maintains the ability to detect group differences at decreased scan qualities. The method should be reliable in the sense that the way samples relate to each other when scanning at different resolutions should not change. In other words, if sample A has a volume fraction that is slightly higher than the volume fraction of sample B at high resolution, it should still have a higher volume fraction when the samples are scanned at a lower resolution. In this paper we will refer to this quality of segmentation algorithms with the term ‘reliability’, which was assessed by using regression analysis. If the way in which samples relate to each other is the same at different resolutions, the variation between samples at a low resolution is explained completely by the variation at a high resolution, which is expressed by the R^2 value. R^2 was assessed for each parameter and each thresholding method by regressing the outcomes for the data sets with 35 and 53 μm on the outcomes of the 18 μm data sets.

Finally, the different segmentation methods were analysed visually by overlaying the cross-sections for the different methods.

Comparing the influence of noise on the different segmentation methods

The effect of noise on the segmentation methods was investigated by adding noise to the 35 μm data sets described in the previous section. The original 35 μm data sets served as the low-noise reference. Data sets with medium and high noise levels were created by adding gaussian distributed noise with a standard deviation of 0.005 (medium) and 0.01 (high) to the virtual shadow projections of the 35 μm data sets.

After reconstruction, all data sets were segmented using the three different methods described above (*GlobalArch*, *GlobalHisto* and *LocalAuto*).

The *LocalAuto* parameter settings for the low noise data sets as determined in the previous section were taken as a reference for the data sets with higher noise levels. *GradientCutOffLow* was kept constant for these data sets, while *GaussRadius* was increased until no more noisy structures were present in the data sets.

The segmented data sets were analysed in the same way as in the study of the effects of decreasing resolution.

¹ The software can be downloaded at: www.eur.nl/jgg/orthopaedics/Downloads.html

Comparing segmentation methods for whole bone scans at different scan qualities

The tibia of a rat was scanned in-vivo using the Skyscan 1076 in-vivo system. Scanning time was kept short (20 minutes) to limit radiation dose absorbed by the living tissue, resulting in a data set with high noise levels. The resulting data set had a voxel-size of 18 μm . After sacrifice, the tibia of the rat was dissected and scanned in-vitro in a Skyscan 1072 micro-CT system. A long scan was made (3 hours) to obtain a high signal to noise ratio.

Both the high-quality (in-vitro) and low-quality (in-vivo) scans were segmented using both the automated local threshold algorithm and by using the most optimal global threshold value. When the global threshold was chosen too high, no trabecular bone was included in the segmentation. On the other hand, when the global threshold was chosen too low, all trabecular bone was included, but cortical bone was oversized. For a range of threshold values the difference in volume estimates between the globally and locally segmented data sets for cortical and trabecular bone was calculated as a percentage of the cortical, respectively trabecular bone

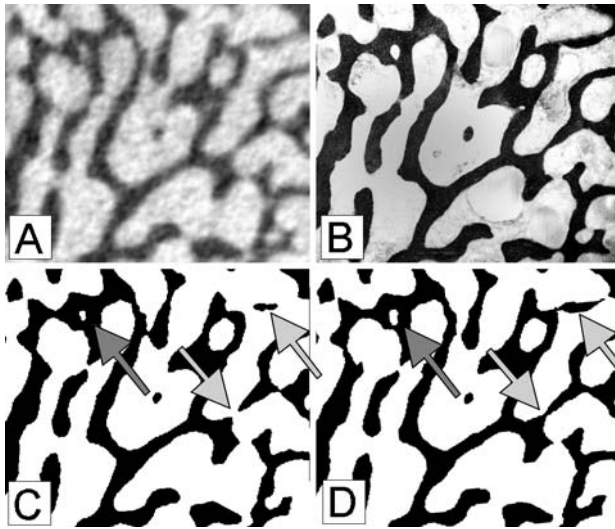


figure 2.3 Comparing micro-CT scans with a voxel size of 11 μm (A) with histological sections with a pixel size of 2 μm (B). The micro-CT image was segmented using the global threshold method (C), set at a level where the resulting volume fraction was equal to the volume fraction resulting from the local method, and was segmented by the local threshold method (D) Light grey arrows indicate thin structures that were not detected by the global method in this section. Also notice the hole that was almost filled up in the globally thresholded image (dark grey arrow).

volume in the locally segmented data set. The minimum in total difference was chosen as the most optimal global threshold value.

Animal procedures formed part of a larger experiment for which approval was obtained of the Animal Ethics Committee.

2.3 Results

Comparison with histological sections

Using the local threshold method as well as applying the global threshold, set at a threshold value that resulted in the same volume fraction as with the local method, resulted in very good representations of the bone. For both thicker and thinner structures, the histological images were nearly identical to the segmented cross-sections obtained with the local threshold method (figure 2.3). Quantitative analysis of bone area showed an average difference of -0.5% between the corresponding locally and globally thresholded cross-sections and the histological sections. Where the locally thresholded cross-sections gave differences in bone area when compared to the histological sections that varied between -0.4% and -0.6%, the globally thresholded cross-sections gave differences that varied between -1% and 1%. Detailed examination showed that the most negative differences of the globally thresholded cross-sections were measured in sections that contained thin structures that were less well detected by the global method than by the local method (figure 2.3).

The influence of a reduction in resolution on segmentation methods

When resolution of the data sets was decreased from 18 to 35 μm , the local segmentation method (*LocalAuto*) gave the least change in parameter values. Parameters changed on average by about 7% for the local method, while the global methods resulted in changes of 12% and 13%. Reliability was very high for all methods, with R^2 values ranging from 0.96 to 0.98. Changes in parameter values and the results of the reliability test are summarized in table 2.2 and table 2.3. When resolution was further decreased to 53 μm , the performance of all methods deteriorated strongly resulting in changes of approximately 30%.

At high resolution the *LocalAuto* method resulted in a slightly higher value

table 2.2 Relative change in parameter value (%) for decreasing resolution

	18-35 μm			18-35 μm		
	<i>GlobalArch</i>	<i>GlobalHist</i>	<i>LocalAuto</i>	<i>GlobalArch</i>	<i>GlobalHist</i>	<i>LocalAuto</i>
BV/TV	1	10	2	1	24	7
Tb.Th	10	13	3	21	28	17
SMI	18	5	7	33	16	22
Cd.	23	19	14	69	47	61
Mean	13	12	7	31	29	27

table 2.3 R^2 Values obtained from regression analysis of high resolution to low resolution

	18-35 μm			18-53 μm		
	<i>GlobalArch</i>	<i>GlobalHist</i>	<i>LocalAuto</i>	<i>GlobalArch</i>	<i>GlobalHist</i>	<i>LocalAuto</i>
BV/TV	1	1	0.99	1	0.93	0.98
Tb.Th	1	1	0.99	0.98	0.95	0.57
SMI	0.95	0.84	0.95	0.82	0.27	0.92
Cd.	0.98	0.98	1	0.59	0.95	0.75
Mean	0.98	0.96	0.98	0.85	0.78	0.81

for volume fraction than the two global methods (figure 2.4). When resolution was decreased, the volume fraction for the *GlobalHist* method increased rapidly and rose above values for the *LocalAuto* method. For all resolutions the *LocalAuto* segmentation method gave thinner trabeculae and a more plate-like structure, indicated by SMI values close to one. In absolute values, connectivity density did not show much difference between the segmentation methods.

Visual inspection of the segmented data sets showed that, in general, both global methods resulted in more bone on the outside of the core samples, while the *LocalAuto* method resulted in more bone at the inside of the core sample (figure 2.5). This difference became stronger as resolution decreased.

The influence of noise on segmentation methods

Adding noise had the least effect on the parameter values estimated with the *GlobalArch* method. On average the values changed 6% when medium noise levels were added and 7% when high noise levels were added. The *GlobalAuto* method gave changes of respectively 8% and 10% for the

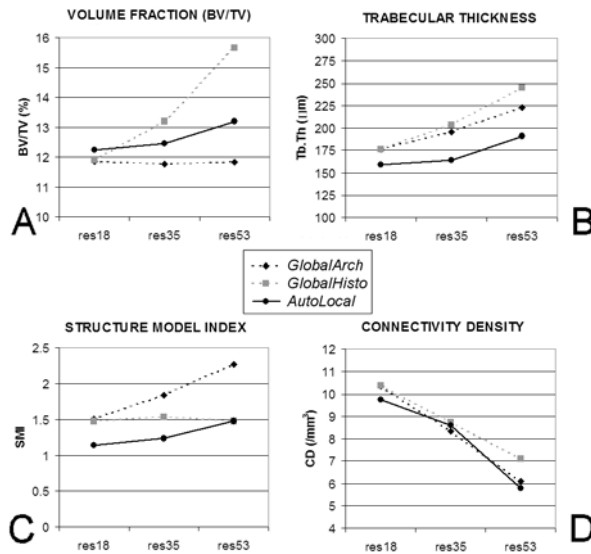


figure 2.4 Parameter values averaged over all samples for the different methods (*GlobalArch*, *GlobalHist*, *LocalAuto*) as a function of the different resolutions (18, 35 and 53 μm). A) Volume Fraction B) Mean trabecular thickness C) Structure Model Index and D) Connectivity Density

table 2.4 Relative change in parameter value (%) for adding noise

	18-35 μm			18-35 μm		
	<i>GlobalArch</i>	<i>GlobalHist</i>	<i>LocalAuto</i>	<i>GlobalArch</i>	<i>GlobalHist</i>	<i>LocalAuto</i>
BV/TV	1	1	0.99	1	0.93	0.98
Tb.Th	1	1	0.99	0.98	0.95	0.57
SMI	0.95	0.84	0.95	0.82	0.27	0.92
Cd.	0.98	0.98	1	0.59	0.95	0.75
Mean	0.98	0.96	0.98	0.85	0.78	0.81

table 2.5 R^2 Values obtained from regression analysis of low to high noise levels

	18-35 μm			18-35 μm		
	<i>GlobalArch</i>	<i>GlobalHist</i>	<i>LocalAuto</i>	<i>GlobalArch</i>	<i>GlobalHist</i>	<i>LocalAuto</i>
BV/TV	1	1	0.99	1	0.93	0.98
Tb.Th	1	1	0.99	0.98	0.95	0.57
SMI	0.95	0.84	0.95	0.82	0.27	0.92
Cd.	0.98	0.98	1	0.59	0.95	0.75
Mean	0.98	0.96	0.98	0.85	0.78	0.81

addition of medium and high noise, and the *LocalAuto* method gave changes of 10% and 17% (table 2.4). *GlobalArch* gave similar results for reliability as *LocalAuto*, with R^2 values of about 0.97 for addition of medium noise levels and 0.94 for addition of high noise levels. *GlobalHist* gave the least reliable results with R^2 values of 0.87 for addition of medium noise levels and 0.84 for addition of high noise levels (table 2.5).

The effects on the various parameters showed strong differences between the segmentation methods. The *GlobalArch* method had problems with representing connectivity: the reliability went down to 0.82 for the highest noise level. *GlobalHist* had problems with estimating the volume (BV) and especially with SMI (R^2 as low as 0.56 for the addition of the highest noise level). The *LocalAuto* method gave strong increases in the absolute value for SMI, and had problems with trabecular thickness, where reliability decreased to 0.86 when high noise levels were added.

Comparison of the segmentation methods for whole bone scans

Applying the local threshold algorithm to the high quality in-vitro scan of a whole rat tibia resulted in a visually convincing segmentation. The local segmentation of the lower quality in-vivo scan showed only minor differences compared to the high quality data set; Metaphyseal trabeculae were slightly thicker (figure 2.6B2 and C2).

For high global threshold values the cortical bone in the globally segmented data set resembled the cortical bone in the locally segmented data set. However, no trabecular bone was included in the data set. Adjusting the global threshold value downwards resulted in the inclusion of more trabecular bone, but this was accompanied by a strong increase in cortical bone volume. Setting the global threshold at the value where there was no difference in total bone volume with the locally segmented data set, would still result in a trabecular bone volume that was more than 40% less

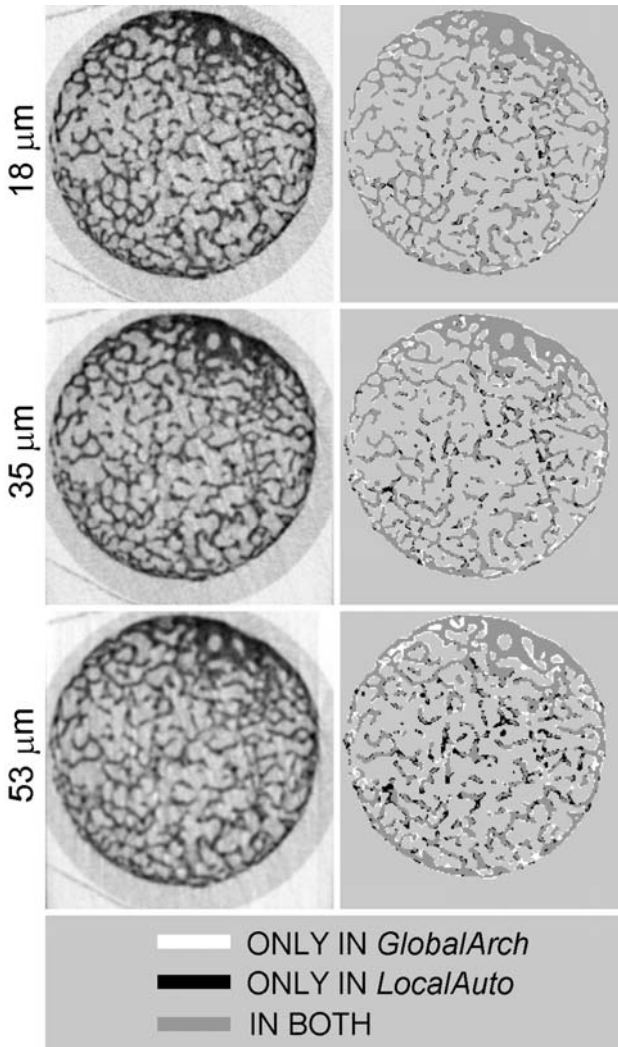


figure 2.5 Same cross-section at three different resolution. Shown here are the original reconstructed image, together with the GlobalArch and LocalAuto segmented images laid on top of each other (white is GlobalArch only, black is LocalAuto only, grey is both). Notice that the globally segmented images have more bone on the outside of the circle, while the images segmented with the local threshold method have more bone on the inside.

than the trabecular bone volume resulting from the local segmentation algorithm (figure 2.6A).

At the optimal global threshold, where the summed difference in cortical and trabecular volume between globally and locally segmented data sets was smallest, the globally segmented data set showed a cortex that was thicker

than the cortex of the locally segmented data set while less trabecular bone was detected. Compared to the globally segmented data set of the high quality scan, the globally segmented data set of the in-vivo scan showed few differences. The trabecular structure appeared slightly more fragmented (figure 2.6B3 and C3).

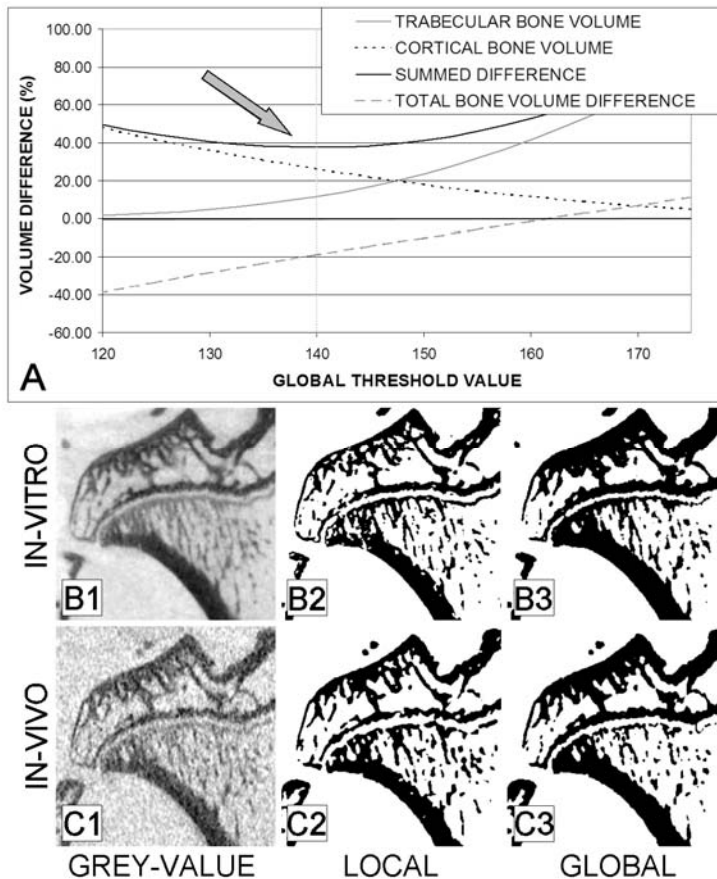


figure 2.6: The effect of global and local thresholds on in-vitro and in-vivo scans of whole bones. A) Absolute difference in the estimation of cortical bone and trabecular bone with respect to the locally segmented data set as a function of the global threshold value. The minimum of the summed difference indicates an optimum. Note that at the optimum (grey arrow) there is a difference between the volumes of the locally and globally segmented data set. B) Example of in-vitro scan, showing a grey-value cross-section (B1), that is segmented with the local method (B2) and the global method using the optimal threshold (B3). C) Example of in-vivo scan, showing a grey-value cross-section (C1), both segmented with the local method (C2) and the global method (C3). Notice the overestimation of the cortical bone and the subchondral bone in the globally segmented cross-sections.

2.4 Discussion

Segmentation of micro-CT data sets is not a trivial issue and its complexity is often neglected or underestimated. In this paper we have tried to clarify this issue by comparing different segmentation techniques and by introducing a new segmentation algorithm using local threshold values.

Applying this local threshold method gave very accurate results. For high quality scans, the segmented dataset was a nearly exact representation of the real bone, as could be seen by comparison with histological sections (figure 3). All trabeculae, both thick and thin, were represented with the correct thickness. The structural integrity of the trabecular network was represented correctly as well and no connections between trabeculae were missed. Applying a global threshold performed almost equally, but some of the thinner connections between trabeculae were lost. These connections could be recovered by adjusting the global threshold value, but this would result in thickening of the trabeculae, and thus in an overestimation of the bone volume.

The global segmentation method could only give such a good result given prior knowledge about the real volume of the bone, a pre-requisite that is not needed for the automatic local threshold algorithm. In many situations information about the volume of a bone sample is not present or difficult to get. When scanning core biopsies, the bone volume can only be obtained after a cumbersome measurement procedure based on Archimedes' principle. For entire bones it is even practically impossible to get the real volume of the bone, which excludes the global segmentation method based on knowledge about bone volume.

Another situation in which it is impossible to obtain the real volume of a bone is when animals are scanned in-vivo. The added value of scanning living animals lies in the fact that the longitudinal study design allows comparison of scans of different time-points of the same animal, such that temporal changes in bone architecture can be followed at the level of single trabeculae (194). Since radiation load on living tissues should be as small as possible, the quality of the scans is limited. The resulting images contain more noise and have a lower resolution than in conventional micro-CT. This situation places high demands on the method of thresholding. Even though the influence of noise seems rather small on both local and global segmentation methods, global thresholding methods fail to give a good representation of the bone. This is partly caused by the relative low resolution of the system that makes thin structures appear less dense. Besides, the result of global thresholding will also be affected by differences in mineralization between cortical and trabecular bone (figure 2.6). Thus, in-vivo scanning is more powerful when combined with local segmentation techniques.

This study indicates that when good quality scans are made at high resolution, and the samples have a homogenous structure, a global threshold performs just as well as the local threshold method. A typical situation that satisfies these conditions is when studies are undertaken in which bone biopsies are scanned at high resolution and compared. The convenience and speed of applying a global threshold makes using this method very tempting. However, the implications of the choice of global threshold value should not be underestimated. In most studies, bone biopsies of subjects with a certain pathological condition or biopsies resulting from some intervention study are compared to controls. The possible changes in bone morphology and bone mineralization caused by these pathologies or interventions will affect the distribution of densities of the scans and thus might interact with the choice of threshold value. This problem can be reduced when the real volume of the samples are known. However, often this volume is not known. In general, using a global threshold might result in uncertainties about which part of the measured difference between groups are caused by the choice of threshold value. Since the result of the local threshold method is not influenced by changes in mineralization and is less sensitive to changes in architecture (especially to changes in the amount of thick versus thin trabeculae), using this method could reduce the uncertainty about measured differences between groups. Although the results presented in this study support this assumption, more tests are needed to see if the local segmentation method is truly better at predicting group differences.

Local segmentation of high resolution scans resulted in accurate representations of the volume. However, when resolution was decreased, the local segmentation method started to overestimate the volume of the scan. This phenomenon is related to the smearing out of thin structures. The lower the resolution, the more trabeculae are smeared out around their real edge, and compensation starts to become problematic. Global methods were also affected by this phenomenon resulting in a strong increase in trabecular thickness with decreasing resolution (figure 2.4b). The average increase in trabecular thickness resulted in extra volume being added to the thickened trabeculae. For the *GlobalArch* method, in which the volume of the data sets was fixed, this extra volume was balanced by an equal decrease in the volume of thinner trabeculae and thus to changes in structure. This is clearly reflected in the change of structural parameters like connectivity density and especially SMI for this method (figure 2.4). As indicated by the less severe changes in SMI and connectivity, the *GlobalHist* method favoured structural integrity above volume. As a consequence, there was a strong rise in trabecular thickness and especially in volume fraction. The local segmentation combined the strong points of both global threshold methods, since it combined preservation of structural integrity with good

representation of bone volume.

A further decrease in resolution to a voxel-size of 53 μm resulted in unreliable results for all segmentation methods. At this resolution, average trabeculae have a real thickness of less than 2 or 3 voxels, which is not sufficient for good representation of the bone. Still the results show that the *LocalAuto* method gave better volume estimates than the *GlobalHist* method, and a better structural integrity than the *GlobalArch* method. A study by Laib and R  gsegger (111) tried to extract volume related parameters from human in-vivo scans at much lower resolutions than were used in the present study (165 μm voxel-size). Their methods gave surprisingly good reliability values for the measured parameters, comparable to the global methods in this paper. However, the low resolution made it impossible to extract the exact structure.

The effects of noise on the different segmentation methods could mostly be explained by the effects of the smoothing filter needed to remove this noise. Filtering the noisy data sets blurred out the smallest details and thinnest trabeculae. Logically, this had the greatest influence on those methods that were most sensitive to thin structures. Blurring the thinnest structures did not influence the *GlobalArch* method, which favoured the detection of thick trabeculae above the detection of thin trabeculae, since it already failed to detect the thin trabeculae in the low noise situation. The *LocalAuto* method on the other hand, detected both thick and thin trabeculae and was therefore very sensitive to blurring of the thin trabeculae. As a result, the thickness of the blurred thin trabeculae was overestimated and the average thickness increased. The thickness measure was affected less for samples with mainly thick trabeculae than for samples with both thin and thick trabeculae, explaining the decrease in reliability of the trabecular thickness measure for the *LocalAuto* method when high noise levels were added to the samples (table 2.5).

Overlaying the globally thresholded data sets with the data sets obtained with the local threshold algorithm illustrated an interesting phenomenon (figure 2.5). The local segmentation method detected more bone in the centre of the bone sample, while the global method resulted in thicker structures on the outside of the bone sample. Imperfect beam hardening correction in a reconstructed data set generally causes the outside of a cylindrical object to appear denser than the inside. Using a global threshold therefore resulted in overestimation of the thickness of the trabeculae in the outer section of a bone sample, while it underestimated the thickness on the inside of the sample. Since this difference of apparent density did not influence the local edges of the bone in a reconstructed data set, beam hardening artefacts have little influence on the local segmentation algorithm, as is demonstrated with the overlaid cross-sections (figure 2.5).

In conclusion, the local threshold method gives a nearly exact representation of a scanned bone at high resolutions without the need for a priori knowledge about the volume of the bone. When analysing high resolution scans of homogenous structures, e.g. bone biopsies, the performance of global threshold methods perform similarly to the local threshold method. As soon as the scanned structures are not homogenous and include e.g. both thick cortices and thin trabeculae, or when scan resolution is relatively low, the local threshold method outperforms the global methods. This makes the local threshold method ideally suited, and perhaps even crucial, for use with in-vivo micro-CT.

The local segmentation algorithm is included in the software for the 3D-Calculator project, and can be downloaded at:
www.eur.nl/fgg/orthopaedics/Downloads.html

Acknowledgements

This work was supported by European Union grant QLRT-1999-02024 (MIAB).

3

Detecting and tracking local changes in the tibiae of individual rats: A novel method to analyse longitudinal in vivo micro-CT data

J.H. Waarsing, J.S. Day, J.C. van der Linden, A.G.H. Ederveen, C. Spanjers, N. De Clerck, A. Sasov, J.A.N. Verhaar, H. Weinans

Reprinted from: Waarsing et al. BONE, 2004 Jan;34(1):163-9

Abstract

- **Introduction:** In this study we present the analysis of in vivo micro-CT scans, using a new method based on image registration that accurately evaluates longitudinal micro-CT studies. We tested if detailed changes in bone architecture could be detected and tracked in individual animals.
- **Methods:** A prototype in vivo micro-CT scanner (Skyscan 1076) was developed in which tibiae of rats that are lying on a bed under gas-anaesthesia, were scanned. For this study, three female Wistar rats were used: a sham operated rat, an ovariectomised rat, and one rat that served as a reproducibility control. The reproducibility control rat was scanned twice in one day. The other animals were scanned at week 0, just before surgery, at week 4 and at week 14 after surgery. Architectural changes over time were detected by overlaying two data sets made at different time points, using an algorithm that uses mutual information for optimal registration. The scans were segmented into binary data sets using a local thresholding algorithm.
- **Results:** The reproducibility test showed small errors of less than 3% in bone volume measurements and errors less than 0.5% in measurements of trabecular thickness. The sham operated rat showed no changes in total bone volume, though thinning and eventual loss of some small trabeculae could be detected, which could be related to the age of the animal. The OVX rat lost large amounts of trabecular bone volume, especially in the metaphysis (60% at week 4, 75% at week 14). Remaining trabeculae slowly increased in thickness. Following the different scans in time showed the forming of new trabecular structures. Additionally, small longitudinal growth at the growth plate could be detected after the first 4 weeks. Further, the OVX rat showed extensive modelling at the proximal endosteal lateral cortex.
- **Conclusion:** We have shown a new method that can detect and track changes in local bone architecture and individual trabeculae in time, in an individual living animal. This method enables longitudinal in vivo micro-CT studies and has the potential to greatly contribute to experimental rat/mouse studies on pharmacological intervention and transgenic models.

3.1 Introduction

Micro-CT scanning makes it possible to analyse the architecture of bones at the trabecular level non-destructively, both qualitatively by visual inspection of informative three dimensional (3D) images of the trabecular network, and quantitatively by calculation of model-independent 3D morphometric parameters (146). In vivo scanning of small animals allows longitudinal study designs, which largely increases research possibilities. Until recently, only in vivo experiments using synchrotron x-ray sources had been described (101, 113). By now, technological progress made it possible to develop a table-top in vivo micro-CT scanner using polychromatic x-ray sources.

In this paper we present illustrative results of one of the first table-top in vivo micro-CT scanners and introduce a method to evaluate follow up in vivo micro-CT scans of the proximal tibia of rats, based on image registration (matching). We specifically tested if detailed changes in architecture at the trabecular level could be detected in individual normal and OVX rats during a 14-week period.

3.2 Method

A prototype in vivo micro-CT scanner (Skyscan 1076: Skyscan, Antwerp, Belgium) was developed which consists of an animal-bed, around which the x-ray source and the camera rotate. The machine is equipped with a 100 kV x-ray source with a spot size of 5 μm . During the scan, the animals were lying on the bed under gas-anaesthesia, while the right hind-leg was fixed in a cylindrical plastic holder. Only the leg was radiated, thus minimising the effects of radiation. During the scan the soft tissue in the leg of the animal received a radiation dose of about 0.4 Gy, as measured by a dosimeter.

A scan lasted about 20 minutes, resulting in shadow projections with a pixel-size of 10 μm . A modified Feldkamp algorithm, using under-sampling to reduce noise, was applied to the scan data, resulting in reconstructed 3D data sets with a voxel-size of 20 μm .

For this study the right tibiae of three 10-month-old female Wistar rats were scanned. One rat served as a reproducibility control and was scanned twice in one day. The remaining two rats were scanned at three time-points. The rats were scanned at week 0, after which one rat was ovariectomised (OVX) and the other was sham-operated. The micro-CT measurement was repeated at week 4 and week 14. The sham and OVX animals received calcein labelling ten days and one day before sacrifice. The scans form part of a larger animal experiment, for which approval was obtained from the Animals Ethics Committee (Organon, Oss, The Netherlands).

Architectural changes over time can be detected by overlaying two data sets, provided that the data sets have equal orientations. Unfortunately this is not the case, since a rat-leg cannot be fixed in the holder in exactly the

same position twice. Therefore data sets need to be reoriented before they can be laid on top of each other. Data sets of different time points were matched by rotating and translating one data set with respect to the other. We used registration (matching) software developed at the University of Leuven, which automatically matches two data sets using an optimisation criterion based on maximising mutual information (122). Epiphyseal and metaphyseal areas of the tibiae were registered separately to ensure that possible growth of the bone did not affect the registration. Further, the fibulae were removed from the data sets.

Correct registration of the metaphysis of the OVX-animal was hindered by the relatively large architectural changes that occurred as a result of the ovariectomy. To overcome this problem, small Volumes of Interest (VOI) were selected around details, like trabeculae and arterial openings in the cortex that could be identified in all scans of the different time-points. New data sets were created containing only the information inside the VOIs. These altered data sets served as input for the registration algorithm, and the resulting transformation matrix was used to rotate and translate the original data sets. Data sets of week 0 and week 14 were rotated using the data sets of week 4 as reference.

The registered data sets were segmented into binary images. Because of the noise and the relative low resolution of the data sets, simple global thresholding methods were not sufficient to segment the data. We used a local segmentation algorithm consisting of a standard edge-detection algorithm, extended to 3D, to find the location of the actual surface of the bone. CT-numbers at the position of the bone surface were used to construct a local threshold matrix, which was used to segment the data set. An option in the algorithm was used to accurately represent thin trabeculae that have a size close to resolution limits. A detailed description and validation of the algorithm is published elsewhere (196).

Cortical and trabecular bone were separated manually using in-house software. Thickness of the trabeculae in the data sets was calculated using a model independent thickness method (75).

To verify if the formation of new bone that was suggested by comparing the scans of two time points really represented new bone, the tibia of the OVX rat was prepared and embedded in black epoxy resin (148). The tibia was cut longitudinally and microphotographs were taken of the calcein labelled surface. The images were taken en-block to prevent geometric distortion caused by cutting thin slices. Using the registration software, these sections were matched with the scan-data.

3.3 Results

The reproducibility study showed an error in the bone volume measurement smaller than 3% and a small error of 0.5% in the measurement of the

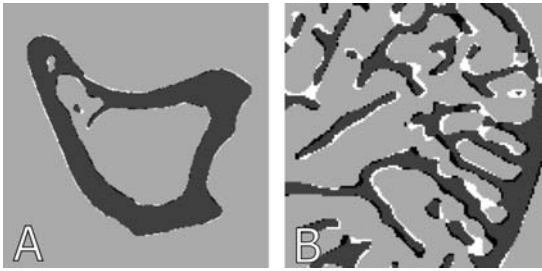


figure 3.1: Registered overlaid cross-sections from the reproducibility study. Grey indicates where the scans overlap, black and white show the difference. A) Diaphyseal cross-section with mainly cortical bone. B) Detail of epiphyseal trabecular bone.

average trabecular thickness. Limitations in the precision of the registration algorithm caused a shift of about one pixel between the positions of the bone surfaces of the two scans as seen when laid on top of each other (figure 3.1). Over the total bone scan, the one-pixel shift sums up to a volume of 15% that does not exactly match, due to the relatively large surface to volume ratio of cancellous bone. This matching error has no influence on measurements of total bone volume and architectural parameters, and only minor influences on measurements of local bone apposition and resorption.

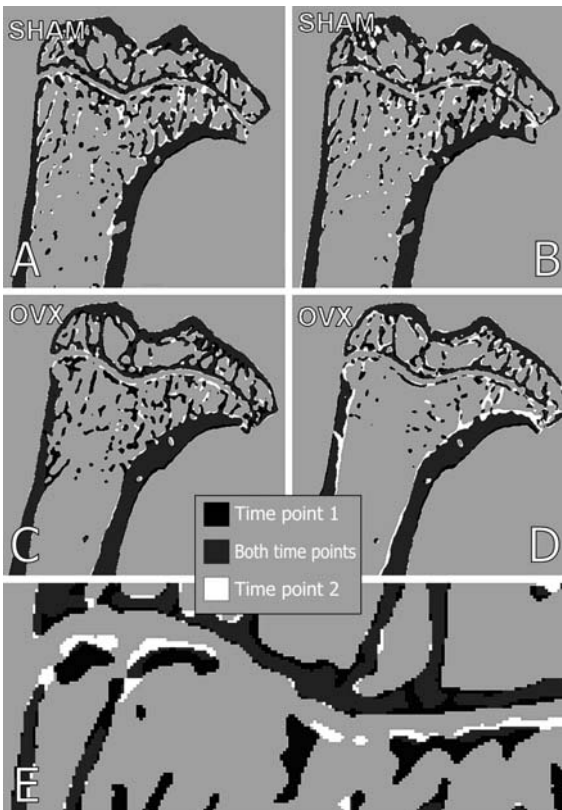


figure 3.2: Longitudinal cross-sections of the tibiae, overlaid after applying the registration algorithm. Black indicates bone that was only present in the older scan and white indicates bone only present in the newer scan. A) Sham operated rat, week 0/4. B) Sham operated rat week 4/14. C) OVX rat, week 0/4. D) OVX rat, week 4/14. E) Detail of the growth plate of OVX rat, showing growth between week 0 and 4 (in white).

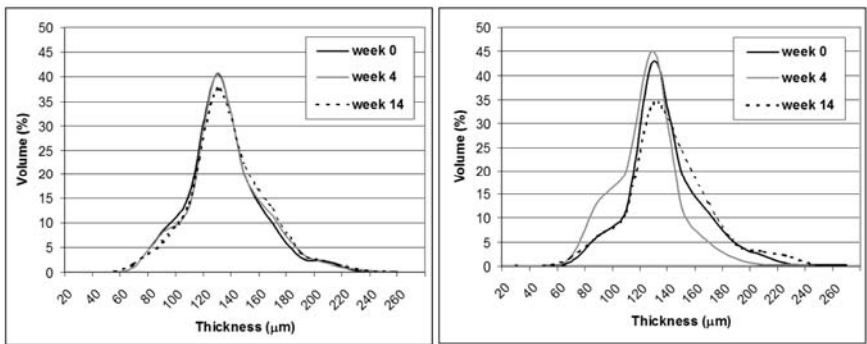


figure 3.3: Thickness distribution of the trabecular bone at the metaphysis of the sham operated rat (A) and OVX rat (B).

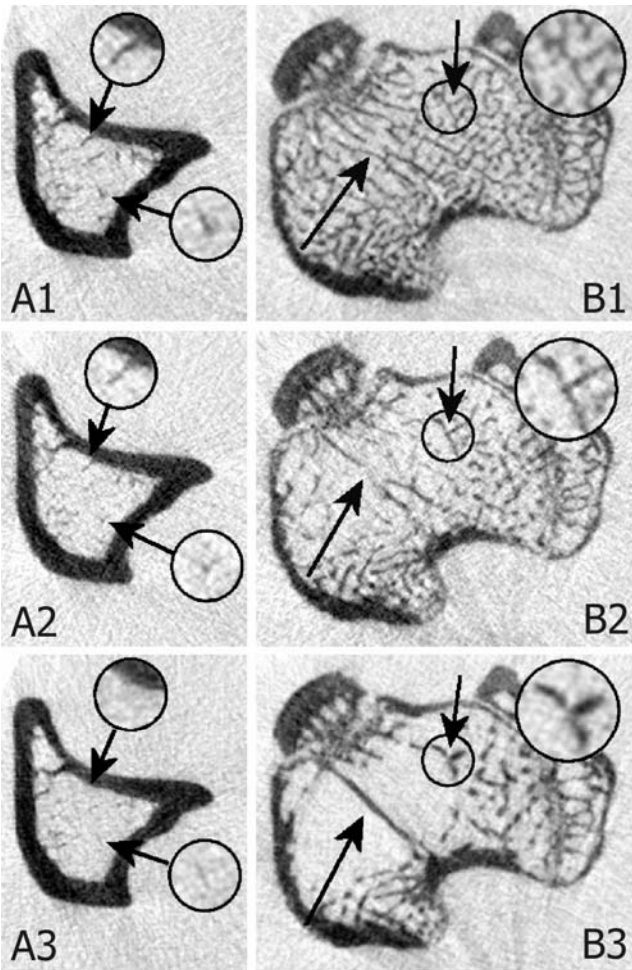


figure 3.4: Each cross-section (not segmented) represents the same area of the bone at week 0 (A1, B1), week 4 (A2, B2) and week 14 (A3, B3). A) Example of thinning trabeculae in the sham operated rat. B) Example of thickening of the remaining trabeculae in the OVX rat.

In the 14 weeks in which the animals were followed, the sham operated rat showed no changes in bone volume larger than the detection limit of 3% (figure 3.2a, b). The trabeculae showed a small increase in average thickness during the duration of the study (figure 3.3a) (epiphysis: 116 μm in week 0 to 121 μm in week 14; metaphysis: 99 μm in week 0 to 102 μm in week 14). More locally, detailed examination of the matched data sets showed thinning and eventual loss of more distally situated metaphyseal trabeculae (figure 3.4). No changes could be detected in the thickness of the cortex. The average cortical thickness for all time points was 390 μm .

As expected, ovariectomy induced a dramatic loss of both epiphyseal and metaphyseal trabecular bone (figure 3.2c, d). After 4 weeks the OVX rat had lost about 25% of its epiphyseal trabecular bone volume and 60% of its metaphyseal trabecular bone volume. In the following 10 weeks the loss proceeded even further to about 30% in the epiphysis and 75% in the metaphysis. Initial thinning of the trabeculae in the first 4 weeks (epiphysis: from 130 μm to 116 μm ; metaphysis: from 108 μm to 96 μm) was followed by a gradual increase in thickness of the few remaining trabeculae from week 4 to 14 (epiphysis: from 116 μm to 122 μm ; metaphysis: from 96 μm to 110 μm) (figure 3.3, figure 3.4).

Detailed examination of the matched data sets revealed between 20 to 40 μm of growth at the growth plate of the OVX animal after 4 weeks (figure 3.2e). This growth did not continue in the following ten weeks. This second period is characterised by large modelling activities at the lateral side of the cortex resulting in shape changes in the cortex (figure 3.2). Resorption takes place at the periosteal surface of the proximal side of the tibia, while bone apposition occurred at the endosteal surface. Areas of endosteal bone apposition corresponded well with areas of double calcein labelling (figure

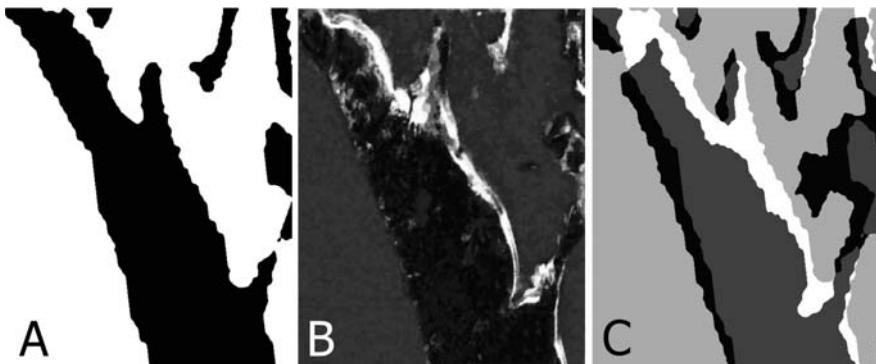


figure 3.5: Comparison of the overlaid registered scan data (C) with calcein labels (B) and segmented image of the detail A). All images represent the same area in the bone. White in C) represents new bone formation and corresponds to the calcein label in B). Black indicates resorbed bone, which cannot be seen in the histological section.

3.5). The average thickness of the cortex of the OVX rat increased from 420 μm at week 4 to 480 μm at week 14.

3.4 Discussion

In this paper we have shown that it is possible to detect and track local changes in bone architecture in small animals in vivo. By combining in vivo Micro-CT and 3D image registration, we could follow the resorption of some trabeculae and the slow increase in thickness of other trabeculae, as well as the effects of growth at the growth plate and geometric changes of the lateral cortex.

Noise was the limiting factor in the detection of small local changes in the bone scans; it limited both the accuracy of the segmentation algorithm in the exact localisation of the bone surface and the precision of the registration algorithm. Despite the trade-off between image noise and radiation dosage, noise can be reduced while keeping scanning times short, by improving scanner geometry and using improved CCD cameras.

An exact biological match of two scans made at different time-points, would be a match in which a bone packet present in one scan falls on top of the same bone packet in the second scan. The bigger the morphological changes in the bone between two time-points, the more likely it is that the mathematical match given by the registration software deviates from the optimal biological match. The solution to this problem would require prior knowledge about which parts of the bone do change, and which parts do not. In our analysis we have assumed that during OVX small details like remaining, non-resorbed, trabeculae and arterial openings in the cortex do not change, or at least to a much lesser extent than the general shape of the bone. This assumption leads to a match in which extensive reshaping in the lateral cortex of the proximal tibia can be seen, consisting of resorption of the periosteal surface and apposition at the endosteum. Double labelling present at the endosteal surface of the cortex, indeed confirms the endosteal apposition and thus supports the registration method (figure 3.4).

A good measurement method is a method in which the measurement does not influence what is measured. Using ionising radiation calls for some concern on this aspect, especially since bone marrow is rather sensitive to radiation: In humans, whole body dosages starting at about 250 mGy lead to reduced lymphocytes counts (26). Studies about the effects of small dose irradiation on bone remodelling are rather scarce, though evidence seems to point to higher threshold values for bone cells. A single dose of 5 Gy impairs bone regeneration in rats, but no clinical effects could be measured at 2.5 Gy (88). At microscopic levels, doses down to 2 Gy resulted in changed growth-plate structure (17). Lower doses of 400 mGy and less showed no effects on osteoblast differentiation and activity in a cell-culture study (39). It is therefore unlikely that any of the changes in bone seen

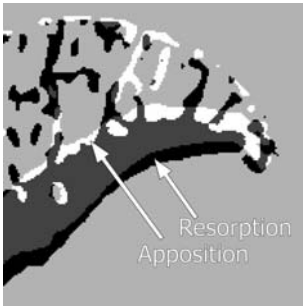


figure 3.6: Detail of the lateral cortex of the metaphysis of the OVX rat, showing extensive modelling (resorption and apposition at different locations) of the cortex between week 0 (black) and week 14 (white).

during this study could have been caused by the radiation dose of 400 mGy exerted during the scans.

Loss of trabecular bone due to ageing is a well-known phenomenon. It has been reported in rats in several studies, where bone loss starts to occur after 9 months of age (9, 126, 200). The thinning and loss of small trabeculae in the more distally located area of the metaphysis as seen in the sham operated rat could well be explained by ageing, since the rat was over 9 months old.

Estrogen depletion caused by ovariectomy induces dramatic trabecular bone loss and changes in trabecular architecture(109, 113), which was clearly seen in the OVX rat. The thickness of the trabeculae decreased in the first 4 weeks and increased in the following weeks, which was also noticed by Laib et al.(109). Besides loss of bone, following the changes in bone over time revealed the forming of new trabecular structures. Old trabecular structures are remodelled into new, thicker and clearly distinct structures, of which the trabecular rod in figure 4 is the most striking example. Aging rats form bony bridges across the growth plate, functionally fusing it. It is considered that these bony bridges make longitudinal growth impossible in aged rats (for females of 10 months and older) (124). Still, the 10-month-old OVX rat showed a small but clear longitudinal growth by apposition of new bone at the growth plate. This might be related to estrogen depletion, since estrogen has been shown to interact with growth plate function (186, 199).

After ovariectomy, the lack of estrogen increases remodelling activity on the entire bone surface, and within a few remodelling cycles large amounts of trabecular bone are lost. This suggests very low osteoblast activity. On the other hand, large endosteal bone apposition on the lateral side of the cortex is seen, and remaining trabeculae increase in thickness, suggesting high osteoblast activity. At the proximal periosteal surface bone is being resorbed, while at the same time osteoblast activity at the endosteal surface of the cortex results in the formation of new bone, a phenomenon that normally accompanies longitudinal bone growth (figure 3.6). It is not understood why these bone cells behave differently at different sites under the same conditions (here: estrogen depletion). It is not clear to what extent

this difference in cell behaviour is spatially and temporally determined: Immediately after OVX some trabeculae are resorbed while others stay intact, which points to spatial differences in cell activity. Nevertheless, most bone apposition can be seen in the latter ten weeks of this study, pointing at temporal differences in cell behaviour. Over time, different hypotheses have been introduced trying to explain this difference in cell behaviour. It was suggested that cells might possess positional information (209), or that cell behaviour is determined by local and time-varying stimuli, like mechanical deformation of the bone matrix (74) or strain energy density (84). Using *in vivo* scanning we are now able to further study this phenomenon. Together with finite element modelling and computer simulations of the remodelling process (188, 190), *in vivo* micro-CT might contribute to the discussion on whether bone cells possess positional information, or act on spatially or temporally distributed (mechanical) stimuli.

These new developments of *in vivo* micro-CT scanning make it possible to perform longitudinal studies in small animals, reducing the numbers of animals needed, while accurately measuring local architectural changes of the bone over time. The methods we introduced here will greatly contribute to experimental studies in small animals concerning orthopaedic or pharmacological intervention and transgenic mouse models.

Acknowledgements

The authors like to thank Pieter Sijrier (Erasmus Medical Center) for his help with scanning.

This work was supported by European Union grant QLRT-1999-02024 (MIAB).

4

Bone loss dynamics result in trabecular alignment in aging and ovariectomised rats

J.H.Waarsing, J.S.Day, J.A.N. Verhaar, A.G.H.
Ederveen, H.Weinans

Reprinted from: Waarsing et al. JOR, 2006, May;24(5):926-35

Abstract

- **Introduction:** Because of the destructive nature of techniques used to measure bone morphometry, studies of architectural changes and bone loss have utilized cross-sectional study designs, with all its inherent limitations in nuances. Here, the results of a longitudinal study using in-vivo micro-CT are presented elucidating the dynamics of bone loss and architectural adaptation in rat models of aging and post-menopausal bone loss.
- **Methods:** Using 3D analysis methodology, we observed the changes in bone architecture in the proximal tibia of normally aging and ovariectomised rats for 54 weeks.
- **Results:** Spatial patterns in bone resorption were observed that were similar for both groups. Remaining trabeculae increased in thickness or were remodeled into new trabecular structures, especially in the ovariectomised animals. The combination of bone loss and bone formation resulted in alignment of trabeculae across the growth plate. Cortical modeling that was associated with growth continued after cessation of longitudinal growth in the ovariectomised animals, resulting in shape changes of the proximal tibia.
- **Conclusion:** The organized nature of the changes in bone architecture that occurred after ovariectomy and the high similarity with the changes observed in the normally aging animals suggest that estrogen depletion resulted in an acceleration of a normal bone adaptation process. The observed aligning of trabeculae suggests regulation through mechanical loading.

4.1 Introduction

In the later years of life, both men and women gradually lose bone leading to an increased risk of fractures. In women, this phase of slow decline of bone mass at old age is preceded by a phase of rapid bone loss shortly after menopause. Early histomorphometric studies of age-related bone loss in humans led to the generally held idea that men lose bone preferentially by thinning of trabeculae, while women lose bone by perforation and loss of entire trabeculae (1, 37, 130, 152, 170).

The process of bone loss has been studied in more detail in rat models of aging (200) and especially in models of post-menopausal bone loss (211). Again, the general picture is that bone loss preferentially occurs due to loss of entire trabeculae (47, 109, 112). Immediately after ovariectomy (OVX), bone remodeling accelerates and entire trabeculae are lost (47). This initial phase of rapid bone loss is followed by a gradual decrease of bone mass, which is also observed in normally aging rats (85, 210). Many studies showed regional differences in bone loss, even within bones (8, 207). While almost all trabeculae are lost in the metaphyseal bone of the proximal tibia, hardly any changes have been observed in the epiphysis.

A common factor in the previously mentioned studies is the cross-sectional study design, which is a necessity for classical histomorphometry or conventional micro-CT studies, because of the invasive and/or destructive nature of these methods. Conclusions drawn from studies that utilize cross-sectional designs invariably contain an aspect of speculation on how observed changes in bone have occurred. This is part of the reason why knowledge on bone dynamics is still limited.

The drawbacks of cross-sectional study designs can at least partly be overcome by using longitudinal study designs. Besides the obvious statistical advantages in that baseline variation in the population can be eliminated, it further allows one to observe the development of certain changes over time. For bone morphometry, such a study design is made possible by novel in-vivo micro-CT technology. When combined with image registration methods, in-vivo micro-CT can visualize architectural changes in bone at the level of single trabeculae (194). In this study we have used this novel technology and tried to further elucidate the process of bone loss in rat models of age-related and post-menopausal bone loss.

4.2 Methods

Study Protocol

Ten adult 10-month old female Wistar rats were randomised into two groups of 5 animals each. One group was sham operated and the other was ovariectomised (OVX). During the experiment, the rats were housed

individually in cages and were fed pelleted food (RMH-B diet; Hope Farms, Linschoten, The Netherlands). Animals in both groups were fed 16 grams per day to limit weight gain in the OVX group. The animals were scanned in the in-vivo micro-CT scanner at week 0, prior to operation, and at week 4, week 14, week 34 and at week 54. The body weight of each rat was measured weekly.

To investigate the possible influence of radiation on bone, another group of 4 animals was sham operated and served as a non-radiated control group. These animals were only scanned at week 54.

All animals formed part of a larger experiment for which approval was obtained from the Animals Ethics Committee.

In-vivo micro-CT scanning

At each time point, the right tibias of the rats were scanned in a prototype Skyscan 1076 in-vivo micro-CT system. During the scanning procedure, the animals lay on a bed under Isoflurane anaesthesia. The right hindlimb was fixed in a cylindrical plastic holder to prevent movement of the limb during scanning. Only the scanned leg of the animals was radiated during the process, thus minimizing the effects of the radiation. A scan lasted about 20 minutes and the absorbed radiation during a scan was approximately 0.4 Gray. The scans resulted in reconstructed 3-D data sets with a voxel-size of 20 μm .

Analysis of the micro-CT scans

The different scans of each individual rat were reoriented in three dimensions to match the scans at week 0, using image registration techniques (122). Since the growth plate in the rat never completely closes, epiphysis and metaphysis were registered separately to avoid miss-matches due to growth by apposition at the growth-plate. This method resulted in accurate matches of the consecutive scans, which was shown elsewhere (194). The registered data sets were segmented into binary data sets using a specially developed algorithm based on local thresholds (197).

Trabecular and cortical bone were separated by drawing regions of interests, using software provided with the scanner. For the metaphyseal trabecular bone, bone volume fraction (BV/TV) and 3-D trabecular thickness (Tb.Th) (75) were calculated as measures of trabecular bone mass and its distribution, while trabecular architecture was quantified by calculating structure model index (SMI) (76) and connectivity of the trabecular network (Conn.) (149). SMI indicates whether the trabeculae are more rod-like (SMI=3) or more plate-like (SMI=0). Conn. was obtained by calculating the connectivity of the trabecular network and normalised by dividing the connectivity by bone volume (BV) and not by tissue volume (TV), thus avoiding the artificial decrease of Conn. by large metaphyseal

marrow areas without trabecular bone. Before Conn. was calculated, pieces of trabecular bone that were not connected to the main structure after applying a region of interest were removed. These loose particles generally constituted less than 1% of the trabecular bone volume. Cortical thickness was calculated for the metaphysis (C.Th). All morphometric parameters were calculated using software of the freely available CT-Calculator project²

The longitudinal growth at the proximal growth-plate between the different time-points was obtained by comparing the difference between the registration results for the epiphysis and the metaphysis. The image registration procedure resulted in a different transformation matrix for the metaphysis than for the epiphysis. From this difference a vector was derived of which the length represented the amount of growth by apposition of cartilage and its mineralization within the growth-plate.

Statistical analysis

For each measured parameter the main effects of time (TIME) and the interaction between time and group (GROUP: ovx or sham) were tested using a General Linear Model (GLM) for repeated measures in SPSS 10.0 (SPSS Inc.). The effect of TIME indicates whether the treatment (ovx or normal aging) changed the tested parameter over time, while the interaction between TIME and GROUP indicates whether the effect of TIME was different for the two groups. For each parameter the assumption of sphericity (homogeneity of variance for the difference of parameter values between successive time points) was tested. If sphericity was not valid, a Greenhouse-Geisser correction on the degrees of freedom for the F-statistic was used. Further, for each group separately, the differences between the parameter values at the different time points were tested. Simple contrasts were used to test the hypothesis that a parameter value at a certain time point was different than the value at week 0, and repeated contrasts were used to test the hypothesis that there was no change between a parameter value at a certain time point and the previous time point.

4.3 Results

Metaphyseal trabecular bone

The OVX animals rapidly lost bone after the surgical removal of the ovaries. After week 14, bone loss slowed down. Between week 34 and week 54, bone volume fraction was almost constant. The sham animals had a much lower but constant rate of bone loss during the entire study period (figure 4.1a). While bone was lost, the thickness of the remaining trabeculae increased, especially in the ovariectomised rats (figure 4.1b).

² The software can be downloaded from: www.eur.nl/jgg/orthopaedics/Downloads.html.

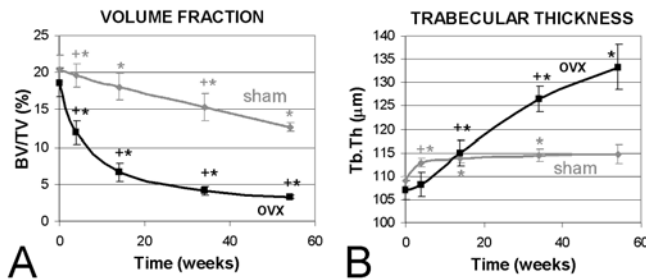


figure 4.1 Trabecular bone volume fraction (A) and trabecular thickness (B) as a function of time for ovx animals (black line) and normally aging animals (grey line). ‘+’ time point is significantly different from previous time point ($p < 0.05$); ‘*’ time point is significantly different from week 0 ($p < 0.05$).

The change in connectivity of the trabecular network in both groups reflected the change in bone volume fraction: the ovx animals showed a strong decrease in connectivity of 80% in the first 14 weeks after which the decrease slowed down and remained constant between week 34 and week 54 (Table 4-1). In the sham animals, the decrease in connectivity was almost linear. While bone was lost, the remaining trabecular structure became more rod-like in the ovx animals, as indicated by an increasing SMI until week 34 (Table 4-1). The sham animals did not show an increase in SMI.

The spatial patterns of trabecular resorption were not homogenous in both groups. Some areas experienced a stronger loss of trabecular bone than others. Especially the central areas lost more bone than areas close to the cortex or growth-plate. However, even in areas with high resorption not all bone was lost. In these areas of high resorption, all ovx animals showed that remodeling activity transformed previously existing trabeculae into new trabecular structures, forming a transversal rod between the anterior and posterior endocortical surfaces (figure 4.2). These spatial resorption patterns were very similar between the two groups, only the time scale in which these patterns evolved was different. The state of bone loss reached after 54 weeks by the normally aging rats was similar to that of the OVX rats at week 14 (figure 4.2).

Spatial differences in bone resorption were also present at sub-regional or trabecular levels. While one trabecula was resorbed, the neighboring trabeculae were preserved and increased in thickness. This could be observed in both groups (figure 4.3).

The main effects of TIME and the interaction between TIME and GROUP were highly significant for all measured parameters. In other words, both OVX and aging significantly affected all measured parameters in the 54 weeks of this study, and OVX affected these parameters differently from normal aging.

Table 4-1 Mean and SEM for Connectivity per bone volume (Conn.), Structure Model Index (SMI) and Cortical Thickness (C.Th) for Sham and OVX groups at all time points.

Time point	Conn. (/mm3)		SMI		C.Th (µm)	
	SHAM	OVX	SHAM	OVX	SHAM	OVX
Week 0	154± 10	155± 4	2.0± 0.06	2.1± 0.09	461± 18	461± 18
Week 4	133± 9***	75± 11****	2.1± 0.05**	2.4± 0.07****	472± 19 ⁺	459± 15
Week 14	134± 8***	32± 6****	2.0± 0.04	2.7± 0.09****	479± 16	503± 18**
Week 34	91± 14***	12± 1***	2.0± 0.09	3.1± 0.06****	473± 11	519± 16 ⁺
Week 54	71± 5* ⁺	8± 2 ⁺⁺	2.0± 0.04	3.1± 0.12 ⁺	477± 5	516± 19*

Significantly different from previous time point *(p<0.05) **(p<0.01); significantly different from values at week 0 +(p<0.05) ++(p<0.01)

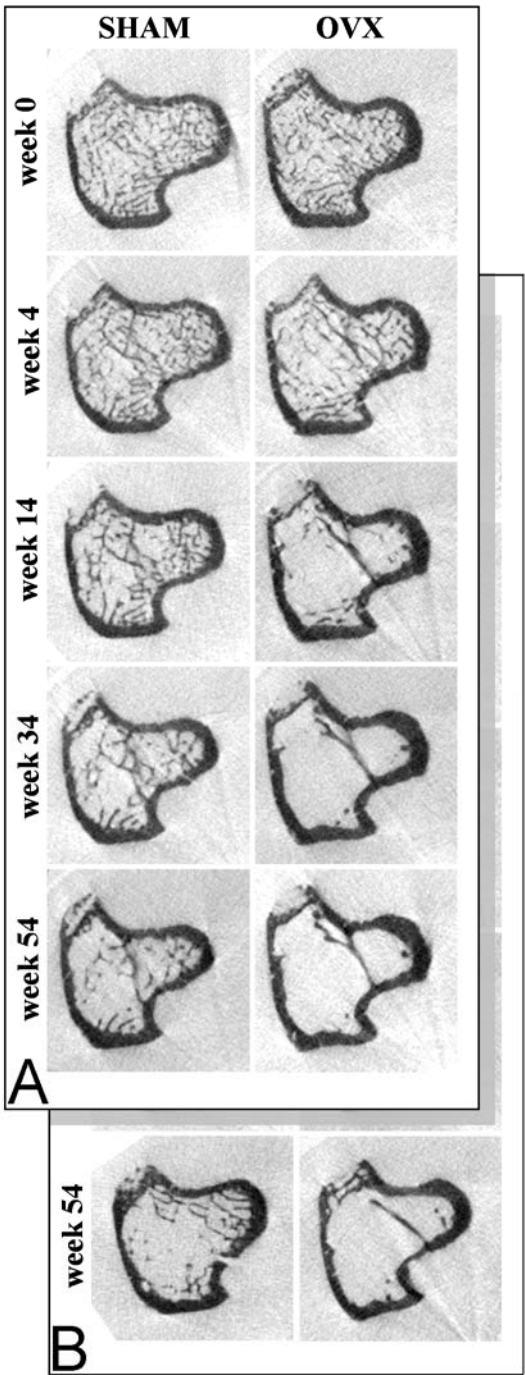


figure 4.2 Transversal cross-sections of the metaphysis of the tibia of a normally aging (sham) and an ovx rat for all time points (A). B shows the situation at week 54 of another sham and ovx animal. Notice how some areas experience more resorption than others. Also notice how remaining trabeculae increase in thickness in the ovx animal and how a new trabecular structure is formed. The spatial resorption pattern of the sham rat at week 54 most resembles the ovx situation at week 14

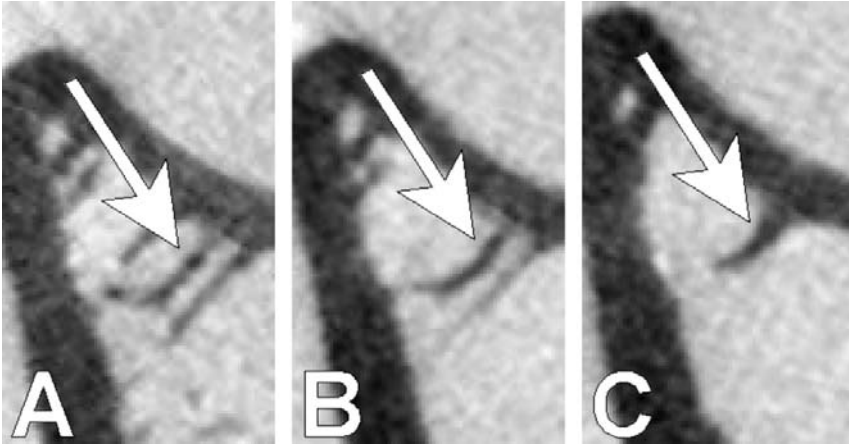


figure 4.3 Transversal cross-section from an ovx animal at the same location at week 0 (A), week 4 (B) and week 14 (C), showing how one trabecula gets thinner and is eventually resorbed, while its neighbour is preserved and increased in thickness.

During the study period, all animals showed a linear increase in body weight. At week 54, normally aging rats weighed 8% more than at baseline, while the animals in the ovx group had a mean increase in bodyweight of 32%. No relation between changes in bodyweight and changes in bone parameters were found.

Cortical bone

Registration of the tibial metaphysis of the ovx rats showed periosteal resorption on the posterior tibial cortex and apposition at the endosteal side between week 0 and week 4 (figure 4.4A). This process continued until week 34. Between week 34 and week 54 no change could be observed. The combined effects of endosteal bone formation and periosteal resorption resulted in maintenance of the bone's shape during longitudinal growth, as can be visualized by performing the registration on the epiphysis (figure 4.4B). The shape of the bone was preserved until the end of the active growth period (until week 14). By week 34 growth had slowed down (figure 4.4C), but the cortical resorption and formation still continued resulting in changes in the shape of the bone.

The sham animals showed the same relation between endocortical apposition and periosteal resorption and longitudinal growth. When the animals were growing, the combined effects of cortical formation and resorption maintained the shape of the bone. Although total bone shape was preserved during longitudinal growth in both groups, the net effect of resorption and apposition in the ovx animals was that of an increase in

proximal metaphyseal cortical thickness after week 4. The sham animals did not show a significant change in cortical thickness (Table 4-1).

Trabecular realignment

In the ovx rats, loss of trabecular bone on the metaphyseal side of the growth-plate appeared to be related to the epiphyseal trabecular structure on the proximal side of the growth-plate: metaphyseal trabeculae opposing epiphyseal trabeculae were preserved while metaphyseal trabeculae that did not have opposite epiphyseal trabeculae were resorbed (figure 4.5). After week 14, trabeculae appeared to change their position resulting in an almost exact alignment of epiphyseal and remaining metaphyseal trabeculae across the growth-plate at week 54.

Similar processes were seen in the sham rats. Changes in trabecular bone structure were again stronger in the metaphysis than in the epiphysis, resulting in trabeculae that were more or less aligned across the growth-plate (figure 4.5).

Non-radiated controls

The non-radiated sham controls did not show differences in bone volume fraction when compared to age-matched controls. However, small differences could be observed in SMI and trabecular thickness. While the radiated sham animals showed no changes in SMI (SMI=2.0, Table 4-1) and showed an increase in trabecular thickness of 4.8% (figure 4.1B), the non-radiated controls had slightly more rod-like trabeculae than the age-matched radiated animals (SMI=2.4, $p<0.01$) and a trabecular thickness that was not significantly different from the baseline control of week 0 (Tb.Th=108 μm).

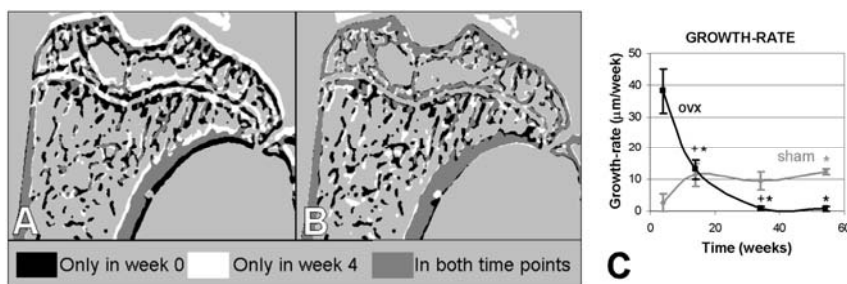


figure 4.4 Overlaid registered longitudinal cross-sections of an ovx rat scanned at week 0 and week 4 (A+B). A) Registration done on metaphyseal bone: note that trabeculae and arterial openings in the metaphysis match. Due to longitudinal growth, the epiphysis does not match. This match visualises periosteal resorption and endosteal apposition. B) Registration done on epiphyseal bone: Note the shift in metaphyseal trabeculae and arterial opening shows otherwise. The apparent good match of total bone shape shows that the net effect of periosteal resorption and endocortical apposition is no change in total bone shape. C) Growth-rate for ovx and sham rats as a function of time.

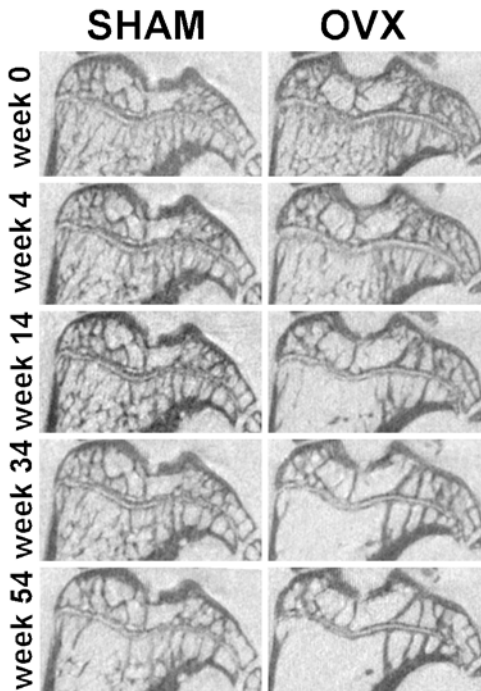


figure 4.5 Longitudinal cross-section of the proximal head of the tibia of a sham and an ovx rat for all time points. Remodeling in the metaphysis in both animals led to alignment of trabeculae across the growth-plate and fortification of the trabeculae in the ovx animal. Note that the end result of the sham animal at week 54 is similar to the situation in the ovx animal at week 14.

4.4 Discussion

Estrogen deficiency is generally considered to cause massive bone loss and deterioration of the trabecular structure, which over time can lead to increased fracture risk. The data presented in this longitudinal study of a rat model does not contradict this view, but the process of alterations in bone structure visualized and quantified in this study does show that the bone remodeling process associated with estrogen depletion is much more complex. It not only resulted in bone loss, but also in the formation of new bone. Bone loss was not general but limited to certain areas and certain trabeculae (figure 4.2 and figure 4.3). Remaining trabeculae increased in thickness and, remarkably, existing trabeculae merged together to form new trabecular structures. Remaining trabeculae changed their position within the bone resulting in the alignment of metaphyseal and epiphyseal trabeculae across the growth-plate (figure 4.6). Instead of describing estrogen deficiency as only a state of bone loss, it might be more appropriate to describe it as a state of rapid bone metabolism in which bone remodeling is high and adaptation is accelerated, resulting in strong changes over time. Problems related to osteoporosis could be caused by an over-adaptation of the bone structure in which it is optimized for daily loads but not for unusual loads due to, for example, falls (80, 203).

We will never be sure whether all the changes that occur in the tibia of the ovx rats would occur eventually in the sham animals if they would live long enough. However, the observed similarities between age-related bone loss and bone loss caused by ovariectomy were striking enough to further support the view that changes occurring after loss of estrogen are the result of an accelerated but otherwise normal adaptation process. A similar process of ongoing trabecular adaptation after cessation of growth has been observed in pigs (179).

Traditionally, age-related bone loss in humans has been assumed to be due to secondary hyperparathyroidism and the related increase in bone remodeling (170), although hyperparathyroidism might be at least partially induced by estrogen deficiency (158). When female rats age their estrous cycle becomes irregular and estrogen serum levels are lowered (58, 118). Further, age-related bone loss in rats was related to increased remodeling (210). The cellular mechanisms by which bone was lost, however, seemed to differ from those associated with estrogen depletion (9). Whether or not the underlying causes and mechanisms of age-related bone loss are similar to those of estrogen depletion related bone loss could not be addressed in our study. However, we showed that at least the result of the bone loss process was very similar in both situations.

The spatial differences in resorption and formation observed in this study lead to an interesting question. How do bone cells in a certain area of the bone “know” that the trabeculae need to be resorbed, while in other areas the trabeculae need to be preserved? Even at the level of single trabeculae, the remodeling process resulted in the thinning and eventual disappearance of one particular trabecula, while the trabecula next to it was preserved and even increased in thickness at the same time (figure 4.3). The differences in resorption patterns seen in this study may have been driven by initial differences in trabecular properties. Thin trabeculae are more prone to perforation by osteoclast activity and subsequent complete resorption than thicker ones. Another possibility is that these differences were driven by gradients in signaling molecules induced by, for instance, the growth-plate

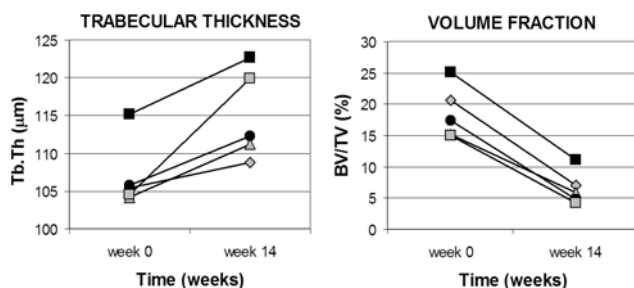


figure 4.6 Change in trabecular thickness and bone volume fraction in the first 14 weeks for all 5 ovx animals. While bone is lost, Tb.Th increases in all animals.

or perhaps the periosteum (27). This would be supported by the observation that more trabecular bone was preserved close to the growth-plate and the cortex. Further, the well-known mechanical responsiveness of bone might have driven the spatial differences in behavior of bone cells. Widely accepted theories suggest resorption of lesser-loaded trabeculae above the more-loaded ones (59, 115). Formulated differently: competition for the load stimulus caused lesser loaded trabeculae to disappear in favor of the more loaded ones, in an ongoing process (205). Although this study is purely observational and does not provide information on mechanical stimuli, the realignment of trabeculae in the metaphysis and epiphysis across the growth-plate does suggest the presence of a mechanical optimization process driven by loading through the femoral condyles.

An interesting issue related to the regulating mechanism of remodeling, is the question whether a complete new trabecula can form that connects two trabecular surfaces that were previously unconnected. In-vivo micro-CT would be an ideal imaging modality to deliver proof of such a phenomenon. However, no evidence could be found whatsoever in our scan data. Though not less remarkable, the new trabecular structures observed in this study clearly originated from previously existing trabecular structures at the same location.

These questions go back to the very basics of bone development and bone adaptation. Much speculation can be found in the literature, but until now very limited data have existed to support such assumptions. For this, data is needed that shows the result of bone adaptation as it occurs in-vivo, such as the unique set of data presented in this study. In-vivo micro-CT has the ability to follow changes in trabecular architecture in individual animals and can visualize regions of both bone formation and resorption, what has been validated by histology previously (194). Only because of these abilities we were able to shine a different light on the process of ovx related bone loss in rats, even though this process has been studied extensively in the past.

Previous cross-sectional studies indicate a strong positive correlation between trabecular bone volume fraction and trabecular thickness (43, 152, 174, 180). In the baseline measurement at week 0 of this study we observed the same relation. However, our longitudinal data showed an opposite relation: Trabecular thickness increased when bone was lost (figure 4.6). The positive relation between volume fraction and trabecular thickness might be a result of development in which, for instance, genetics relate more bone to thicker trabeculae. During life, other factors that influence bone remodeling and bone adaptation (e.g. loading history, certain pathologies, estrogen depletion) might cause bone structure to deviate from this relation. However, bone morphometric studies in humans generally have not shown a deviation from this positive relation with age, or after menopause, though

results were not consistent between studies. At least one study did report an increase of trabecular thickness in older women (16). Cross-sectional variation and limitations in methodology and sample size in most of the previously mentioned studies might have hidden an increase in trabecular thickness during aging. Still, the response in rats might be different from that in humans.

The radiation dose the animals received during a scan (0.4 Gray) was not high, but certainly not negligible. Bone marrow is a radiosensitive tissue that is affected by radiation dosages as low as 0.2 Gray (26). Therefore, a group of sham rats was included that were only scanned at week 54 to compare with the age matched scanned animals. We found a small but significant effect of the scanning procedure in the sham operated animals. Although there was no effect on volume fraction, the trabecular structure in the animals that were not scanned during the study period was slightly different than that of the scanned sham rats. This effect could be due to radiation effects, but a possible effect of the Isoflurane anesthesia or of temporary unloading in the hind leg caused by clamping the ankle during scanning might have contributed as well. Unlike the longitudinal comparisons and the related high statistical power in the rest of this study, the number of animals and thus the power in this cross-sectional comparison was relatively low and the small experimental effect could be due to a statistical type II error. However, the possible serious effects of radiation on bone metabolism calls for concern and further research is needed to address this issue in in-vivo micro-CT scanning.

In summary, this longitudinal in-vivo micro-CT study showed bone adaptation dynamics in age-related bone loss and bone loss due to estrogen depletion. The dynamics were very similar in both groups, leading to vertical alignment of trabeculae and the groups mainly differed in the time scale at which the changes occurred. Describing estrogen depletion as a state of bone loss would not do justice to the dynamics of bone remodeling as observed in this study, which would better be described as a state of accelerated bone metabolism that resulted in fast, possibly mechanically driven, bone adaptation.

Acknowledgements

This work was supported by European Union grant QLRT-1999-02024 (MIAB).

5

Effects of tibolone treatment on trabecular architecture in the tibia of mature rats: an in-vivo micro-CT study

J.H. Waarsing, J.S. Day, J.A.N. Verhaar, D.R. Sumner,
A.G.H. Ederveen, H. Weinans

Submitted

Abstract

- **Introduction:** Tibolone is a tissue selective compound that prevents post-menopausal bone loss through estrogenic activity. Since bone quality is not only determined by bone mass but also by bone architecture, we investigated the effects of long-term tibolone use on trabecular architecture in aged, ovariectomised rats. We performed a longitudinal study using in-vivo micro-CT, which facilitates the detection of subtle changes in trabecular architecture in individual rats.
- **Methods:** 126 Ten-month old female Wistar rats were randomized over 3 treatment groups and 5 time-points. The animals were either sham operated (SHAM), ovariectomised (OVX) or ovariectomised and treated with tibolone at a dose of 2 mg/kg/day (OVX+T). At each time point (0, 4, 14, 34 and 54 weeks) 9 animals were sacrificed and serum osteocalcin and urinary DPD were determined. From the animals that lived until week 54, 7 animals were selected out of each of the three treatment groups, of which the proximal tibias were scanned in an in-vivo micro-CT scanner at each time point. Image registration was used to overlay the data sets of each animal at the different time points. Registration allowed determination of longitudinal growth and visualization of the bone loss process. Morphometric parameters were calculated for the metaphyseal trabecular bone (BV/TV, Tb.Th, SMI, Conn.) and cortex. Further, backscatter scanning electron microscopy (bSEM) was used to determine the tissue mineralization in the distal femur of the animals sacrificed at week 54.
- **Results:** Treatment with tibolone significantly reduced the effect of ovariectomy on all morphometric and biochemical parameters. Ovariectomised-induced changes in trabecular thickness and cortical geometry were completely blocked in the OVX+T group and were even less than those found in the SHAM group. While ovariectomy temporarily stimulated longitudinal growth, treatment with tibolone suppressed this effect to below sham levels. At week 54, no significant difference in tissue mineralization could be detected between SHAM and OVX+T animals, while OVX animals had a lower mineralized bone tissue.
- **Conclusion:** Treatment with a sub-optimal dose of tibolone partially prevented ovariectomised-induced bone loss, but completely inhibited the increase in trabecular thickness, cortical changes and the longitudinal growth that was found in both sham and ovx animals.

5.1 Introduction

Tibolone is a tissue selective compound that prevents post-menopausal bone loss and relieves climacteric complaints, similar to treatment with estrogens, but does not stimulate breast and endometrium as estrogens do (103). In the body, tibolone is rapidly metabolized into three compounds, two of which have estrogenic effects, and one that has both progestogenic and androgenic effects (103). In bone, tibolone acts almost entirely through activation of the estrogen receptors (52).

Studies of tibolone use by post-menopausal women have shown that tibolone prevents bone loss and increases bone mineral density (13, 62, 153, 154, 167, 176). Tibolone prevents bone loss by reducing bone remodelling as is indicated by a decrease in markers of bone metabolism in post menopausal women that used tibolone (157, 176).

Animal studies have yielded information on the effects of tibolone on the mechanical quality of bone. Three-point bending tests on femurs and compression tests on lumbar vertebrae in rat models of osteoporosis have shown that treatment with tibolone, besides preserving bone mass, also preserved the mechanical competence of bones in a dose dependent manner (53, 212). A similar prevention of the loss of bending strength due to tibolone treatment was found in the femurs of ovariectomised monkeys (36).

Bone mass is a good predictor of its strength in the main loading directions, but off axis the relative importance of the architecture itself seems much more important (35, 42, 80). Since most falls exert impacts in the off-axis directions, this might explain the poor predictability of fracture risk by bone mass alone, and stresses the importance of knowing how drugs that prevent bone loss affect trabecular architecture. Data on how tibolone treatment influences trabecular architecture is inconclusive and limited to two studies using histology on vertebrae and femurs of young growing ovariectomised rats. Tibolone treatment reduced bone loss by limiting the reduction in trabecular number and trabecular separation in lumbar vertebrae (212). In the femur, administration of tibolone, besides preserving bone mass, reduced the decrease in trabecular thickness (155).

Our aim was to investigate the long-term effects of tibolone treatment of ovariectomised rats on 3-dimensional bone architecture of the tibia, relative to changes in architecture induced by ovariectomy and due to normal aging. We applied a longitudinal study set-up using in-vivo micro-CT which allows the precise detection of subtle changes in trabecular and cortical architecture and longitudinal growth, and to follow the development of these changes over time in individual animals (194).

5.2 Methods

Study design

126 six-month old unmated female Wistar rats were purchased from Harlan (Horst, The Netherlands) and were housed individually until 10 months of age, the baseline time point of this study. All animals had unlimited access to tap water and were pair fed with 16 g per day (RMH-B diet; Hope Farms, Linschoten, The Netherlands). At the start of the experiment 18 animals were killed to serve as baseline controls. The remaining animals were randomized over 3 treatment groups and 4 time points. Thus, each subgroup contained 9 animals. The animals were either sham operated (SHAM), ovariectomised (OVX) or ovariectomised and treated with tibolone (OVX+T). Animals were sacrificed at 4, 14, 34 and 54 weeks. At baseline, surgery (OVX or SHAM) was performed and treatment of the OVX+T group with tibolone started directly thereafter. Tibolone was administered orally at a daily dose of 2 mg/kg, which is known to be sub-optimal in the rat for prevention of OVX-induced bone loss in the long-bones (53). The dose was chosen to be sub-optimal in order to guarantee that changes in bone structure would be present.

Before sacrifice, the animals were deprived from food for 16 h (but with access to demineralised water) while housed in metabolic cages for urine collection. At autopsy blood samples were collected from the abdominal aorta. Urine and blood samples were used to determine biochemical markers of bone metabolism. Bodyweight of all animals was measured at all time points.

From the groups that lived until week 54, 21 animals (7 out of each treatment group) were selected randomly and micro-CT scanned once at each time point.

All animal handling formed part of a larger experiment for which approval was obtained from the Animal Ethics Committee.

Biochemical markers of bone metabolism

Urinary deoxypyridinoline (DPD), a marker of collagen I breakdown, was determined by ELISA (Pyrilinks-D, Metra Biosystems, Inc., Palo Alto, CA, USA), and expressed as a fraction of urinary creatinine (Cr) as determined by a standard autoanalyser. Plasma osteocalcin, a marker of osteoblast activity, was determined by radioimmunoassay (193).

In-vivo micro-CT scanning

At each time point, the proximal one-third of the right tibias of the rats that were selected for micro-CT scanning were scanned in a prototype Skyscan 1076 in-vivo micro-CT system. During the scanning procedure, the animals lay on a bed under Isoflurane anaesthesia. The right hind limb was fixed in a

cylindrical plastic holder to prevent movement of the limb during scanning. Only the scanned leg of the animals was radiated during the process, thus minimizing the effects of the radiation. A scan lasted about 20 minutes and the absorbed radiation during a scan was approximately 0.4 Gray. Although this dose is not negligible, the scanning scheme as used during this study did not result in differences between the tibias of scanned and non-scanned animals previously (195). The scans resulted in reconstructed data sets with a voxel-size of 20 μm .

At the final time point (week 54) only 3 animals from each treatment group were scanned due to problems with the prototype micro-CT scanner.

Analysis of the micro-CT scans

The different scans of each individual rat were reoriented to match the scans at week 0, using image registration techniques (122). Since the growth plate in the rat never completely closes, the epiphyses and metaphyses were registered separately to avoid miss-matches due to growth at the growth-plate. This method resulted in accurate matches of the consecutive scans, as demonstrated previously (194). The registered data sets were segmented into binary images using a specially developed algorithm based on local thresholds (197).

Trabecular and cortical bone were separated manually, using the software package CT-analyser (Skyscan, Antwerp, Belgium). The trabecular Volume of Interest (VOI) chosen was the metaphyseal trabecular bone from just underneath the growth-plate to the end of the scanned volume. In the VOI, bone volume fraction (BV/TV) and trabecular thickness (Tb.Th) (75) were calculated as measures of trabecular bone mass and its distribution, while trabecular architecture was quantified by calculating structure model index (SMI) (76) and connectivity of the trabecular network (Conn.) (149). SMI indicates whether the trabeculae are more rod-like (SMI=3) or more plate-like (SMI=0). Conn. was obtained by calculating the connectivity of the trabecular network after removal of possible loose trabecular pieces. Conn. was expressed as a fraction of bone volume (BV) rather than the more common tissue volume (TV). Correction of connectivity by tissue volume is sensible for homogenous pieces of trabecular bone, but not for whole bones in which large marrow areas exist without trabecular bone. Correction by tissue volume would then correlate to the fraction of the marrow cavity that is filled with trabecular bone, and not to the connectivity of the trabecular bone network within this part of the marrow cavity.

Cortical morphometry was determined on 1 mm of metaphyseal cortical bone taken 7 mm from the top of the tibia (about 3 mm below the growth-plate). Trabeculae were removed from the piece of cortex as described above. Mean 3D cortical thickness (Ct.Th) of the piece of cortical bone was calculated. Further, cross-sectional polar moment of inertia (Ct.J) was

calculated which represents the distribution of bone tissue around the centre of mass and is a geometrical measure of torsional strength. Periosteal perimeter (Ps.Pm) was calculated to detect cortical expansion and endocortical area (Ec.Ar) to detect endocortical resorption. Ct.J, Ps.Pm and Ec.Ar were calculated for each cross-section of the cortical piece and expressed as an average.

All morphometric parameters were calculated using software of the freely available CT-Calculator project³.

The longitudinal growth at the proximal growth-plate between the different time-points was quantified by comparing the difference between the registration results for the epiphysis and the metaphysis. The image registration procedure resulted in a different transformation matrix for the metaphysis than for the epiphysis. From this difference a vector was derived of which the length represented the amount of growth by apposition of new bone at the growth-plate.

Backscatter Scanning Electron Microscopy

From each group sacrificed at week 54 (SHAM, OVX and OVX+T) the femurs of 7 rats were excised and embedded in 4 blocks of Methylmethacrylate (MMA), such that each block contained 6 distal femurs: 2 rows of 3 femurs. Each row contained a femur out of each group in random order. Within a block, all femurs were placed within a plane, such that the longitudinal lateral-medial plane of the femurs coincided with the plane of embedding. Embedding several samples in one block enabled us to image these samples within one SEM session, thus decreasing the variance in the measurements.

After embedding, the blocks were cut on an electric bandsaw (Exakt, Norderstedt, Germany), resulting in a slab of plastic with two parallel surfaces, parallel to the plane of embedding of the femurs. Starting from the posterior side of the bones, material was removed using an automatic grinding system (Buehler Phoenix 4000) with p400 grid paper until an interior surface, halfway between the ventral and dorsal external surfaces, was exposed. To reduce the roughness of the surface the blocks were ground with p1200 paper, followed by polishing using 3 µm diamond paste with polishing paper (Buehler Texmet 1000). The resulting surface had a roughness (Ra) smaller than 0.05 µm. The blocks were cleaned, sonicated and sputter coated with a thin layer of carbon (Bio-Rad Temcarb Carbon Coater, Bio-Rad Microscience Division) to enable conduction of the electron beam to the sample surface.

Backscatter scanning-electron microscopy images (bSEM) were taken of trabecular bone of the metaphyseal and epiphyseal regions of each bone

³ The software can be downloaded from: www.eur.nl/jgg/orthopaedics/Downloads.html

sample, and of the cortex using methods described in detail previously (20). The images were taken at an accelerating voltage of 25 kV, a working distance of 17 mm and 50x magnification. Before and after imaging calibration images were taken of an aluminium standard embedded in each block and of the MMA material. The equivalent Z-value (atomic number) of the MMA was obtained by calibration with aluminium (Z=13) and carbon (Z=6) standards (Micro Analysis Consultants).

A normal distribution was fit to the histogram of Z-equivalents for each image. The mean of this normal distribution represented the mean mineralization of the bone surface.

Statistical analysis

Since only three animals in each group were scanned at the final time point (week 54), statistical analysis of the micro-CT data was limited to the data from week 0 to week 34.

For each measured micro-CT parameter the main effects of time (TIME: 0, 4, 14 or 34 weeks) and the interaction between time and group (GROUP: sham, ovx or ovx+t) were tested using a General Linear Model (GLM) for repeated measures in SPSS 10.0 (SPSS Inc.). For each parameter the validity of the assumption of sphericity (homogeneity of variance for the difference of parameter values between successive time points) was tested. If the assumption was not valid, a Greenhouse-Geisser correction on the degrees of freedom for the F-statistic was used. When a significant interaction was found, each group was analysed separately. Simple contrasts were used to test the hypothesis that a parameter value at a certain time point was different than the value at week 0. At week 34, group differences in the relative change in parameter values were tested using a one-way ANOVA and Bonferroni post-hoc testing.

For the biochemical markers, which were cross-sectional data, a similar procedure was followed as with the micro-CT parameters, but using a normal General Linear Model and Bonferroni post-hoc testing. Group differences in the SEM data, only measured at one time point (week 54), were tested using one-way ANOVA and Bonferroni post-hoc testing.

5.3 Results

Biochemical markers of bone turnover and bodyweight

No difference was detected in remodelling rate as indicated by osteocalcin and DPD/Cr levels between the SHAM and OVX+T groups. The OVX group had significantly higher levels than the SHAM and OVX+T groups for both biochemical markers (figure 5.1). Both markers showed an increase from baseline to week 4 in all groups. After week 4, levels decreased in all groups, with the SHAM and OVX+T groups approaching baseline levels.

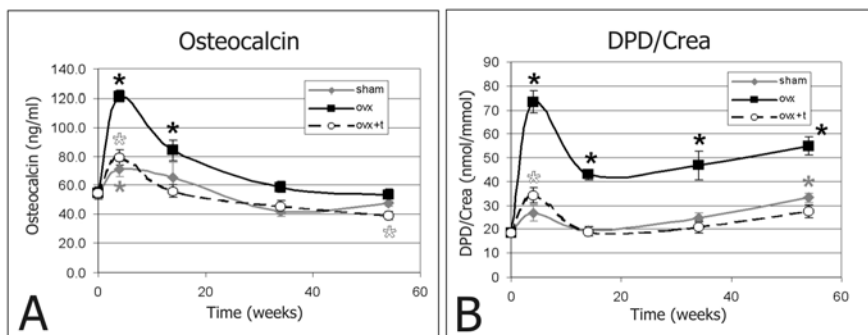


figure 5.1: Biochemical markers of bone remodeling for the different time-points and different treatment groups. These markers were assessed cross-sectional. A) Osteocalcin, a marker of osteoblast activity. B) DPD/Creatine, a marker of bone resorption. (* Significantly different from week 0, $p < 0.05$)

Between week 14 and week 54 the bone marker osteocalcin declined while the DPD/Cr levels increased in all groups suggesting a shift in the balance between bone resorption and formation upon aging.

Bodyweight increased in both the SHAM and OVX group. The gradual increase was strongest in the OVX animals (27%: 315 gr. at week 0 to 400 gr. at week 54). The weight of the SHAM animals increased from 310 at week 0 to 348 grams at week 54 (12%) with a small but significant dip at week 4 (307 gr.: $p < 0.01$). Tibolone prevented the increase in bodyweight completely. The weight of the animals stayed relatively constant after an initial decrease of 10% at week 4 (304 gr. at week 0 to 281 gr. at week 54).

table 5-1: Absolute micro-CT parameter values (mean \pm sem) at week 0 and week 34 and relative change (mean \pm sem) from week 0 to week 34 for trabecular bone volume fraction (BV/TV), trabecular thickness (Tb.Th), structure model index (SMI) and connectivity per bone volume (Conn.)

		Week 0		Week 34	
		absolute		absolute	relative
BV/TV (%)	Sham	22.1 \pm 1.66		17.1 \pm 1.67	-23.44 \pm 3.93 ^{+x}
	Ovx	19.8 \pm 1.53		4.33 \pm 0.52	-78.32 \pm 1.49 ^{*x}
	Ovx+t	22.6 \pm 1.04		12.2 \pm 1.59	-46.92 \pm 4.95 ^{*+}
Tb.Th (μm)	Sham	114.9 \pm 4.37		120.3 \pm 3.96	4.81 \pm 1.26 ⁺
	Ovx	113.0 \pm 4.69		133.5 \pm 6.86	17.91 \pm 2.18 ^{*x}
	Ovx+t	117.7 \pm 4.68		119.4 \pm 4.70	1.44 \pm 0.43 ⁺
SMI	Sham	2.01 \pm 0.04		2.04 \pm 0.06	1.35 \pm 2.25 ^{+x}
	Ovx	2.10 \pm 0.07		1.95 \pm 0.03	48.49 \pm 4.13 ^{*x}
	Ovx+t	1.95 \pm 0.03		2.33 \pm 0.08	16.86 \pm 3.78 ^{*x}
Conn. (/mm³)	Sham	154.4 \pm 9.67		90.7 \pm 13.6	-35.62 \pm 7.58 ⁺
	Ovx	171.7 \pm 11.5		15.6 \pm 3.45	-91.21 \pm 1.31 ^{*x}
	Ovx+t	190.3 \pm 13.9		86.5 \pm 17.0	-55.71 \pm 6.44 ⁺

Significantly different from sham * ($p < 0.01$), from ovx + ($p < 0.01$) or from ovx+t * ($p < 0.01$)

Trabecular architecture

In the OVX+T group, bone mass decreased rapidly in the first weeks after start of the experiment, similar to the OVX group, but to a much lesser extent. After 14 weeks bone loss slowed down and the rate of bone loss was similar to that in the SHAM group (figure 5.2a). At week 34, treatment with tibolone reduced trabecular bone loss to 50% as compared to the 80% bone loss in the OVX group, while the animals in the SHAM group lost 25% of their trabecular bone mass (table 5-1).

The change in most of the parameters that describe trabecular architecture followed a similar pattern as the rate of bone loss. The trabecular network in the OVX+T group became more rod-like as indicated by an increase in SMI, though not as much as the OVX group, while the SHAM group showed no changes in SMI (figure 5.2c). The loss of trabecular bone mass resulted in a decrease in connectivity of the trabecular network for all groups, which again was strongest for the OVX group, and

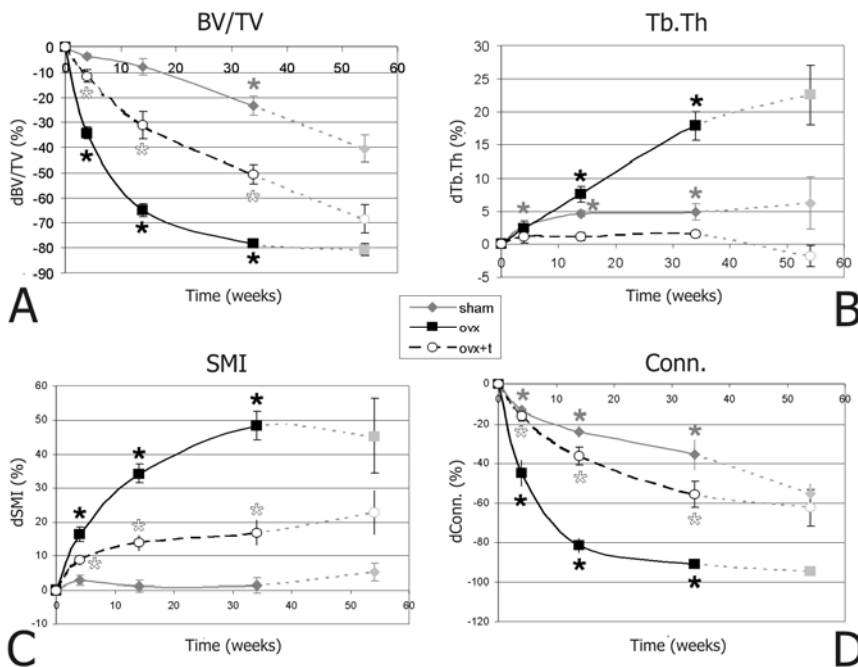


figure 5.2: Relative changes in trabecular bone architecture expressed as percentage of the value at week 0, for the three treatment groups. The error bars represent the standard error of the mean. A) Changes in trabecular bone volume fraction. B) Changes in trabecular thickness. C) Changes in structure model index D) Changes in connectivity per bone volume. (* Significantly different from week 0, $p < 0.05$) At week 54 only three animals per group were available, this time point is not used for statistical testing. In the graphs this is indicated by dashed grayed out lines.

smallest for the SHAM group, while treatment with tibolone partially prevented the decrease in connectivity to in between OVX and SHAM levels (figure 5.2d).

The changes in trabecular thickness (Tb.Th) however, deviated from the pattern observed for the other morphometric parameters. In the SHAM group low levels of bone loss were accompanied by a mild but gradual increase in trabecular thickness, and the OVX group showed rapid bone loss accompanied by a strong increase in trabecular thickness. Although bone loss in the OVX+T group was in between SHAM and OVX levels no accompanying changes in trabecular thickness could be observed (figure 5.2b). This resulted in a significant lower change in thickness of the trabeculae at week 34 for the OVX+T group when compared to the other two groups ($p < 0.05$).

Examination of the registered follow-up scans revealed that the patterns of bone loss were very similar in all groups. Bone was preferentially lost in regions more distal to the growth-plate, and within the medullar canal away from the endocortical surface (figure 5.3). The resorption pattern in the metaphysis seemed to be influenced by the trabecular network in the epiphysis. Metaphyseal trabeculae that were in line with trabeculae in the epiphysis on the opposite site of the growth-plate were preserved, while

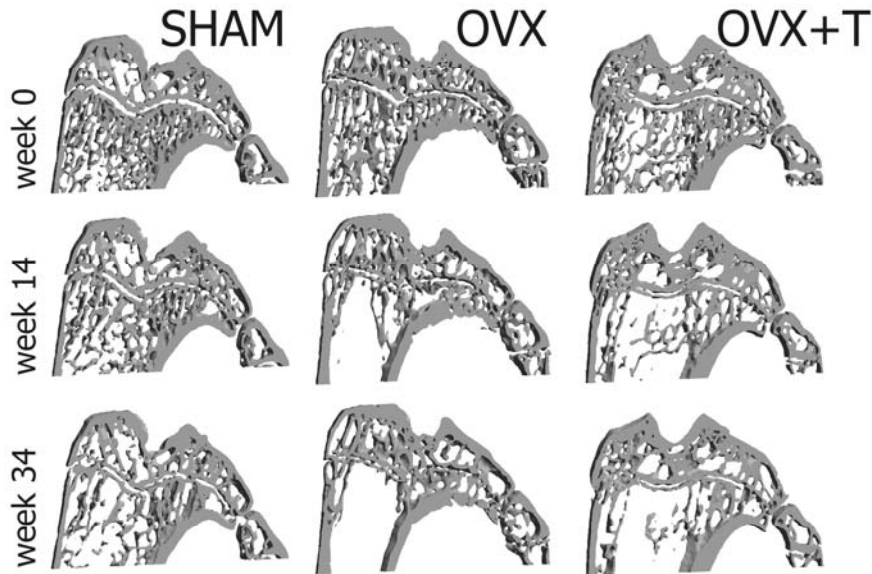


figure 5.3: Three-dimensional longitudinal slices out of the proximal tibia of a typical SHAM, OVX and OVX+T animal, scanned at different time points. All animals lost metaphyseal trabecular bone. Bone was mainly lost by removal of entire trabeculae. Initially, bone is preferentially lost from regions away from the cortical shell or growth-plate. Bone loss in the OVX+T animal was partially prevented.

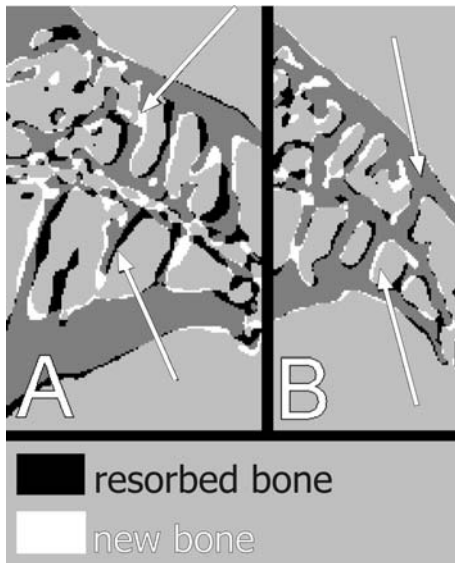


figure 5.4: Details out of a longitudinal cross-section of the proximal tibia of an OVX (A) and OVX+T (B) rat, showing aligning trabeculae. By overlaying scan images of two time points regions of bone resorption and of formation of new bone can be visualized. Resorption of old bone (black) and apposition of new bone (white) appear regulated such that alignment of the trabecular structure across the growth-plate becomes stronger. The arrows indicate trabeculae that appear to be 'moving' toward each other.

other trabecular structures were removed (figure 5.4). Remodelling activity occurred such that the initial complex trabecular network in the metaphysis turned into a structure with longitudinal rods that were aligned with the trabeculae at the opposite side of the growth-plate, in the epiphysis. This process took place in all three groups, but was strongest in the OVX group and weakest in the SHAM group.

table 5-2: Absolute micro-CT parameter values (mean±sem) at week 0 and week 34 and relative change (mean±sem) from week 0 to week 34 for cortical geometry: periosteal perimeter (Ps.Pr), cortical thickness (Ct.Th), cross-sectional polar moment of inertia (Ct.J.) and endocortical area (Ec.Ar)

		Week 0	Week 34	
		<i>absolute</i>	<i>absolute</i>	<i>relative</i>
BV/TV (%)	Sham	15.1±0.77	15.5±0.80	2.45±0.72
	Ovx	15.1±0.56	15.7±0.60	4.00±0.82*
	Ovx+t	15.2±0.61	15.4±0.65	0.62±0.28*
Tb.Th (µm)	Sham	489.6±37.4	496.4±23.5	1.69±2.10*
	Ovx	500.6±37.9	550.8±34.6	10.3±2.66**
	Ovx+t	488.5±21.4	508.6±44.2	1.28±1.75*
SMI	Sham	20.6±1.60	21.1±1.69	1.77±1.84
	Ovx	20.7±1.20	20.9±1.22	1.26±2.17
	Ovx+t	21.5±1.84	21.8±1.82	1.64±0.80
Conn. (/mm³)	Sham	4.84±0.97	4.75±0.98	-1.97±1.38*
	Ovx	4.91±0.46	4.32±0.52	-2.04±1.65**
	Ovx+t	4.93±1.04	4.90±1.06	0.63±1.86*

Significantly different from sham * (p<0.01), from ovx + (p<0.01) or from ovx+t * (p<0.01)

Cortical bone

Treatment with tibolone prevented any changes in cortical bone for all parameter. The cortex of the SHAM and OVX animals increased in thickness (figure 5.5a), resulting from both periosteal expansion (figure 5.5b) and endocortical bone formation (figure 5.5c). In the SHAM animals, the initial decrease in endocortical area was followed by a slight increase and an accompanying decrease in cortical thickness to baseline levels. The observed changes in the cortex did not alter the cross-sectional polar moment of inertia for all groups at all time-points (figure 5.5d) up to week 34. Except for the polar moment of inertia, at week 34 the tibolone treated group differed significantly from the OVX group for all parameters (table 5-2).

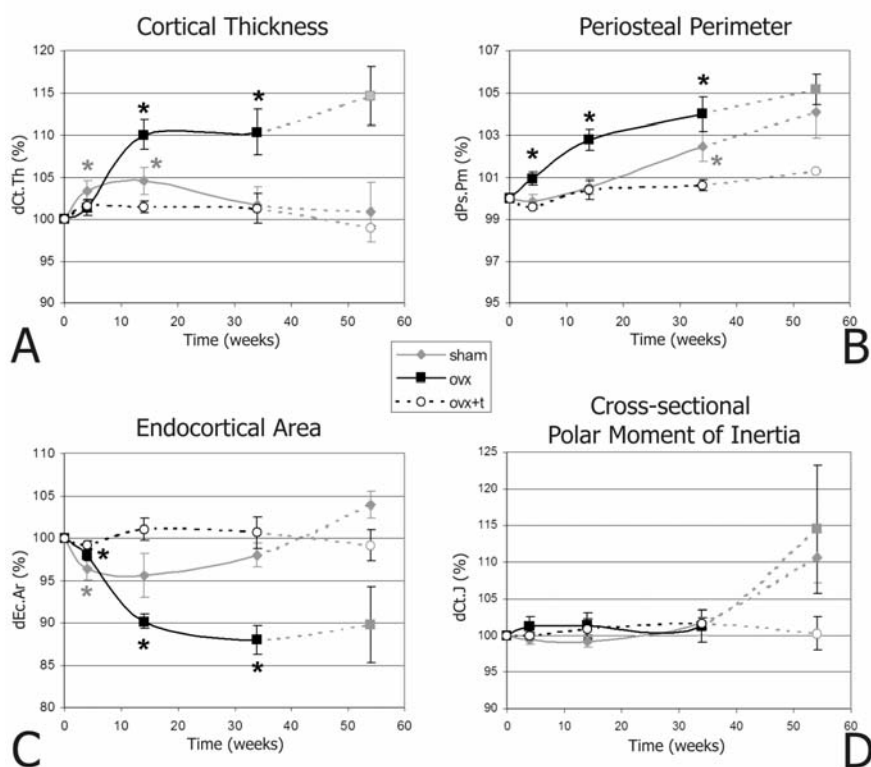


figure 5.5: Relative changes in cortical geometry expressed as percentage of the value at week 0, for the three treatment groups. The error bars represent the standard error of the mean. A) Changes in cortical thickness. B) Changes in periosteal perimeter. C) Changes in endocortical area. D) Changes in cross-sectional polar moment of inertia. (* Significantly different from week 0, $p < 0.05$) At week 54 only three animals per group were available, this time point is not used for statistical testing. In the graphs this is indicated by dash greyed out lines.

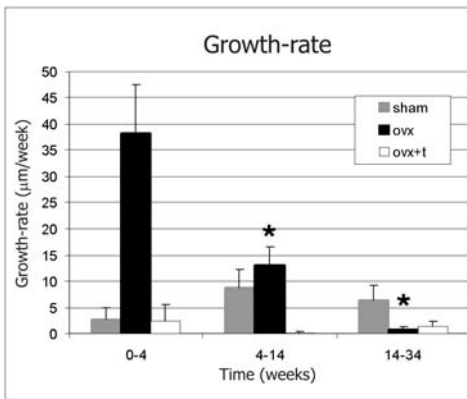


figure 5.6: Average growth-rate for the different groups for the periods between the different time-points (mean with standard error of the mean). (* Significant difference from week 0-4, $p < 0.05$)

Longitudinal growth

Treatment with tibolone halted longitudinal growth in the tibia of ovariectomised animals almost completely at all time points. OVX alone initially increased longitudinal growth-rates well above SHAM levels (figure 5.6). At later time points, growth-rate in OVX animals decreased and no growth could be observed between week 14 and 34. In the SHAM animals, longitudinal growth stayed relatively constant at a mean rate of between 5 and 10 μm per week. After 34 weeks, this resulted in an average total growth at the proximal growth-plate of 225 μm for the SHAM group, 250 μm for the OVX group and 37 μm for the OVX+T animals.

Backscatter Scanning Electron Microscopy

Treatment with tibolone for 54 weeks prevented the decrease in mineralization that occurred in bone tissue of ovx rats (figure 5.7). The lower mineralization of bone tissue due to ovx only reached statistical significance in epiphyseal trabecular bone tissue, but similar trends were noted in both metaphyseal trabecular bone and cortical bone tissue as well.

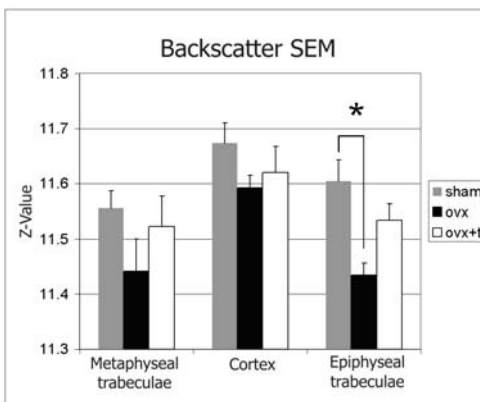


figure 5.7: Tissue mineralization expressed as equivalent Z-value (mean and standard error of the mean) as measured with backscatter SEM for the three treatment groups. (* significant difference, $p < 0.05$)

5.4 Discussion

Treatment with tibolone significantly reduced the effects of ovariectomy, both on bone mass and on selected parameters of bone architecture. Changes in trabecular bone volume fraction (BV/TV), structure model index (SMI) and connectivity density (Conn.) were reduced to levels between OVX and SHAM. Surprisingly, changes in trabecular thickness were even prevented to below SHAM levels. Furthermore, treatment with tibolone prevented all cortical changes and slowed down longitudinal growth to below SHAM levels. Measures of bone metabolism, i.e. urinary DPD/Cr levels and plasma osteocalcin levels, showed a complete prevention of the increase associated with OVX over the whole time period. This, however, did not result in a complete prevention of the OVX-induced bone loss.

In general, treatment with tibolone did not alter the way in which bone remodelling removed bone mass. Patterns of bone loss were very similar in all three groups, and only differed in the speed of bone loss. Observation of the follow-up scans showed that in all three groups, bone was lost preferentially by removal of entire trabeculae, and not by a general thinning. These observations are corroborated by the measured morphometric parameters. The decrease in connectivity indicates a loss of entire trabeculae, while the increase in SMI indicates a perforation of plate-like trabeculae. Since perforation of plates and removal of entire trabeculae have opposite effects on connectivity, the net negative change in connectivity density we measured indicates that loss of entire trabeculae must have been the major contributor to the loss of trabecular bone.

The increase in periosteal perimeter in both SHAM and OVX animal is a well known phenomenon occurring both after ovariectomy and due to aging (6, 158). Although periosteal expansion normally occurs together with, or in reaction to, expansion of the marrow cavity, our data actually showed a decreasing marrow cavity. It is possible that the analyzed part of metaphyseal cortical bone in this study was too close to the growth-plate to show the mostly diaphyseal expanding effects described in literature. Previously we have shown that cortical changes in the metaphysis are closely related to longitudinal growth (195). This result is emphasized by the data of the present study since tibolone both prevented longitudinal growth and prevented any change in cortical geometry.

The biochemical markers showed a peculiar temporary peak at week 4 in all groups. In the SHAM group a temporary disturbance was also present in bodyweight and longitudinal growth-rate: both showed a dip at week 4. Such early and temporary changes in especially biochemical bone markers has been noticed previously (173) and was suggested to be related to cytokine release as a consequence of surgery.

Similar to a few other studies (104, 150), but contrary to one study (18), we found that estrogen deficiency lowered the mean mineralization of the bone tissue, though the changes are rather small. Since the secondary mineralization of bone tissue normally slowly continues over time, it is likely that the decrease in mineralization after OVX relates to the relatively 'young' bone tissue that has been formed by the active remodelling process. In particular, the newly formed thick trabecular structures mainly consist of young and thus lowly mineralized bone tissue. Treatment with tibolone prevented the increase in bone remodelling and thus prevented the decrease in tissue mineralization to non-significant differences ($p=0.44$). The changes in mineralization may also be related to other factors, such as the composition of the bone matrix. For instance, human osteoporotic bone has a lower ratio of non-collagenous matrix proteins than non-osteoporotic bone (66).

It is intriguing that treatment with tibolone completely prevented the changes in trabecular thickness, even to below SHAM levels, while changes in all other parameters of trabecular bone architecture were only partially prevented. In both SHAM and OVX groups, bone loss was associated with an increase in trabecular thickness. Presumably, the remaining trabeculae were 'reinforced' as a reaction to increased local strains caused by loss of mechanical strength (195). Mechanisms that compensate for the loss of mechanical competence by adding more bone are considered quite common. The fact that trabecular thickening was not observed in the OVX+T group not necessarily means that the mechanical responsiveness in these animals was hindered, as is shown by the continuing aligning of trabeculae across the growth-plate. Mechanical strength of the trabecular network is not only determined by architecture, but can also be influenced by changes in tissue stiffness (44, 187). A recent study of the effects of tibolone on the mechanical competence of rat vertebrae suggested an increase in tissue properties with respect to sham controls associated with long term tibolone treatment (49). This could indicate that no need exist to reinforce trabeculae by putting more material since tibolone treatment already reinforced the trabeculae by increasing material properties. The backscatter SEM data indicate that the possible increase in mechanical properties of the bone tissue due to tibolone treatment cannot be explained by changes in tissue mineralization. If stiffer bone tissue is indeed the reason behind the unaltered trabecular thickness, the changes need to be in the organic bone matrix. Further study is needed to investigate this possibility.

The preventive effect of tibolone is thought to originate from the inhibitory actions on osteoclasts by the estrogenic metabolites. At the dose used in this study, the increase in osteoclast activity associated with ovariectomy was prevented completely as is shown by urinary levels of DPD/Cr, a marker for bone resorption. Still, this dose is considered sub-

optimal since it did not completely prevent ovx-induced bone loss. Removal of estrogen results in an increase in remodelling and thus in an increase in the number of active bone remodelling units (Basic Multicellular Units: BMU) (47). Since tibolone treatment inhibited the increase in the levels of bone remodelling markers, it is reasonable to assume that the number of BMUs in the tibolone treated animals was not increased. Bone remodelling in the OVX animals resulted in removal of entire trabeculae and an increase in thickness of remaining trabeculae, what could correspond to an increase in resorption depth (152) and a positive balance of the BMUs. Following this line of argumentation, the fact that tibolone treatment inhibited the increase in trabecular thickness but not the removal of entire trabeculae (figure 5.3), suggests that the increase in BMU balance was inhibited, while the increase in resorption depth was not prevented or only mildly so. Since osteoblast activity determines both the balance of the BMU as activation of the BMU through the RANK/RANKL/OPG pathway (5), the current findings could suggest that tibolone in the dose used in this study affected osteoblasts more than osteoclasts.

However, the organized manner in which these architectural changes occurred, both trabecular and cortical, suggest that remodelling is not random but locally regulated and thus the observed effects on trabecular architecture cannot only be explained from general actions of tibolone on specific cells. Hence, we are left with an unresolved question: How do changes in the remodelling process result in these organized changes in bone architecture? Although the data in this study cannot answer this question, it does show that tibolone activity cannot be understood without knowing how its metabolites influence local regulation of bone cell activity.

This study was designed to investigate the macroscopic effects of tibolone on bone architecture and does not address the question of what the cellular basis is for the observed changes. Future research could be targeted at the potential role of ER α and ER β in the effect of tibolone on bone architecture (120, 168, 172), since it has been shown that the estrogenic metabolites of tibolone have stronger affinities for ER α (45). In this light it would be interesting to compare treatment with tibolone with treatment with estrogen or estrogen like compounds, in combination with receptor-type specific anti-estrogens.

Further, the changes in bone architecture could also be influenced indirectly, for instance by the inhibitory effects of tibolone on longitudinal growth.

Although the molecular and cell physiological origins and the mechanical consequences of the observed changes remain unclear and speculative, our data showed that treatment with a sub-optimal dose of tibolone partially prevented ovariectomised-induced bone loss and completely inhibited the

increase in trabecular thickness, cortical alterations and longitudinal growth that was found in both aging sham and ovx animals.

Acknowledgement

This work was supported by European Union grant QLRT-1999-02024 (MIAB) and a travel grant from the Netherlands Organization for Scientific Research (NWO)

6

In the rat, bone adaptation is regulated by local mechanical stimuli, while ovx-induced bone loss is regulated by local bone density

J.H. Waarsing, J.C. van der Linden, H. Weinans

Abstract

- **Introduction:** Bones are capable of adapting their structure to the mechanical environment. It has been suggested that a failure in this mechanism is responsible for post-menopausal bone loss. After estrogen withdrawal bone is supposed to switch to a disuse state in which low loaded bone is lost. The exact relations between bone loss or formation and mechanical signalling are not known however. In this study we examined the role of mechanical and non-mechanical signals in the alterations in bone structure due to aging and estrogen depletion.
- **Methods:** Local bone loss and formation were assessed in the tibia of an aging sham and ovariectomised rat by comparing in-vivo micro-CT scans made at baseline and at 4 weeks follow-up. We examined the relation between local bone resorption and formation as assessed by in-vivo micro-CT and various strain-related and non-mechanical signals derived from FE-models of the tibiae. The most promising strain-related signal was incorporated in a simulation of the remodelling process.
- **Results:** Our results indicated that local bone resorption and formation was related to local deviations in strain. This relation did not explain bone loss, but associated with alignment of metaphyseal and epiphyseal trabeculae. Gross ovariectomy-induced bone loss was not related to any mechanical signal, but to local bone density or the inverse, local marrow density.
- **Conclusion:** We concluded that alterations in bone structure were regulated by two possibly independent mechanisms. One mechanism was the mechanical adaptation of the trabecular architecture, which was driven by local deviations in strain. The second mechanism regulated ovariectomy-induced bone loss, and was not related to mechanical signalling. This mechanism was driven by local bone (or marrow) density, which could indicate the involvement of bone preserving factors from the bone tissue or resorption stimulating factors from the surrounding marrow.

6.1 Introduction

Bone is known as an organ that adapts its structure to the mechanical environment. This phenomenon, often referred to as Wolff's law (208), has inspired much research to unravel the biophysical and chemical mechanisms of bone adaptation. Animal experiments have shown that bone indeed reacts to its mechanical environment (3, 46, 82, 115, 143). Bone is added when loads are high, while bone is removed when loads are low, both in cortical and cancellous bone. Experiments using cell cultures have shown that especially cells of the osteoblast lineage are sensitive to mechanical stimuli caused by stretching and fluid flows (12, 91, 133).

However, details on how the local sensing of the mechanical environment by bone cells is translated into changes in bone structure are not known. The well-known mechanostat theory of Frost (59) poses that bone adaptation might be regulated similar to a simple thermostat: above a certain set-point, mechanical stimulation results in the addition of new bone, while stimulation below another set-point results in the removal of bone. He suggested that the values of these set-points are 'known' by the sensor cells in bone. However, these set-points cannot be fixed values since they have to vary between bones, and perhaps even within bones (82). Further, bones appear to react only to time varying stimuli and not to static loads (183).

Failure of the mechanical adaptation mechanism could result in bone disorders like post-menopausal osteoporosis. Because of the similarities between post-menopausal and disuse related bone loss, it was assumed that especially the less loaded trabeculae are resorbed when estrogen levels decrease (114, 161, 207). In the tibia of ovariectomised rats, it is principally the more distal trabecular metaphyseal bone that is resorbed while the trabecular bone in the epiphysis which is considered to experience higher loading is relatively unaltered (207). The increase in anisotropy in human osteoporotic bone due to resorption of the 'horizontal' trabecular connections in favour of the load carrying vertical trabeculae, gives further support to this theory (80, 132). Frost's mechanostat theory accommodates this phenomenon by stating that estrogen influences the value of the set-point. When estrogen levels decrease, the value of the resorption set-point increases such that more trabecular bone is loaded below this set-point and is thus subject to resorption. In other words, estrogen sensitizes bone to mechanical stimulation (115). Several studies exist that apparently support this generally accepted theory (34, 117, 119). However, evidence is not rock-solid, and other studies exist that give contradictory evidence and show that the responsiveness of bone to mechanical stimulation increase in the absence of estrogen (92). At least the interaction between estrogen and mechanical sensing in bone is more complex in that estrogen suppresses the

initiation of the osteogenic response to mechanical loading, but enhances the bone formation phase (90).

In this study we have explored the interaction between mechanical loading and changes in bone architecture as it occurs in-vivo during aging and because of decreasing estrogen levels. For this we used follow-up in-vivo micro-CT scans of the tibia of a normally aging and an ovariectomised (ovx) rat. We compared the changes in the bones that occurred in-vivo with strain distributions yielded by finite element models and with changes predicted by load-driven remodelling simulations.

6.2 Methods

In-vivo micro-CT scanning

The proximal right tibias of two 10 month-old female Wistar rats were scanned in an in-vivo micro-CT scanner (prototype Skyscan 1076). The scans resulted in reconstructed datasets of the proximal tibia with a voxel-size of 21 μm . After the baseline scan one animal was sham operated and the other ovariectomised. Ovariectomised rats are used as a model for post-menopausal osteoporosis (98). After surgery, the animals were scanned at week 4, 14, 34 and 54. All animal procedures formed part of a larger experiment for which approval was obtained from the animal ethics committee (DEC).

The reconstructed data sets were segmented into binary sets consisting of bone and non-bone voxels by an automated segmentation algorithm using local thresholds (197).

The subsequent scans of each animal were repositioned to match the scan at week 0 using an automatic registration algorithm that maximizes mutual information as an optimization criterion. The registration procedure has been described in detail previously (194).

Finite Element Modelling

The strain and stress distributions in the proximal tibiae were assessed using Finite Element (FE) modelling. The FE models were constructed using micro-CT scans of 1 cm of the proximal tibia as input. Each bone voxel in the scan data represented a bone element in the FE model.

Load was applied to the tibia through a model of the femoral condyles. The condyles were modelled as an elliptical block of which the distal end was an inverse mask of the tibial plateau. A cylindrical groove between the two condyles was taken out of the block. The block was modelled such that load transfer from femur to tibia did not take place at one position as would be the case with a real femur at a specific angle of the knee, but load transfer took place over the entire tibial plateau, thus simulating the summed load transfer during a complete gait-cycle. The block was positioned 400 μm

above the tibial plateau and the space between the femoral condyles and the tibia was filled with cartilage elements (figure 6.1). One point of the tibial cortex at the bottom of the model was fixated in all directions and another in the vertical and one horizontal direction, so that the tibia could neither translate nor rotate, but could become wider. The fibula was only fixated in the vertical direction, so that the fibula was free to move in the horizontal plane.

The space within the metaphysis and epiphysis was filled with marrow elements, except for the non-mineralized tissue in the growth-plate, which was modelled as cartilage. The models contained approximately 6.5 million bone elements, 4 million cartilage elements and 6.5 million marrow elements.

Bone was modelled with a Poisson Ratio of 0.3 and a Young's Modulus of 10 GPa, which lies in between reported values of 5 GPa (192) and 20 GPa (156). Bone marrow (approximated by fat) has a very low Young's Modulus, but the material is nearly incompressible (the Poisson Ratio is close to 0.5). Thus in confined compression the apparent stiffness can be relatively high. Marrow indeed has a substantial contribution to the whole bone stiffness, which is referred to as hydraulic stiffening (144, 145). Cartilage has non-linear mechanical properties and the apparent stiffness depends on the rate of compression. In our models we approximated the

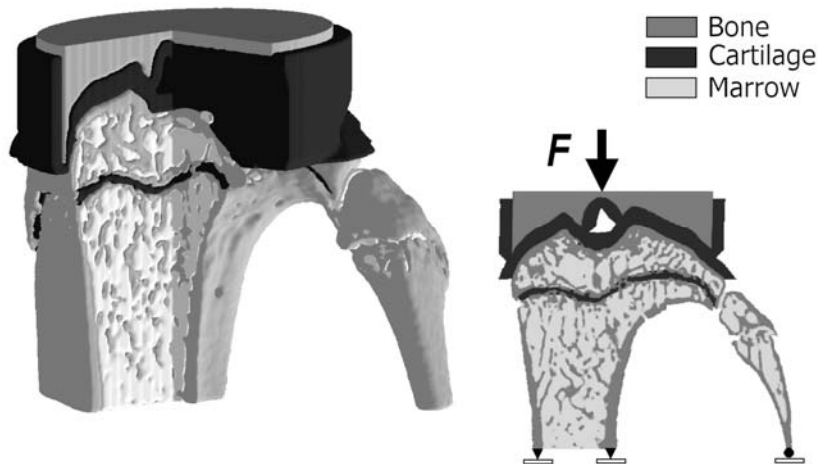


figure 6.1: Example of an FE model used in this study, represented as an opened 3D model and a schematic 2D cross-section. The model contains bone, cartilage and marrow elements. The model is compressed by applying a load (F) to the model of the distal femur. The tibia is fixed in all directions at two cortical points at the bottom end of the model, while the fibula is only fixed in the vertical direction and thus can move in the horizontal plane.

mechanical behaviour of bone marrow and cartilage elements and investigated the sensitivity of the outcome measures for variation in modulus values for these tissues. The models were run with modulus values for marrow and cartilage of resp. 5 GPa and 8 GPa (*HighStiff*); 2 GPa and 5 GPa (*MediumStiff*) and 1 GPa and 2 GPa (*LowStiff*).

Part 1: Analysis of the strain distributions

In the first part of this study we investigated if relations existed between bone resorption and formation as suggested by the in-vivo follow-up scans and various potential mechanical and non-mechanical signals. The mechanical signals were derived from FE-models that used a baseline scan as input. The non-mechanical signals were related to local bone morphology: local bone density and local 3D thickness. This latter signal was chosen to see if thin trabeculae are more likely to be resorbed than thick trabeculae.

By comparing the scans at week 0 with the registered scan of the next time point (week 4) we could classify the voxels in the original scan as 1) voxels that were resorbed after 4 weeks (*Resorption*), 2) voxels that were not resorbed and received a neighbouring new bone voxel after 4 weeks (*Formation*) and 3) voxels that were not associated with any change after 4 weeks (*NoChange*).

Scanning noise, partial voxels and small registration errors will reduce the accuracy of the voxel classification, especially at the surface of the bone. To reduce these errors, edge voxels were excluded. However, edge voxels were excluded solely if they were present in one scan and not in the other scan. Edge voxels that were present in both scans were less likely to be the result of noise or other artefacts and thus were considered to be ‘real’.

Trabecular bone was separated from cortical bone using in-house software. The bones were divided into three compartments: epiphysis, proximal metaphysis (first 2.5 mm below the growth-plate) and distal metaphysis (final 2.5 mm of the metaphysis). The two metaphyseal compartments touched, but did not overlap.

Six different types of signals were defined and calculated for each voxel. Four signals were strain related and two were related to bone morphology. The strain related signals were derived from FE models that were run using the baseline scan of the sham and ovx rat as input. The morphology related signals were derived from the baseline scans themselves. The following signals (S) were derived for each voxel (i):

1. *Absolute Strain*: the signal at voxel location i was defined as the Maximum Principle Strain (MPS), calculated from the FE model at that location.

$$S_i = \varepsilon_i$$

2. *Total Strain*: The signal at location i was defined as the sum of all MPS values of the bone voxels in neighbourhood R with radius r .⁴

$$S_i = \sum_{j \in R} \varepsilon_j$$

3. *Relative Strain*: The signal at location i was defined as the absolute MPS of each voxel divided by the average MPS of its neighbourhood R with radius r .

$$S_i = \frac{\varepsilon_i}{\frac{1}{N_R} \sum_{j \in R} \varepsilon_j}$$

4. *Deviation in Strain*: The signal at location i was defined as the difference between the local MPS and the regional MPS.

$$S_i = \varepsilon_i - \frac{1}{N_R} \sum_{j \in R} \varepsilon_j$$

5. *Local Bone Density*: The signal at location i was defined as the bone density in a local neighbourhood R with radius r .

$$S_i = \frac{1}{\frac{4}{3}\pi r^3} N_R$$

6. *Local 3D Thickness*: The signal at location i was defined as the local 3D thickness of the bone at location i . The set of distances were calculated using the method introduced by Hildebrand and Ruegsegger (75).

$$S_i = (3D.Th)_i$$

NR = number of bone voxels in neighbourhood R with radius r , which was set at 16 voxels (320 μm)

The distributions of the signals throughout the bone were represented as probability density distributions. The density distributions of the different voxel classes (*Resorption*, *Formation* and *NoChange*) were compared among each other within the entire bone, and within each bone compartment separately (epiphysis, proximal metaphysis and distal metaphysis).

Comparing the distributions of the various signals is hampered by the fact that each signal has different units and differently shaped distributions. To facilitate the comparison, the difference between the distribution means of the *Resorption* and *Formation* voxel classes were expressed as effect size, which is the difference between the means of the distributions, normalized by the pooled standard deviation of the two distributions:

$$EffectSize = \frac{\mu_1 - \mu_2}{\sqrt{\frac{1}{2}(\sigma_1^2 + \sigma_2^2)}}$$

⁴ This signal was derived from work of Mullender et al. (31) and Ruimerman et al. (32). They applied a remodelling stimulus that was a distance weighted sum of the mechanical stimuli in a neighborhood with radius D . The weights (w) were calculated as follows: $w_j = e^{-d_{j,i}/D}$, with d_{ij} the distance between the location of an 'osteocyte' (j) and the location where the remodelling stimulus is applied (i). Our situation is a special case in which the weight function is approximated by $w=1$ if $d_{ij} < D$ and $w=0$ if $d_{ij} > D$

Thus, the difference between two distributions is expressed relative to the width of the distributions and can be seen as the ‘strength’ of the separation between the two distributions.

Part 2: Simulation of the remodelling process in the OVX rat

Bone adaptation was simulated in a stepwise process. At each step the stress and strain distribution in the proximal tibia was assessed using an FE-model as described above. Next, surface bone elements were added or removed depending on the evaluation of a decision rule using a local criterion. The *Deviation in Strain* signal defined under part one was used as input for the decision rule. The MPS of a bone surface element was compared to the average MPS of the neighbouring bone elements in a spherical neighbourhood with radius $r=16$ voxels ($=320\text{ }\mu\text{m}$). When the MPS of the bone element under consideration was more than one standard deviation (SD) below the local average, the element was substituted for a marrow element. If the MPS was more than one standard deviation (SD) above the local average, the element’s non-bone neighbour that had the most bone neighbours was substituted for a bone element. When multiple non-bone neighbours fitted this criterion, a random element was selected from these non-bone neighbours. Thus the signal range between -SD and +SD can be considered as the width of a lazy zone, similar to the lazy-zone in the mechanostat theory, but without ‘pre-programmed’ fixed set-points. Stimulation within the boundaries does not result in any changes, while stimulation outside the boundaries results in removal of the voxel, or apposition of a new neighbour.

The discrete steps in the simulation were not intended to correspond to a certain fixed time frame of the continuous biological remodelling process. The remodelling simulation was run for 8 cycles.

Sensitivity of the remodelling simulation

The sensitivity of the remodelling simulations for changes in parameter settings was determined by running the simulation with different settings for the radius r of the spherical neighbourhood R , and by varying the set-points of the lazy-zone. For the radius r the following values were used: 4, 8, 16 and 32 voxels (80, 160, 320 and 640 μm); for the set-points, the following values were used: 0.5, 1 and 2. The radius was varied at a set-point of 1 SD, while the set-points were varied at a radius of $r=16$ voxels.

Analysis of trabecular architecture

Trabecular architecture was analysed for the scans of all of the five time points and for all simulation results of each of the eight cycles.

Trabecular and cortical bone were separated manually, using the software package CT-analyser (Skyscan, Antwerp, Belgium). For the metaphyseal trabecular bone, bone volume fraction (BV/TV) and trabecular thickness

(Tb.Th) (75) were calculated as measures of trabecular bone mass and its distribution, while trabecular architecture was quantified by calculating structure model index (SMI) (76). SMI indicates whether the trabeculae are more rod-like (SMI=3) or more plate-like (SMI=0).

All morphometric parameters were calculated using software of the freely available CT-Calculator project⁵.

6.3 Results

Part 1: Analysis of strain distributions

Strain

The medial side of the proximal tibia was mostly compressed uniformly along the entire length of the bone. The epiphysis hardly experienced any deformations and was pushed downward, resulting in bending of the metaphysis at the side where the fibula was attached. Strains were highest at the distal cortex (figure 6.2). The mechanical deformation resulted in low average strains in the epiphyseal trabecular bone and high strains in the trabecular bone at the distal metaphysis for both animals (figure 6.2a).

Overall signal distributions

No difference in strain (MPS) existed for the trabecular bone between the voxels that were associated with resorption and the voxels that were associated with new bone formation, neither for the sham nor for the ovx animal (figure 6.3, table 6-1). The strain categories that were based on deviations from a regional average (*Relative Strain* and *Deviation in Strain*),

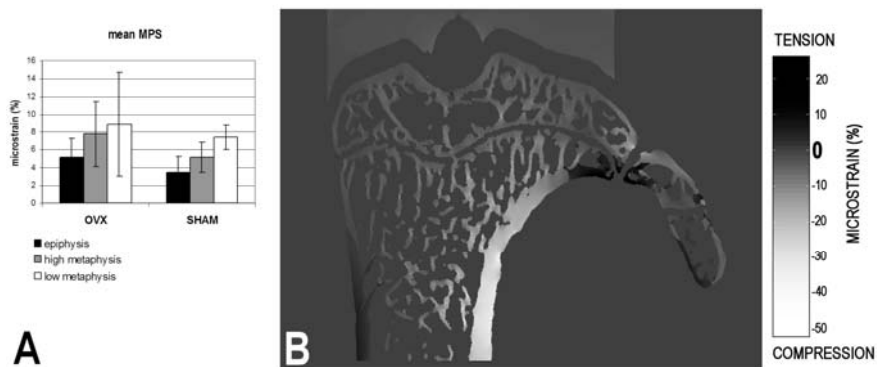


figure 6.2: Average MPS +/- SD in the three trabecular bone compartments for the SHAM and OVX animal (A). The distribution of compressive and tensile strains are depicted in a longitudinal cross-section of the tibia of the OVX rat under compression (B).

⁵ The software can be downloaded from: www.eur.nl/jgg/orthopaedics/Downloads.html

table 6-1: Difference between resorption and formation voxels expressed as effect size, which is the standardized difference between the means, for trabecular bone

	SHAM			OVX		
	<i>Mean resorption</i>	<i>Mean formation</i>	<i>Effect size</i>	<i>Mean resorption</i>	<i>Mean formation</i>	<i>Effect size</i>
NORMAL	4.28	4.25	0.01	6.78	6.92	-0.04
TOTAL	77.7	70.6	0.18	125.8	129.2	-0.05
RELATIVE	0.93	0.96	-0.25	0.89	0.97	-0.33
DEVIATION	-0.07	0.08	-0.24	-0.51	0.08	-0.31
MASS	37.4	35.6	0.14	39.6	42.1	-0.20
THICKNESS	109.0	100.8	0.27	110.4	111.4	-0.03

however, exhibited a small but clear shift in strain distribution, such that the *Resorption* voxels had a lower mean signal value than the *Formation* voxels. This difference was present in both animals (figure 6.3). The shift in distributions as expressed by the effect size was similar for both deviation categories, but stronger in the ovx animal than in the sham animal (table 6-1). The voxels that were associated with no change, and which generally did not reside on the bone surface, mostly showed a narrower strain distribution, which overlaid the distribution of the *Formation* voxels for all strain categories (figure 6.3).

The distributions of the morphology derived signals showed patterns that showed a difference between *Resorption* and *Formation* voxels (effect size = -0.20), due to a shift in the distributions. For the sham animal, both morphology-derived signals gave a positive effect size. However, this difference was due to changes in the shape of the distributions, not due to a shift.

The various signal distributions obtained from the cortical bone voxels did not show clear patterns. The difference between resorption and formation as expressed by the effect size was generally small and present in one animal and not in the other, or the effect size was different in sign for both animals. Further, the small differences could not be attributed to a clear shift in the distributions (figure 6.4, table 6-2).

table 6-2: Difference between resorption and formation voxels expressed as effect size, which is the standardized difference between the means, for cortical bone

	SHAM			OVX		
	<i>Mean resorption</i>	<i>Mean formation</i>	<i>Effect size</i>	<i>Mean resorption</i>	<i>Mean formation</i>	<i>Effect size</i>
NORMAL	4.50	4.38	0.04	11.94	9.57	0.25
TOTAL	139.8	129.1	0.11	347.9	300.0	0.16
RELATIVE	0.90	0.92	-0.13	0.92	0.92	0.04
DEVIATION	0.00	0.11	-0.08	0.09	-0.23	0.18
MASS	58.9	57.5	0.12	61.4	62.4	-0.08
THICKNESS	224.5	213.0	0.14	209.7	213.9	-0.06

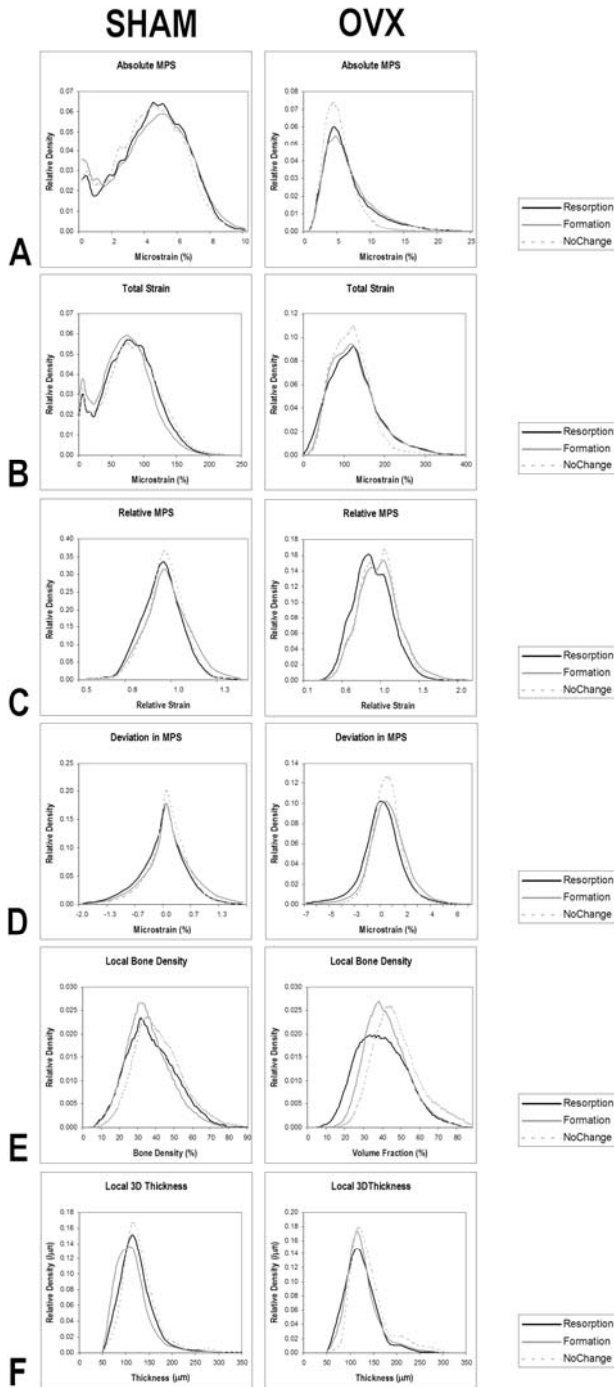


figure 6.3:
Distributions of the different strain and morphology related signals extracted from trabecular bone for both the ovx and sham rat. Each figure shows the distributions of the *Resorption*, *Formation* and *NoChange* voxel classes. A) Absolute Strain, B) Total Strain, C) Relative Strain, D) Deviation in Strain, E) Local Bone Density, F) Local 3D Thickness.

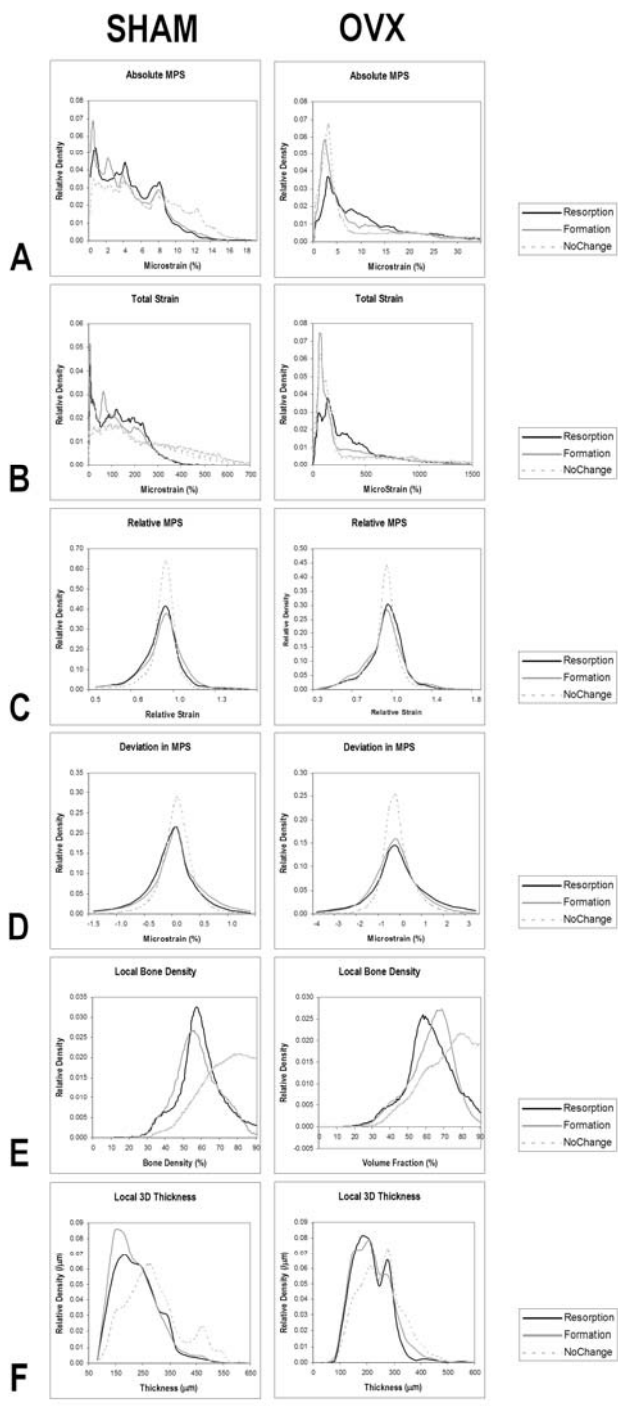


figure 6.4:
Distributions of the different strain and morphology related signals extracted from cortical bone for both the ovx and sham rat. Each figure shows the distributions of the *Resorption*, *Formation* and *NoChange* voxel classes. A) Absolute Strain, B) Total Strain, C) Relative Strain, D) Deviation in Strain, E) Local Bone Density, F) Local 3D Thickness.

Signal distribution per bone compartment

Although the *Deviation in Strain* signal showed a clear shift between the distributions of the *Resorption* and *Formation* voxels when all trabecular bone was concerned, this shift was only apparent within some bone compartments (figure 6.5a,c). The epiphysis did not show a shift of the distribution of the *Resorption* voxels relative to the distribution of the *Formation* voxels in either animal. In the other two trabecular bone compartments a distinct shift was present. In the sham animal the shift was more pronounced in the distal metaphysis (effect size of -0.41 in distal metaphysis compared to -0.21 in the proximal metaphysis; (figure 6.5a) while in the ovx animal the strongest shift showed in the proximal metaphysis (effect size of -0.30 in the proximal metaphysis compared to -0.24 in the distal metaphysis; figure 6.5c). No relation could be found between the amount of bone loss in a compartment and the difference between the *Deviation in Strain* signal distributions.

The distributions for the *Local Bone Density* signal only showed differences between *Resorption* and *Formation* for the ovx animal (figure 6.5b). In the distal metaphysis where bone loss was strongest, the shift was especially strong (effect size of -0.96). The proximal metaphysis did show a difference between the shape of the distributions of the *Resorption* and *Formation* voxels, but the effect size was about zero. No difference was detected in bone compartments where hardly any bone was lost, like the epiphysis of the ovx animal and the three bone compartments of the sham animal (figure 6.5a). Thus, local bone density appeared to relate to the amount of bone loss.

Influence of variation in marrow and cartilage modulus

The influence of the material stiffness of both marrow and cartilage on the above reported results was only minor. Though the effect size of the difference between *Resorption* and *Formation* for the different conditions varied a few percent, this did not change the observed patterns.

Part 2: Remodelling results

In-vivo

In-vivo, the ovx rat lost considerable amounts of trabecular bone over the 54 weeks of the study period. This resulted in a decrease of trabecular bone volume fraction of 86% (figure 6.6a). Most bone loss took place in the central and more distal metaphyseal regions of the tibia. Remaining trabeculae increased in thickness (TbTh.: $131 \rightarrow 150 \mu\text{m}$) and became more rod-like (SMI: $2.0 \rightarrow 3.3$). In general, the remaining trabeculae in the metaphysis appeared to align with the trabeculae in the epiphysis, on the opposite side of the growth-plate (figure 6.7).

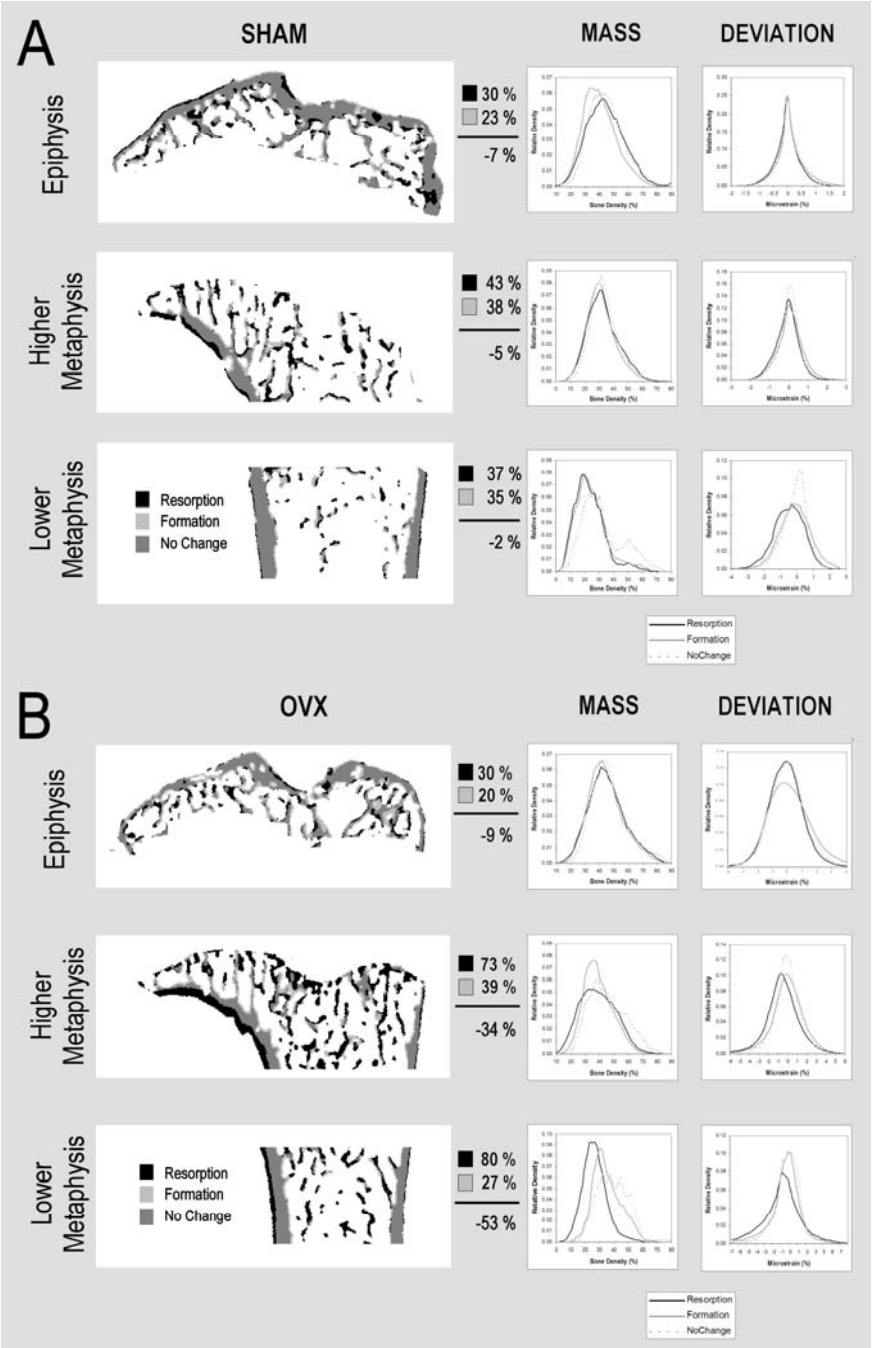


figure 6.5: (previous page) In this figure the *Deviation in Strain* (deviation) and the *Local Bone Density* (mass) signal distributions is related to bone loss in the three compartments of the sham (A) and ovx (B) rat (epiphysis, proximal metaphysis and distal metaphysis). The left panels depict bone loss and formation as suggested by overlaying the in-vivo scans made at baseline with the in-vivo scan made at week 4. Bone that is present in the baseline scan but not in the follow up scan is considered to be resorbed, while bone present at week 4 but not in the baseline scan is considered newly formed bone. The amount of bone classified as resorption or formation and the resulting amount of bone loss is given, expressed as a percentage of the original bone mass.

Although the linear bone loss in the sham rat progressed more slowly than in the ovx rat (29% after 54 weeks, figure 6.6a), bone loss patterns were very similar. The structure model index however did not increase.

Simulation

During the simulation, which started from the week 0 situation of the ovx rat, the trabecular structure changed considerably. Many connecting horizontal struts were lost, while the remaining vertical trabeculae straightened and aligned, increased in thickness and in general became more rod-like, very similar to the in-vivo situation (figure 6.7). The resulting amount of trabecular bone loss however, was only minor (figure 6.6b). Variation in the radius of the neighbourhood R or the cut-off set points hardly influenced this outcome (figure 6.6b). During each step about 0.7%

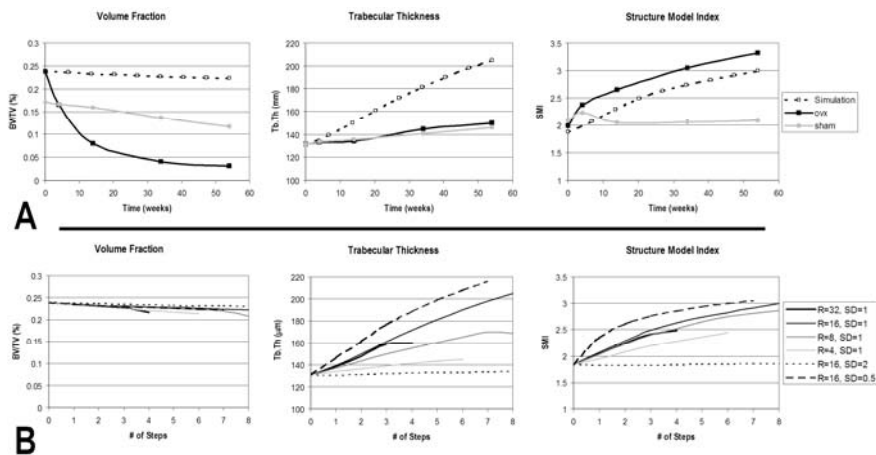


figure 6.6: A) Changes in trabecular structure over time of the ovx and sham animal as expressed by different measures of trabecular architecture (Trabecular bone volume fraction, trabecular thickness and structure model index). The in-vivo measured values are shown together with the values predicted by the remodelling simulation of the ovx rat. The different steps of the remodelling simulation are evenly distributed over the time axis of the in-vivo measurements and thus do not represent real time steps. B) Variation in trabecular structure predicted by the remodelling simulation after varying the radius of the local neighbourhood ($r=4, 8, 16$ and 32 voxels) and the set-points of the lazy zone ($SD=0.5, 1$ and 2)

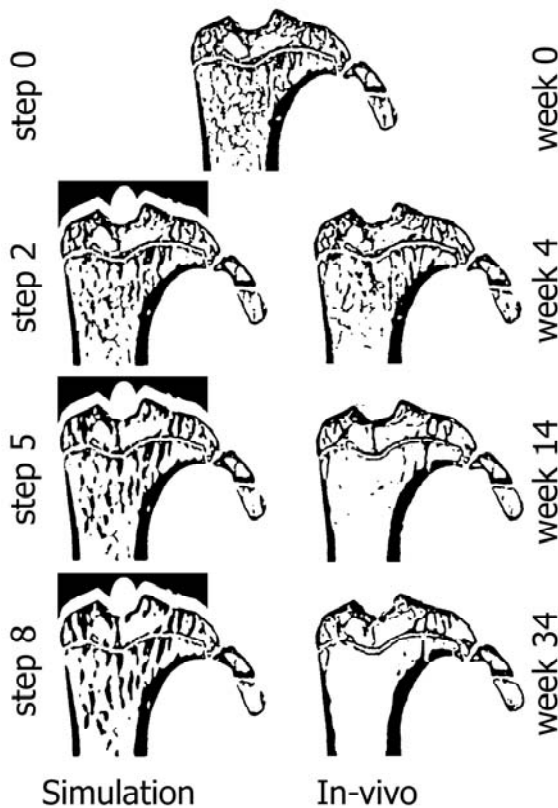


figure 6.7: Longitudinal cross-section out of the tibia of the OVX animal that served as input for the remodelling simulation. The left panels show the structural changes over time as predicted by the remodelling simulation, while the right panels show the trabecular bone changes as measured in-vivo. The different steps from the remodelling simulation do not necessarily match the time points from the in-vivo scans. Notice the alignment of trabeculae that occurs both in-vivo and in the simulation. Also notice the lack of bone loss in the simulation.

of the bone volume was lost resulting in a 6% decrease in trabecular bone volume fraction after 8 steps. The trabecular thickness increased considerably for most settings of the remodelling parameters. The increase in trabecular thickness was influenced most strongly by changes in the width of the lazy zone. When the cut-off points were set at 2.0 SD the thickness hardly changed, while setting the cut-off points at 0.5 SD resulted in the most rapid increase in trabecular thickness. The SMI behaved similar to the trabecular thickness with respect to changes in parameter settings. No changes were observed at the cortex.

6.4 Discussion

In-vivo micro-CT gives the possibility to overlay successive scans of the same bone and thus to identify bone that was resorbed or formed in between two scans. In this study we combined this unique possibility with high-resolution FE models to determine strain distributions and ran

simulations of the remodelling process to explore the relations between bone loss (or remodelling) and mechanical signalling.

Our results indicated that resorption and formation of bone was related to local deviations in strain, but not to absolute mechanical strains (table 6-1 and figure 6.3). Bone that was strained low relative to a local average was associated with resorption, while strains that were high relative to a local average were associated with formation. This relation was present in all metaphyseal compartments in both animals (figure 6.5) what suggests that the regulatory principle behind this relation was rather general. Since the relation was present in both animals, but only the ovx animal lost substantial amounts of bone, local deviations in strain appeared unrelated to total amounts of bone loss. The results of the remodelling simulations that were implemented with the *Deviation in Strain* criterion supported this. The simulations showed that horizontal connections between trabeculae were removed, while the load carrying vertical trabeculae were preserved, which resulted in only minor amounts of bone loss (figure 6.6). Simulated metaphyseal trabeculae became straight, smooth and aligned with trabeculae in the epiphysis. This resembled to a great extent the aligning of trabeculae that occurred in the in-vivo situation as observed in the 54 weeks of the experiment (figure 6.7).

Bone loss that occurred after ovx, on the other hand, did not associate with any mechanical signal, but associated strongly with local bone density. Low local bone density associated with resorption while high local density associated with formation. This relation was strongest in the distal metaphysis of the ovx rat, where bone loss was strongest, and was absent in the epiphysis of the ovx rat and in all three compartments of the sham rat, where no bone was lost. These results suggest that bone loss was inhibited or slowed down when local bone density was high. Of course, the relation could also indicate that bone loss was related to the surrounding marrow, which is the inverse of the local bone density. Thus bone loss was stimulated when marrow density was relatively high. Whether this relation with local bone or marrow density points to insufficient bone preserving stimuli due to small amounts of osteocytes or to high amounts of bone resorbing stimuli coming from the marrow remains to be seen. Considering the osteocyte network as a network of mechanical sensors, one could easily assume that the potential bone preserving stimuli could be the summed strain signal of the osteocytes in a local neighbourhood (136, 165). However, this appears not to be the case, since the *Total Strain* signal, which is the summed strain signal, examined in this study showed no relation with bone loss.

Thus, it appears that two, perhaps independent, mechanisms were at work to regulate changes in bone structure. One mechanism adapted bone to the current loading conditions and was driven by local deviations in

strain. This mechanism had minor influences on bone mass, and was not related to bone loss induced by estrogen withdrawal. However, withdrawal of estrogen might accelerate this mechanism by increasing remodelling rate (195). The second mechanism regulated ovx-induced bone loss and was not related to mechanical strain, but to low local amounts of bone or high local amounts of marrow.

Interestingly, this finding is contrary to the current vision that ovx-induced bone loss is targeted at trabeculae that experience the lowest strains. This vision stems from early observations that post-menopausal bone loss resembles disuse-related bone loss since both situations result in increased remodelling and the initial acceleration of bone resorption wears off (32, 183). However, disuse-induced bone loss does not completely follow the same remodelling patterns as ovx-induced bone loss. After ovx, erosion increases on all bone surfaces, central metaphyseal trabeculae are lost and the diaphyseal cortex expands. Bone loss due to disuse induced by hind-limb immobilization resulted in increased bone loss only on bone surfaces where turnover was high (171) and bone loss was not limited to central metaphyseal trabeculae (7). Further, after immobilization cortical thinning occurred without accompanying periosteal expansion (6).

The idea that ovx-induced bone loss is a form of disuse related bone loss leans strongly on a study by Westerlind et al (207) of bone loss in rats. In a 2D homogenized FE model of the distal femur they showed that areas in which strains were low (the metaphysis) were also the areas where bone loss was strongest, while regions that experienced high strains (the epiphysis) were protected for ovx-induced bone loss. Again, our results are quite distinct. The high-resolution fully 3D FE model of the proximal tibia showed that the highest strains are found in the metaphysis, while the epiphysis is hardly deformed. Apart from the obvious differences in FE models no other reasons are known that could explain the differences in outcome.

The strain patterns observed in our FE models resulted from the fact that the tibia bended in compression. Bending occurred entirely in the distal metaphysis. The epiphysis was hardly deformed and was pushed down on the metaphysis. Thus, structurally, the epiphysis, or more general, the area around the growth-plate was stiffer than the more distal metaphyseal areas. Most long bones bend in compression due to the bone's natural curvature. Thus, bones sacrifice strength in order to gain predictability of where the highest strains occur (14). Apparent from the strain distributions seen in this study, this could be to direct the highest strains away from the sensitive growth-plate.

The findings discussed in this study give some indications about the regulatory mechanisms at work in bone adaptation and bone loss induced by removal of estrogen and normal aging. It does not give an explanation for

disuse related bone loss. After hind limb unloading bone is also lost from surfaces that are relatively untouched by estrogen-induced bone loss, and that experience relatively low amounts of strain, like the epiphysis (171, 207). Although our study did not find any relation between absolute strain and bone loss, disuse related bone loss does suggest that such a relation exists.

During development bones adapt themselves such that an equilibrium state is reached in which all strains sensed are above the disuse threshold (30). Thus the strains experienced within the tibia during this experiment can be assumed to have been above the disuse threshold, and thus it is logical that we did not find a relation between resorption and absolute strain in our study. Besides, disuse related bone loss could be caused by the changes in load at the onset of the disuse period more than by the lack of mechanical signalling itself. This would explain the decay in bone loss during disuse (32). In this case the disuse phenomenon can easily be incorporated into our findings when considering the theory posed by Lanyon that bone remodelling is in principle ‘error-driven’ (115). Normally this refers to the idea that bone is resorbed when the experienced strain becomes lower than previously experienced strains (reference strains). The theory explains among others why static strains do not affect bone remodelling, while dynamic strains do, and could also explain the initial increase in bone loss at the onset of disuse. The current findings can be incorporated into this theory by posing that the reference strain in the error-driven bone adaptation theory is determined, not only by previously experienced strains, but also by current strains averaged over a certain area.

One of our strain signals, the Total Strain, was derived from studies by Mullender (136) and Ruimerman (165). The idea in these studies is that the remodelling stimulus at a location on the bone surface is the combined stimulus communicated to the surface from osteocytes lying within the bone. The signal is assumed to decay exponentially with the travelled distance. The resulting stimulus is thus a distance-weighted sum of stimuli, resembling the *Total Strain* signal presented in this study. Although in our study we did not see any relation between *Total Strain* and resorption or formation, the mentioned studies showed convincing results from remodelling simulations driven by this stimulus. The models showed the aligning of the trabecular structure to the main loading directions, a process that is also seen in-vivo (195). Our data however showed that such behaviour related to deviations in strain, not to absolute strains. An explanation of this seeming contradiction might be that these models represented rather small homogenous pieces of trabecular bone. In such situations, comparing local (summed) strain-related stimuli to a fixed reference value is similar to comparing local strains with a regional mean, since in homogenous samples regional means will be homogenous as well.

When whole bones are studied in which strains are not homogenous, using an absolute strain related stimulus with a global reference value mainly resulted in resorption of bone in regions where strains were low, and not in subtle alignment of trabeculae (data not shown).

The difference between the distribution of resorption and non-resorption voxels was obviously present for the local *Deviation in Strain* and the *Local Bone Mass* criteria, but the differences were fairly small, especially considering the width of the distributions. A large part of the voxels that were classified as being resorbed must have been part of the remodelling space and were thus only temporarily 'removed'. This might or might not be related to mechanical strain. Other 'truly' resorbed voxels could be the result of resorption targeted at the removal of micro-cracks or be the result of 'random' resorption. These confounding issues undoubtedly contributed to the width of the distributions and thus to the relatively small observed differences between the distributions.

Despite the fact that the methodology used in this study is on the edge of what is feasible at this moment, the results seem consistent and for the most part could fit within existing theories on how bone adaptation is regulated. The exception is the finding that estrogen related bone loss was not related to mechanical stimuli, which is contrary to the currently held opinion that estrogen related bone loss is targeted at the less loaded trabeculae. However, removal of estrogen accelerates the remodelling process, which certainly influences mechanical bone adaptation. Further, the acceleration of the adaptation process is mixed with not-mechanical bone loss what could cause further (apparent) interactions between changes in bone structure and mechanical loading. Thus, it is understandable that studies investigating the influence of estrogen on loading regimes in-vivo do find an effect of estrogen on the mechanical response (90, 92, 207).

In conclusion, by combining FE analysis and in-vivo micro-CT scanning we found that structural changes in bone appeared to be regulated by two possibly independent mechanisms. The first mechanism regulated bone adaptation, which resulted in the alignment of the trabecular structure to the main loads by local deviations in strain. This mechanism was not responsible for gross bone loss after ovx. The second mechanism regulated ovx-induced bone loss and was associated with low local bone density or high local marrow density. Identifying biochemical factors that influence these mechanisms separately might result in treatment of post-menopausal bone loss without affecting the mechanical responsiveness of bone.

7

General discussion

7.1 Introduction

The bones that form the skeleton are active organs with a complex structure that are an inseparable part of a complex living organism. And like other organs in the organism, just like the organism itself, its nature is dynamic, not static. It reacts and acts towards its environment and is capable of adaptation of its complex structure. This adaptation is mostly seen in the light of gaining or losing bone mass. For a large part this is due to the fact that most of the accessible imaging modalities are merely capable of measuring bone mass. Further, since it is not really known what this adaptation process actually does and how it works, it is difficult to attach a meaning to the changing bone structure that is the result of this adaptation process. The current change in paradigm from bone mass to bone quality is a sign that awareness is changing. Thus, the idea of an in-vivo micro-CT scanner that would have the capabilities to scan the bones of living animals at resolutions high enough to resolve the individual trabeculae raised a lot of excitement and expectations. As with most ideas, the realization of this particular one involved the conquering of many obstacles. The first chapters in this thesis reflect a few aspects of that development phase, namely the post-processing of the scan images, while the final chapters report the first scientific harvest using the developed method. We hope that this body of work does meet with the expectations aroused by the idea of an in-vivo scanner. We believe that the findings presented here can shed some light on the way the bone adaptation mechanism works and will contribute to the understanding of bone quality and what it entails.

7.2 Thoughts on the methods

In-vivo versus in-vitro micro-CT

As mentioned above, a new imaging modality like an in-vivo micro-CT scanner raises a lot of expectation. Have these expectations been met? What are the advantages of in-vivo micro-CT above in-vitro scanners? In other words, could the results presented in this body of work also have been obtained by traditional in-vitro micro-CT scanning?

The most obvious advantage has a statistical nature. Longitudinal studies have stronger statistical power than cross-sectional studies, since treatment effects can be measured independent of variations at baseline. Thus by using in-vivo micro-CT, smaller changes could be detected at an earlier stage by scanning fewer animals than when we would have used in-vitro micro-CT. Although this gives in-vivo micro-CT a strong advantage, it does not mean that such results could not have been obtained by traditional in-vitro micro-CT.

What makes in-vivo micro-CT unique is the combination with image registration techniques. This way we were able to determine locally where new bone was formed and where old bone was resorbed. In chapter 6 we showed that this local information on changes in bone structure could be related to local bone morphometry and to the local mechanical environment. Such studies could greatly enhance our knowledge on how structural adaptation of trabecular bone is regulated. Further we could assess small changes in longitudinal growth rate. Both possibilities do not exist in in-vitro micro-CT studies.

7.3 Radiation and in-vivo scanning

One of the biggest concerns when using x-ray based imaging modalities on living organisms are the destructive effects of the ionizing radiation on living cells. In the discussion of chapter three we have expressed this concern and given a very brief review of the limited literature on the effects of low intensity x-ray radiation on bone. In chapter four we reported small and probably clinically insignificant differences in bone structure between animals that had been imaged for a year and animals that were not imaged. These differences, if real, may or may not be attributed to the radiation. Ongoing studies in our lab show that subjecting young three-month old growing female Wistar rats to 6 scanning sessions in 4 weeks (day 0, 3, 7, 14, 21 and 28) resulted in considerable bone loss in the scanned leg when compared to the contra-lateral leg. Another report on a study where aged female rats were scanned in-vivo weekly for 8 weeks showed no detectable changes in bone architecture (21). Two more abstracts about similar studies in mice however did see mild to considerable bone loss due to x-ray radiation (97, 102). Further, another study reported up to 40% loss of trabecular bone volume after 110 days due to a single 2 Gy dose of gamma irradiation in mice (70).

The exact local dose is not known. Reported values refer to the surface dose. The local dose, for instance in marrow or at the bone surface, might actually be lower. Studies that apply Monte-Carlo simulations using mathematical phantoms or micro-CT scans as input can shed more light on the exact local dose (127).

The effects of radiation on bone architecture in experimental animals are likely strongly dependent on species, age, strain, bone site and treatment, probably due to differences in bone remodelling rate. At this moment it is not known what the exact effects are of radiation on bone metabolism, and no rule of thumbs are available to assess which radiation dose and which scanning regimens can be considered save in the light of the studied experiment. Thus, it is vital to include animals that won't be radiated as controls and to compare bone structure of the scanned leg to the contra-lateral leg at the end of the scanning sessions.

Segmentation

In chapter 2 we have introduced and promoted a new segmentation algorithm that we have used throughout the studies in the rest of this body of work. We showed that using local thresholds clearly has advantages above using a global threshold, and that it certainly is superior when scanning whole bones or when analyzing in-vivo micro-CT scans with lower resolutions. But is it possible to give a final word about whether to use a global or local threshold in ideal scanning situations, when rather homogenous biopsies of trabecular bone are scanned at high resolution? At the moment there isn't. The answer should come from studies where the influence of the choice of threshold method on group differences is investigated.

Data from an ongoing study in our group show that when analyzing homogeneous samples, the sensitivity of most morphological parameters for small variations in global threshold values is rather small. Parameter values do vary with changing threshold value, but they vary in the same way for each sample. Thus, a sample that has a higher value for a certain parameter than another sample will keep a higher value even if the chosen global threshold value is not 'exact' or 'optimal'. In other words, the possibility to detect group differences is not very sensitive to small variations in global threshold value when all samples are segmented with the same global threshold value.

The next question is whether all samples should or can be segmented using the same threshold value. Theoretically, the optimal threshold value can be influenced by the mineralization of the bone tissue. Although rather homogenous between individuals within healthy populations, the tissue mineralization can be considerably affected by bone pathologies (162). Further, artefacts caused by beam-hardening which in its turn can be influenced by bone architecture and the shape of the scanned sample, are another source for changes in grey-values. Thus, different samples could have different optimal threshold values. Indeed, when the real bone volume is determined by for instance Archimedes' method and the threshold is selected based on the true volume, different samples have different threshold values. Of course, assessing the true volume with such methods is not error-free and the question is which error is smaller: the error when determining the true volume of a sample or the error made when one single global threshold is chosen. As mentioned above, more study is needed to resolve this issue.

Morphometric measures

Micro-CT scans are generally analyzed through quantifiable morphometric measures. In this work we have limited ourselves to the use of volume fraction (BV/TV), trabecular thickness (Tb.Th), structure model index

(SMI) and connectivity of the trabecular network. Other parameters that are commonly described in literature are the degree of anisotropy -determined through mean intercept length (MIL) or star volume distribution (147)-, trabecular number (Tb.N), trabecular separation (Tb.Sp) and trabecular pattern factor (69). What do all these parameters tell us? Many of these parameters are actually related, partly theoretically because they describe similar properties of topology (e.g. SMI and pattern factor) and partly because the remodelling process changes bone architecture such that certain parameters are linked. Principle Components Analysis of many morphological parameters has shown that most of the variance in trabecular architecture can be explained using three independent components: bone density, connectivity and anisotropy (42). Bone density explains most of the variance as expected and includes parameters like volume fraction, trabecular thickness and structure model index. The second component explains variances due to variation in connectivity (including connectivity density and trabecular spacing) independent of bone volume and the third component is the degree of anisotropy measured using MIL. It has to be stressed that these findings stem from cross-sectional analysis and need not be valid in longitudinal studies, or when certain pathologies are involved. In chapter 4 for example, although a cross-sectional positive relation existed between trabecular thickness and bone volume fraction, over time, a decrease in bone volume fraction was associated with an increase in trabecular thickness.

Another issue that should be considered when interpreting bone architectural parameters is that most of these parameters were developed for analysis of bone biopsies that were mostly taken from the iliac crest, which are pieces of relative homogenous trabecular bone. In long bones of small animals like rats and especially mice most of the trabecular bone is far from homogenous and substantial areas without trabecular bone are present. Some parameters loose or have a different meaning within this context. MIL is ideally calculated on a spherical volume of rather homogenous trabecular bone, which is generally impossible in long bones of mice and rats. Volume fraction is strongly influenced by medullar areas without any bone and thus does not give the true relative density as it does in a piece of homogenous trabecular bone. The meaning of trabecular thickness is unaltered, but the error caused by artificial cutting at the edge of a volume of interest (called the edge effect) increases when the amount of trabecular bone is low. On the other hand, trabecular separation which is calculated as the 3D thickness of the marrow cavities loses most of its meaning. The value of this parameter will be dominated by large areas without trabecular bone and will thus mainly reflect the size of the medullar area and won't be a measure of the 'separation' or distance between trabeculae. The structure model index generally gives normal values, though values might range beyond the

traditional plate-like ($SMI=0$) and rod-like ($SMI=3$) values. More generalized, the structure model index gives an indication of the convex or concaveness of a structure. Dense structures like the epiphysis can therefore result in negative values, and areas with very low amounts of trabecular struts, artificially cut from the cortex by the used region of interest might give values well above 3.

This does not mean that these parameters cannot be used but one needs to be aware of the altered meaning of these parameters when interpreting results.

Image registration

One of the most interesting aspects of our micro-CT studies involved the fact that we could position scans from different time points on top of each other. This generated the possibility to do detailed observations on how bone structure changed over time or due to treatment. Not only by changes in morphometric parameters, but also by visual inspection of the trabeculae itself. We used registration algorithms, which work sufficiently well when changes in the bone are small. Unfortunately due to some treatments or due to the fact that some time between scans is necessary to avoid radiation problems, changes in the bone can be considerable. Especially when the animal is still rapidly growing, the changes in a bone between two consecutive scans can be such that all trabecular bone in the initial scan has been resorbed or reshaped into cortical bone, while all present trabeculae were newly formed at the growth-plate. Also, cortical expansion could have resulted in complete resorption of the old cortical bone. In such cases registration will, besides being irrelevant, be impossible. We overcame problems of changing bone by performing registration on several details that could be recognized in all the consecutive scans, like certain trabeculae or arterial openings (chapter 3). Comparing the changes suggested by the registration with changes as could be visualized using histology we showed that this is a workable procedure that gives accurate results. However, we assumed that trabeculae and arterial openings we selected to perform the registration did not change position relative to each other. This assumption is not completely accurate. In chapter 4 we have shown that trabeculae can shift their position to align with other trabeculae. Further we have seen evidence of closing and slightly shifting arterial openings. Thus, to obtain accurate result it is crucial to include many details such that small errors due to shifting of some of these details will average out.

Remodelling simulation

In chapter six we have compared the outcome of computer simulations of the remodelling process occurring after ovx with the changes occurring in bone in-vivo. A potential interest in studies that combine in-vivo scanning

with remodelling simulations would be the possibility to validate simulations of the remodelling process, whereas traditional remodelling simulation studies can at their best only claim ‘real’ looking results. Though the results we obtained are interesting, we did not ‘perfectly’ simulate the real situation. Thus, it is fair to question whether this study benefited from the in-vivo scans. In general, modelling a certain biological process means leaving things out. Partly because it is not possible to include all factors that influence a living organism, but mainly because the idea is to find generalized ‘rules’ that can explain the behaviour of certain averaged aspects of an organism. Thus it is unlikely that a model would correspond exactly with the behaviour of an individual organism. Still, using longitudinal data to validate a model can enhance the potential of simulation studies. The potential becomes apparent when a generalized model can predict part of the biological variation between organisms, which can only be shown using longitudinal data to validate the model. In the case of this study, it could for instance be tested if a model can explain why a certain animal would loose more bone over time than another animal.

7.4 Thoughts on the role of imaging in bone research

Bone research comprises different areas of research in which research on bone cells and molecular biology are the most extensive. They mostly aim at unravelling molecular mechanisms that play a role in the regulation of bone metabolism. Studies like the one described in this thesis form another area of research that involves imaging of bone and which appears to be on the other side of the spectrum since it does not yield ‘functional’ information. Although research on cellular level has yielded many pieces of information, they do not state how cellular activity affects bone architecture. The very complicated puzzle that is formed by this information is practically unsolvable. Such a complex puzzle can only be solved when the whole picture is known, from molecular interactions to macro scale regulation of bone structure. Imaging studies like ours form thus an indispensable part of bone research (94).

However, even though the study described in this thesis gives a highly detailed description of bone changes as they occur after estrogen withdrawal, it appears almost impossible to see how combined molecular events described in literature could result in these highly spatial inhomogeneous changes. Similar questions arise from several studies on knock-out mouse models (48, 77). These studies used micro-CT to phenotype bone changes related to the genetic alterations, but it is almost impossible to explain these changes from the effect these knocked out genes have on cellular activity. What is needed to combine the findings in both areas is knowledge about how bone architecture is regulated, so the control mechanisms at work in bone at a macroscopic scale.

Consider the analogy of an antique standing clock, in which the radar work inside the clock represents the biochemical processes in bone, while the turning of the hands on the dial and the swinging of the pendulum represent the outcome of observational imaging studies. The working of the clock can only be understood when the general control mechanism is known, which would be the understanding that the swinging movement of the pendulum is transmitted to the turning movements of the hands, and that the pendulum is kept swinging by the weights. Only in the light of this understanding can the puzzle of all the small radars and their interactions be understood. Or as Niels Bohr put it, knowing the physical properties of the elements of water is not enough to predict its 'waterish' properties.

Current theories about the regulation of bone metabolism are based on three biological functions that bone is thought to have: it serves as a reservoir of calcium, it protects the more vulnerable organs and it serves as a mechanical structure to allow movement. The regulation mechanism controlling serum calcium levels has been well established and involves regulation of bone remodelling by parathyroid hormone and vitamin D. The mechanical function involves a much more complex regulation mechanism since bone is capable of repairing its damage and of adjusting itself to an altered mechanical environment. But although it has been shown that bone cells respond to mechanical stimuli, principle theories do not state much more than that higher loaded bone is preserved above lesser loaded bone. To get a better understanding on how these regulation-mechanisms work, careful observations are needed on how bone, as a macroscopic structure, behaves within its mechanical environment. This brings us back to the imaging of bone, and especially to the topic of this thesis: in-vivo micro-CT.

However, we should bear in mind that each regulation mechanism that we see underneath the macroscopic changes we have observed in bone are – probably crude- models of the real processes going on in bones. Bone as an organ has not been Intelligently Designed to follow a certain ideal regulation mechanism. All macroscopic behaviour that we observe is the result of many complex interactions between bone cells and biochemical substances, all the result of millions of years of random mutations and selection. Thus bone will never behave completely according to one of our theories. But such is everything else in science and life...

7.5 Thoughts on the interaction between estrogen levels and mechanical driven bone adaptation.

As mentioned several times throughout this paper, the general vision on the relation between estrogen and mechanical driven bone adaptation is that estrogen sensitizes the bone for mechanical stimulation (59, 161, 184). Thus, when estrogen levels drop, bones become less sensitive to its mechanical environment and reacts as if it is in a state of disuse, until a new balance has

been reached. Although not much hard evidence exists in support, this vision is a very persistent one. More elaborate theories exist that try to deal with some inconsistencies, but most are still built on this basic vision (60, 115, 168). A few animal studies support these theories (33) and experiments in humans never found much effect of exercise as treatment for post-menopausal bone loss. However, most reports on animal experiments actually concluded that the bone preserving effects of estrogen and exercise/mechanical loading occur independently (81, 207), while one study even concluded that the positive effect of mechanical stimulation is enhanced in the absence of estrogen (92). Especially the studies investigating the effect in humans suffer from some methodological difficulties related among others to the measurement of bone mass in humans, which is mainly done using DXA. In a perspective paper Järvinen et al. (93) claim that re-analysis of three studies that investigated the effect of hormone replacement therapy after menopause and mechanical exercise actually showed that loss of estrogen makes the skeleton more responsive to mechanical exercise, contrary to the original conclusions in these papers (72, 105, 106). This would correspond with the fact that high-impact sports have stronger bone anabolic effects in girls just before than after menarche (11, 73).

The work described in this thesis confirmed that the effects of loss of estrogen are indeed dramatic. The structure changing process in bone as associated with both ovariectomy and aging is very dynamic and certainly not limited to bone loss, how ever dramatic this loss of bone might be. Bone was not removed randomly, but such that aligned trabecular structures arose across the growth-plate, which strongly suggests an active adaptation process that is regulated by mechanical stimulation. In chapter 6 we could show that these types of structural adaptation indeed are associated with mechanical stimulation. The fact that certain trabeculae were transformed into thick rods at a certain moment in time, but removed at later moments further suggests that the bone adaptation process continues and is not working towards a 'fixed' or stable end stage. Interesting is the fact that removal of estrogen speeded up the adaptation process. From this formulation of the effect of estrogen it would be tempting to say, like Järvinen, that loss of estrogen makes a bone more sensitive to mechanical loading. However, I think it's more accurate to say that the adaptation of bone to its mechanical environment becomes faster. I'd like to quote the title of a well known paper by Westerlind et al. (207) "Estrogen regulates the rate of bone turnover but bone balance is modulated by prevailing mechanical strain." It has been noted previously that the effect of mechanical stimulation seems to interact with bone formation on bone surfaces that are in a state of active remodelling or modelling (11, 171). In an estrogen-deprived state, bone remodelling certainly is more active and

thus the bone adaptation process works faster. It is therefore not unlikely that estrogen levels do not influence the mechanical sensation of bone. Whether bones appear to be more or less sensitive to mechanical signalling might be more dependent on where to look, how to look and how to compare than to the true effect of estrogen itself. This would explain why so many studies report different conclusions.

Above we considered the effects of estrogen on bone adaptation, which does not necessarily include the massive cancellous metaphyseal bone loss that accompanies lowered estrogen levels. In chapter 6 we did not find any association between bone loss and mechanical signalling. In contrary, we saw that regions that experienced the strongest bone loss actually were the regions where strains were highest. The trabeculae in the relatively stiff epiphysis hardly experienced any strains at all and could be considered to be in disuse mode, although hardly any bone was lost. Moreover, in chapter 6 we showed that bone loss is related to local bone density and that no mechanical information is needed to explain estrogen related bone loss. In this light it is interesting to reflect on the influence of estrogen on longitudinal bone growth. When estrogen levels rise at the onset of menarche in girls, the growth-spurt sets in. The estrogenic effect might be indirect by stimulation of the Growth Hormone/ IGF-I axes by increasing estrogen levels (159). When estrogen levels rise further, longitudinal growth slows down and the growth-plate closes. In boys, estrogen, locally obtained from testosterone through aromatase activity, is also responsible for closing of the growth-plate. In animals like the rat in which the growth-plate never closes, removal of estrogen stimulates longitudinal growth (186)

During normal longitudinal growth, new bone is formed at the metaphyseal side of the growth-plate. The dense network of thin trabeculae that is formed is rapidly remodelled into a more coarse trabecular structure with increased thickness. Further distally, the 'old' trabecular structure is removed. At the same time the cortex is being modelled such that the total shape of the bone remains intact, although wider and longer.

After ovariectomy, all these aspects related to growth occur. It is especially the more distal trabecular bone that is resorbed, while the remodelling of the trabecular structure close to the growth-plate into a less dense and courser structure is accelerated, what could increase trabecular thickness and locally decrease bone density. Further, all the modelling activities at the cortex are present as well, including periosteal expansion (2). It must be said that in young and active growing rats removal of estrogen also results in dramatic bone loss, more than would occur by accelerated 'normal' longitudinal growth. This could indicate that certain levels of estrogen are needed to maintain a balance between the various aspects accompanying longitudinal growth.

Since in post-menopausal women the growth-plate has long been closed, no longitudinal growth occurs when estrogen levels drop. However, the way trabecular bone is removed does resemble remodelling as it occurs during growth. Seen in this light, osteoporosis might not be a failure in bone's ability to maintain its strength, but a renewed activation of the growth-process, resulting in weak bones since no growth-plate exist anymore where new bone can be formed.

This viewpoint could also explain why in humans different bone sites respond differently to the post-menopausal situation. In vertebrae, where longitudinal growth is not accompanied by 'distal' loss of trabecular bone as occurs in long-bones, the high remodelling that accompanies reduced levels of estrogen results in adaptation and coarsening of the trabecular structure, which has been described as 'over-adaptation' of the trabecular structure (80). In long-bones, where longitudinal growth is accompanied by removal of distal trabecular bone, large parts of trabecular bone disappear after menopause.

In general, it would be hard to imagine that all molecular, cellular and physical mechanism that an organism applies during development and growth would cease to exist upon reaching the ultimate 'finished' and adult state. The way adult bone adapts to the mechanical environment resembles strongly the way bone develops in embryonic stages, which suggests that the same mechanism is at work (30). It is more likely that these processes are inhibited or perhaps even just slowed down. This means that all these mechanisms can reactivate when the inhibitor is taken away. Estrogen could very well serve the role of all-round inhibitor, since it is one of the most ancient hormones that arose very early in the history of evolution (181).

That bone modelling during growth is a very intricate process that needs accurate regulation can be seen in the above data (chapter 4). Thus the question remains how this is regulated and the potential answers remain speculative. Perhaps the cortical modelling that occurs during longitudinal growth is related to mechanical signalling, though not through loading of the bone as it occurs during daily activity. It could be the local forces where muscles are attached or the tension that occurs due to connective tissues that are stretched during growth that deliver the driving signals (74). The data in chapter 6 suggest that metaphyseal bone loss is not related to mechanical signalling but to other factors, perhaps the proximity of diaphyseal marrow or, related to this, the absence of surrounding signalling osteocytes.

7.6 Thoughts about possible experiments.

The theories set out in the above paragraphs are still speculative and call out for dedicated experimental studies. The above ideas can be separated in a few distinct questions that can be addressed by cleverly designed

experiments. The principle question is how does estrogen interact with mechanically regulated bone adaptation? In detail the following questions can then be considered:

- Does estrogen influence the sensitivity for mechanical stimulation?
- Does estrogen influence the speed of the mechanical adaptation?
- Does adaptation lead to a stable ‘steady state’?

A difficulty in researching these questions is that estrogen might influence other, non- mechanically regulated bone processes that lead to bone loss, as is suggested by the data in chapter 6. Thus the outcome measures that will be evaluated should be carefully considered. In general mere bone volume will not suffice, which is unfortunately a measure that has been used in many previous studies.

Most studies that investigated the mechanical responsiveness of bone have used animal models in which mechanical loading has been applied through treadmill running, jumping or cage climbing (81, 92, 143, 184). Although these methods are relatively animal friendly, the mechanical loading regimens cannot be controlled well. Other animal experiments involved bending of the ulna or tibia in small mechanical testing devices (3, 82). Though these experiments are a heavier load for the animal, mechanical loading can be controlled in detail. The loading will however principally be directed to the diaphyseal cortex and loading of the trabecular structure is very indirect. The most accurate and controllable, but invasive, model described is one in which a tail vertebra of a rat or mouse is loaded through the adjacent vertebrae (89). Metal pins are inserted in the adjacent vertebrae and loading is applied through these pins.

The methods used throughout this thesis are ideally suited to investigate bone structural changes resulting from different loading regimens in combination with various estrogen levels (e.g. sham, ovx, sham+E2, ovx+E2). The confounding of different treatment effects when using bone volume fraction as outcome can be diminished when local changes in bone architecture are measured in-vivo. Further, the in-vivo scanning methodology should be combined with FE analysis that simulates the in-vivo loading regimens. Relating local bone changes with local strain levels can thus yield outcome measures that are ideally suited to investigate the above posed questions and might eventually answer which theory fits reality best: the mechanostat or the ideas described in this thesis.

7.7 Concluding remarks

This thesis is a representation of the introduction of the in-vivo micro-CT scanner in bone research, from the development of post-processing methodology to the first scientific results. To optimally segment the scan images of relatively low quality we developed an automated segmentation

algorithm using local threshold values. In the typical situation of images obtained in-vivo, the newly developed algorithm outperformed tradition segmentation methods that use global thresholds. By combining in-vivo micro-CT scanning with image registration techniques we were able to overlay follow-up scans and thus could identify both new and resorbed bone. We were also able to follow ongoing changes in bone architecture at trabecular level. Using these methods we showed that bone loss dynamics that occur due to aging and ovariectomy result in an aligned trabecular structure in which the remaining trabeculae increase in thickness. These changes could be reduced by tibolone treatment. Interestingly, though the gross actions of tibolone could be described as prevention of ovariectomy induced bone loss, at more detail tibolone affected bone metabolism such that longitudinal growth was halted completely and the remaining trabeculae did not increase in thickness. Further, we showed a relation between the changes observed after ovariectomy and due to aging and mechanical signalling. The bone adaptation process responsible for the aligning trabeculae associated with local deviations in strain, while the gross bone loss did not relate to any mechanical signal, but to local bone density.

In-vivo micro-CT turned out to be an invaluable tool for revealing the subtle bone changes that might prove crucial in the understanding of bone remodelling and bone adaptations.

Summary

Although bone mass or density is still the main clinical measure for fracture risk, the interest is shifting towards measuring bone ‘quality’. Bone quality is a broad and loosely defined term that includes, besides bone mass, bone (trabecular) architecture and tissue properties. Bone histomorphometry is a widely used histological method to quantify bone architecture. The obvious and inherent drawbacks are the fact that 2D measures are used to describe 3D topological features and the invasive and destructive nature of this labor-intensive technique. More recent was the introduction of micro-CT that enabled high-resolution 3D analysis without destroying samples. However, the invasive nature of the method is still present.

This thesis describes the introduction of in-vivo micro-CT to quantify bone architecture in living animals, which allows longitudinal imaging of the changes in bone architecture. Since bone adaptation has a very dynamic nature that is still poorly understood the introduced technology gives rise to high expectations regarding the unraveling of the regulation of bone architecture and the resulting bone quality.

The work in this thesis consists of two parts. The first part has a methodological nature and describes some aspects of post-processing the scan data in order to optimally extract information from the scans. In the second part the first scientific harvest is presented and it gives a detailed analysis of the bone loss process as it occurs in aging and ovariectomised (ovx) rats. The latter is a model of post-menopausal osteoporosis.

The segmentation of the reconstructed micro-CT datasets into binary sets that only contain bone and non-bone is a crucial –and often underestimated– part of the analysis of micro-CT data. Errors made during this step will progress towards the final quantification of architectural parameters. This step becomes especially challenging when analyzing in-vivo micro-CT data because the need to keep radiation doses low during scanning limits the quality of the resulting scans. The standard segmentation techniques using global threshold values perform only moderately under these circumstances. To improve the segmentation, in chapter 2 we have introduced an automated method that segments micro-CT datasets using local thresholds. Gradients in the reconstructed data were calculated in 3D of which the peaks represent the edges of the bone tissue. A large part of the chapter is dedicated to the validation of the new algorithm and to compare it to the standard, easy to use, segmentation methods in which one global threshold is used to separate bone from non-bone. We found that for

high quality, high-resolution scans of homogenous data sets both methods functioned equally well. Both give near perfect representations of the real bone structure when compared to histology. However, this assumes knowing the optimal global threshold which is not always trivial. When non-homogenous datasets are considered, for example those of whole bones at lower resolutions, as is the case in in-vivo scanning, the segmentation quality of the global method became seriously limited and the local method was easily superior.

Next, we explored the possibility to translate and rotate follow-up scans such that they matched with a previous scan in order to be able to detect detailed changes at the level of single trabeculae (chapter 3). The subject of the interest in this possibility is at the same time a cause for methodological difficulties: the gross shape and detailed architecture of bones change. We performed the matching using image registration techniques that optimize the match using mutual information. We prevented inaccuracies due to longitudinal growth by splitting the bone scans at the epiphyseal growth-plate and register the epiphysis and metaphysis separately. Registration of the metaphysis posed additional difficulties, especially in the ovx animals where the bone structure changed considerable between two time-points. Registration could be improved by using details like arterial openings and certain trabeculae that could be identified in all scans to perform the registration. New bone formation as suggested by the registration method resembled to a great extent the new bone formation as indicated by histology. Using this method we could follow changes at the level of single trabeculae, determine the amount of longitudinal growth by new bone formation at the growth-plate and identify bone that was resorbed and bone that was newly formed.

In the second part of this thesis we applied the above described methods to study bone loss and architectural changes that occur during aging and as a consequence of estrogen loss. In chapter 4 we describe the bone loss process in the tibia of ovariectomised and normally aging rats. The rats were 10 months old at the start of the experiment and were scanned 5 times during the following 54 weeks. Bone loss patterns in both groups were very alike. Bone loss occurred primarily in the more distal or central regions in the metaphysis. Especially interesting was the increase in thickness of the remaining trabeculae, and the aligning of these trabeculae with epiphyseal trabeculae on the opposite side of the growth-plate. The main difference between the two groups was the speed with which these changes occurred: very rapidly in the ovariectomised animals and much slower in the normally aging animals. Further, we noted that estrogen depletion influenced longitudinal growth. An initial acceleration in growth in the ovariectomised animals was followed by a complete halt of growth, while new bone kept

being formed at the growth-plate of the normally aging animals. Modeling at the cortex occurred which kept the total bone shape intact during growing.

We concluded that estrogen depletion is not merely a state characterized by strong loss of bone, but that it is better described as a state of accelerated and dynamic (normal) bone adaptation that appears minutely regulated.

A third group of rats was ovariectomised and treated with the drug tibolone of which the results were described in the following chapter (chapter 5). Tibolone is an interesting drug that has proved its efficacy for treatment of post-menopausal bone loss. It has been shown to possess the bone preserving effects of conventional hormone replacement therapies (HRT) using estrogen, without some of the negative side effects that are associated with estrogen use. In this study we examined the effects of the drug on trabecular architecture. Bone loss was indeed slowed down. While bone loss and changes in related architectural parameters was prevented partially at the dose used in this study, changes in trabecular thickness, cortical alterations and longitudinal growth were suppressed completely, even to below sham levels. It appears that the effectiveness of the drug varies with relation to different aspects of estrogen related bone metabolism. It will be difficult to understand how the influence of tibolone on cellular level can result in the observed architectural changes without knowing the way in which bone adaptation is regulated.

In chapter 6 of this thesis we explored just this regulation mechanism. In-vivo micro-CT gives the unique possibility to exactly overlay two successive scans. Comparing scans this way made it possible to identify bone voxels that were resorbed in the next scan, and bone voxels that were newly formed. Thus we have classified voxels in scans of an ovx and a normally aging rat. Next we examined which strain or morphology related criteria were related with this classification. We calculated the strain distributions in the proximal tibia in both animals by high-resolution finite element (FE) models. We did not find any indication that especially the lower loaded trabeculae were resorbed in the ovx rat as is the general opinion. On the contrary, the regions that experienced most bone loss also experienced the highest strains. This bone loss turned out to be unrelated to any of the mechanically related criteria. Although not related to bone loss, relative strain (relative to a local neighborhood) did show a relation with bone remodeling in both animals. On average, the resorbed voxels had a lower relative strain than the voxels that were associated with formation. We performed a remodeling simulation using relative strain as the driving criterion, which showed that this criterion related to the previously observed aligning and thickening trabeculae. Bone loss on the other hand, turned out to be strongly related to the amount of local bone mass. Thus, bone that has much surrounding bone tissue was preserved, while bone that was poorly surrounded by bone tissue was resorbed. We concluded that structural

alterations in bone are regulated by two distinct mechanisms. Bone adaptation to the principle loads is directed by the local relative strain, which leads to aligning trabeculae and removal of horizontal non-load carrying trabeculae. Bone loss as occurs after estrogen loss and probably aging, however, is not related to mechanical strain, but is purely related to the amount of surrounding bone (or the reverse: the amount of surrounding marrow) and could indicate that the amount of neighboring osteocytes is, or factors from the marrow are determinate for resorption.

Samenvatting

Hoewel botmassa of botdichtheid nog steeds de belangrijkste klinische maat is voor het bepalen van fractuurrisico, begint de interesse te verschuiven richting 'botkwaliteit'. Botkwaliteit is een breed en losjes gedefinieerd begrip, dat naast botmassa de trabeculaire architectuur en weefseigenschappen van het bot omvat. Bothistomorphometrie is een algemeen gebruikte, histologische techniek om botarchitectuur te kwantificeren. Duidelijke en aan de methode inherente nadelen zijn dat 2D metingen worden gebruikt om 3D topologische eigenschappen te beschrijven en dat deze arbeidsintensieve methode invasief en destructief van aard is. Een tiental jaren geleden werd de micro-CT geïntroduceerd, waardoor het mogelijk werd om met hoge resolutie 3D analyses uit te voeren zonder de preparaten te vernietigen. Echter, ook deze methode is invasief.

Dit proefschrift beschrijft de introductie van in-vivo micro-CT waarmee de botarchitectuur van kleine levende proefdieren gekwantificeerd kan worden, waardoor het mogelijk wordt veranderingen in architectuur in de tijd te volgen. Aangezien botadaptatie, dat dynamisch van aard is, nog steeds slecht begrepen wordt, schept de geïntroduceerde technologie hoge verwachtingen wat betreft het ontrafelen van de mechanismen die de botarchitectuur (en daarmee de resulterende botkwaliteit) reguleren.

Dit proefschrift bestaat uit twee gedeelten. Het eerste gedeelte is methodisch van aard en beschrijft enkele aspecten van de nabewerking van de scandata, die ontwikkeld werden om zo optimaal mogelijk informatie uit de scans te extraheren. In het tweede gedeelte wordt de eerste wetenschappelijke oogst gepresenteerd. Het geeft een gedetailleerde analyse van het proces, dat leidt tot botverlies zoals dat optreedt tijdens veroudering en na ovariectomie in ratten. Dit laatste wordt gebruikt als een model voor postmenopausale osteoporose.

De segmentatie van een gereconstrueerde micro-CT dataset tot een binaire set, die alleen bestaat uit bot en niet-bot, is een cruciaal –en vaak ondergewaardeerd– aspect van de analyse van micro-CT data. Fouten die tijdens deze stap gemaakt worden zullen doorwerken in de uiteindelijke kwantificatie van de architecturele parameters. Juist deze stap wordt een extra grote uitdaging bij het analyseren van in-vivo micro-CT data, omdat de noodzaak de stralingsdosis laag te houden tijdens het scannen de kwaliteit van de resulterende scan beperkt. De standaard segmentatiemethoden die globale drempelwaarden gebruiken presteren slechts matig onder deze omstandigheden. In hoofdstuk 2 hebben we een geautomatiseerde methode beschreven om micro-CT data te segmenteren met behulp van lokale

drempelwaarden. In de gereconstrueerde datasets werden spatiële gradienten in 3D berekend. De pieken in de spatiële gradienten komen overeen met de randen van het bot in de scan. Een groot gedeelte van dit hoofdstuk is gewijd aan de validatie van dit nieuwe algoritme. Het werd vergeleken met standaard en makkelijk te gebruiken segmentatiemethoden, waarbij één globale drempelwaarde wordt gebruikt om bot van niet-bot te scheiden. Wanneer scans met hoge kwaliteit en een hoge resolutie gemaakt werden van homogene botsamples, presteerden beide segmentatiemethodes even goed. Beide gaven een bijna perfecte representatie van de werkelijke botstructuur zoals dat bleek uit vergelijking met histologische coupes. Echter, dit gold alleen als de optimale globale drempelwaarde bekend was en het vinden van die optimale waarde is niet altijd triviaal. Wanneer sprake is van niet-homogene datasets, bijvoorbeeld scans van hele botten met een lage resolutie, zoals het geval is bij in-vivo scans, was de kwaliteit van de segmentatie van de globale methoden zeer beperkt en was de nieuw ontwikkelde lokale methode superieur.

Vervolgens hebben wij de mogelijkheid onderzocht om follow-up datasets zodanig te transleren en roteren dat ze passend over een voorafgaande scan gelegd konden worden, zodat veranderingen op trabeculair niveau in detail te detecteren zijn (hoofdstuk 3). Dat wat deze mogelijkheid interessant maakt is tegelijkertijd een reden voor methodologische uitdagingen: De totale vorm en de gedetailleerde structuur van het bot zijn onderhevig aan verandering. We hebben het passend over elkaar leggen van de beelden uitgevoerd met behulp van beeldregistratietechnieken die de Mutuele Informatie maximaliseren. We konden onnauwkeurigheden veroorzaakt door lengtegroei voorkomen door de scans van het bot op te splitsen in epifyse en metaphyse en deze apart te registreren. Registratie van de metaphyse werd verder bemoeilijkt, speciaal in de geovariectomeerde dieren, doordat de botstructuur tussen twee tijdstippen aanzienlijk veranderde. We konden de registratie verbeteren door gebruik te maken van details in de scans, zoals arteriële openingen in het bot en bepaalde botbalkjes die in alle scans geïdentificeerd konden worden. Plekken waar volgens de registratiemethode nieuw bot gevormd werd kwamen uitstekend overeen met de resultaten van histologie. Door middel van deze methodologie konden we kleine veranderingen op trabeculair niveau volgen in de tijd, de hoeveelheid nieuw door lengtegroei gevormd bot onder de groeischijf nauwkeurig bepalen en zowel nieuw gevormd als geresorbeerd bot identificeren.

In het tweede gedeelte van dit proefschrift hebben we de hierboven beschreven methoden toegepast om botverlies en architecturele veranderingen te bestuderen die optreden tijdens veroudering en bij oestrogeen verlies na ovariectomy. In hoofdstuk 4 hebben we het botverliesproces in de tibia van geovariectomeerde en normaal

verouderende (schijngeopereerde) ratten beschreven. De ratten waren 10 maanden oud aan het begin van het experiment en werden gedurende de daarop volgende 54 weken vijf maal gescand. De botverliespatronen in beide groepen leken sterk op elkaar. Botverlies vond voornamelijk plaats in de meer distale en centrale regio's in de metaphyse. Bijzonder interessant was het dikker worden van de overgebleven botbalkjes en het uitlijnen van deze botbalkjes met epiphysaire botbalkjes aan de tegenoverliggende zijde van de groeischijf. Het voornaamste verschil tussen de twee groepen was de snelheid waarmee deze veranderingen zich voordeden: snel in de geovariectomeerde dieren en langzaam in de normaal verouderende dieren. We zagen verder dat oestrogeendepletie de lengtegroei beïnvloedde. In de geovariectomeerde dieren werd een initiële versnelling in de groei gevolgd door een complete groeistop, terwijl in de normaal verouderende dieren de lengtegroei nagenoeg constant verliep. De totale vorm van het bot bleef intact tijdens de groei door modellering van de cortex. We concludeerden dat oestrogeendepletie niet slechts een toestand is die gekarakteriseerd wordt door sterk botverlies, maar dat een omschrijving als een toestand van versnelde en dynamische (normale) botadaptatie die minutieus geregeld wordt, beter op zijn plaats lijkt.

Een derde groep ratten werd geovariectomeerd en behandeld met het medicijn tibolone, waarvan de resultaten beschreven staan in hoofdstuk 5. Tibolone is een interessante stof waarvan de effectiviteit voor de preventie van post-menopausaal botverlies bewezen is. Het bezit de botbeschermende werking van conventionele Hormoon Vervangings Therapie (HVT) waarin een oestrogeen gebruikt wordt, zonder enkele van de negatieve bijwerkingen die met oestrogeen gebruik geassocieerd zijn. In deze studie hebben we de effecten van tibolone op de trabeculaire structuur onderzocht. Botverlies werd inderdaad geremd. Hoewel bij de gebruikte dosering botverlies en veranderingen in de daarmee samenhangende architecturale parameters slechts ten dele voorkomen werden, werden veranderingen in trabeculaire dikte, corticale veranderingen en de lengtegroei compleet tegengehouden, zelfs tot onder het niveau van de dieren die een schijnoperatie hadden ondergaan. De effectiviteit van het medicijn lijkt te variëren tussen verschillende aspecten van aan oestrogeen gerelateerd botmetabolisme. Het zal moeilijk zijn om te begrijpen hoe de werking van tibolone op cellulair niveau kan resulteren in de geobserveerde architecturale veranderingen, zonder de manier waarop botadaptatie gereguleerd is beter te kennen.

Precies dat regulatiemechanisme is het onderwerp van onderzoek in het zesde hoofdstuk. In-vivo micro-CT geeft de mogelijkheid om twee opeenvolgende scans exact over elkaar heen te leggen. Het op deze wijze vergelijken van scans maakte het mogelijk om bot voxels (3D pixels) te identificeren die tussen twee opeenvolgende scans geresorbeerd of gevormd werden. In scans van een geovariectomeerde en een normaal verouderende

rat hebben we alle voxels geclassificeerd met deze methode. Vervolgens hebben we onderzocht of er een verband was tussen resorptie of formatie van voxels en lokale mechanische vervorming of architecturale eigenschappen. Voor beide dieren hebben we de rekverdeling in de proximale tibia berekend door middel van Eindige Elementen modellen met hoge resolutie. We vonden geen aanwijzingen dat voornamelijk trabekels met een lage rek geresorbeerd werden, zoals de algemene opvatting is. In tegendeel, de regio's waar het meeste bot verdween waren ook de regio's waar de hoogste rekken voorkwamen. Netto botverlies bleek niet gerelateerd aan mechanische criteria. Relatieve rek (relatief ten opzichte van een lokaal gemiddelde), hoewel niet gerelateerd aan botverlies, liet in beide dieren wel een relatie met botremodellering zien. Gemiddeld hadden de geresorbeerde voxels een lagere relatieve rek dan de voxels die geassocieerd waren met formatie. Vervolgens hebben we het remodelleringsproces gesimuleerd met relatieve rek als sturend criterium. Het bleek dat dit criterium kan leiden tot de in de vorige hoofdstukken geobserveerde uitlijning en het dikker worden van de botbalkjes. Botverlies daarentegen, bleek sterk gerelateerd aan de lokale botdichtheid. Met andere woorden, bot met veel omringend botweefsel bleef behouden, terwijl bot met weinig omringend botweefsel geresorbeerd werd. We concludeerden dat veranderingen in botstructuur gereguleerd lijken door twee verschillende mechanismen. Adaptatie van bot naar de mechanische omgeving wordt lokaal gestuurd door relatieve rek, wat ertoe leidt dat botbalkjes uitlijnen en dat horizontale botbalkjes die geen kracht dragen geresorbeerd worden. Botverlies echter, zoals dat optreedt na oestrogeenverlies en waarschijnlijk ook tijdens het verouderen, is niet gerelateerd aan mechanische rek, maar puur aan de hoeveelheid omringend botweefsel (of de hoeveelheid omringend merg). Dit kan een aanwijzing zijn dat de lokale osteocytendichtheid, of factoren vanuit het merg, bepalend zijn voor resorptie.

References

- 1) Aaron, J. E., Makins, N. B., and Sagreiya, K. *"The microanatomy of trabecular bone loss in normal aging men and women"* Clin Orthop **1987; (215):260-71**
- 2) Ahlborg, H. G., Johnell, O., Turner, C. H., Rannevik, G., and Karlsson, M. K. *"Bone loss and bone size after menopause"* N Engl J Med **2003; 349 (4):327-34**
- 3) Akhter, M. P., Cullen, D. M., Pedersen, E. A., Kimmel, D. B., and Recker, R. R. *"Bone response to in vivo mechanical loading in two breeds of mice"* Calcif Tissue Int **1998; 63 (5):442-9**
- 4) ASTM *"Standard guide for Computed Tomography (CT) Imaging"*. ASTM Standards **E1440-97**. Philadelphia, PA: American Society for Testing and Materials; **1997**.
- 5) Aubin, J. E., and Bonnylye, E. *"Osteoprotegerin and its ligand: a new paradigm for regulation of osteoclastogenesis and bone resorption"* Osteoporos Int **2000; 11 (11):905-13**
- 6) Bagi, C. M., Mecham, M., Weiss, J., and Miller, S. C. *"Comparative morphometric changes in rat cortical bone following ovariectomy and/or immobilization"* Bone **1993; 14 (6):877-83**
- 7) Bagi, C. M., and Miller, S. C. *"Comparison of osteopenic changes in cancellous bone induced by ovariectomy and/or immobilization in adult rats"* Anat Rec **1994; 239 (3):243-54**
- 8) Baldock, P. A., Morris, H. A., Need, A. G., Moore, R. J., and Durbridge, T. C. *"Variation in the short-term changes in bone cell activity in three regions of the distal femur immediately following ovariectomy"* J Bone Miner Res **1998; 13 (9):1451-7**
- 9) Baldock, P. A., Need, A. G., Moore, R. J., Durbridge, T. C., and Morris, H. A. *"Discordance between bone turnover and bone loss: effects of aging and ovariectomy in the rat"* J Bone Miner Res **1999; 14 (8):1442-8**
- 10) Balemans, W., and Van Hul, W. *"Identification of the disease-causing gene in sclerosteosis--discovery of a novel bone anabolic target?"* J Musculoskelet Neuronal Interact **2004; 4 (2):139-42**
- 11) Bass, S. L., Saxon, L., Daly, R. M., Turner, C. H., Robling, A. G., Seeman, E., and Stuckey, S. *"The effect of mechanical loading on the size and shape of bone in pre-, peri-, and postpubertal girls: a study in tennis players"* J Bone Miner Res **2002; 17 (12):2274-80**
- 12) Batra, N. N., Li, Y. J., Yellowley, C. E., You, L., Malone, A. M., Kim, C. H., and Jacobs, C. R. *"Effects of short-term recovery periods on fluid-induced signaling in osteoblastic cells"* J Biomech **2005; 38 (9):1909-17**
- 13) Berning, B., Kuijk, C. V., Kuiper, J. W., Bennink, H. J., Kicovic, P. M., and Fauser, B. C. *"Effects of two doses of tibolone on trabecular and cortical bone loss in early postmenopausal women: a two-year randomized, placebo-controlled study"* Bone **1996; 19 (4):395-9**
- 14) Bertram, J. E., and Biewener, A. A. *"Bone curvature: sacrificing strength for load predictability?"* J Theor Biol **1988; 131 (1):75-92**
- 15) Bikle, D. D., Halloran, B. P., and Morey-Holton, E. *"Space flight and the skeleton: lessons for the earthbound"* Endocrinologist **1997; 7 (1):10-22**
- 16) Birkenhager-Frenkel, D. H., Courpron, P., Hupscher, E. A., Clermonts, E., Coutinho, M. F., Schmitz, P. I., and Meunier, P. J. *"Age-related changes in cancellous bone*

- structure. A two-dimensional study in the transiliac and iliac crest biopsy sites*" Bone Miner **1988; 4 (2):197-216**
- 17) Bisgard, J. D., and Hunt, H. B. *"Influence of roentgen rays and radium on epiphyseal growth of long bones"* Radiology **1936; 26 56-68**
- 18) Boyde, A., Compston, J. E., Reeve, J., Bell, K. L., Noble, B. S., Jones, S. J., and Loveridge, N. *"Effect of estrogen suppression on the mineralization density of iliac crest biopsies in young women as assessed by backscattered electron imaging"* Bone **1998; 22 (3):241-50**
- 19) Bravenboer, N., Engelbregt, M. J., Visser, N. A., Popp-Snijders, C., and Lips, P. *"The effect of exercise on systemic and bone concentrations of growth factors in rats"* J Orthop Res **2001; 19 (5):945-9**
- 20) Broderick, E., Infanger, S., Turner, T. M., and Sumner, D. R. *"Depressed bone mineralization following high dose TGF-beta1 application in an orthopedic implant model"* Calcif Tissue Int **2005; 76 (5):379-84**
- 21) Brouwers, J., van Rietbergen, B., and Huiskes, R. *"In-vivo micro-CT radiation does not affect bone structure in rats"*. 52nd Annual Meeting of the Orthopaedic Research Society. Chicago, IL, USA; **2006**.
- 22) Buhl, K. M., Jacobs, C. R., Turner, R. T., Evans, G. L., Farrell, P. A., and Donahue, H. J. *"Aged bone displays an increased responsiveness to low-intensity resistance exercise"* J Appl Physiol **2001; 90 (4):1359-64**
- 23) Burger, E. H., and Klein-Nulend, J. *"Mechanotransduction in bone--role of the lacuno-canalicular network"* FASEB J **1999; 13 Suppl S101-12**
- 24) Burger, E. H., Klein-Nulend, J., van der Plas, A., and Nijweide, P. J. *"Function of osteocytes in bone--their role in mechanotransduction"* J Nutr **1995; 125 (7 Suppl):2020S-2023S**
- 25) Burt-Pichat, B., Lafage-Proust, M. H., Duboeuf, F., Laroche, N., Itzstein, C., Vico, L., Delmas, P. D., and Chenu, C. *"Dramatic decrease of innervation density in bone after ovariectomy"* Endocrinology **2005; 146 (1):503-10**
- 26) Bushberg, J. T., Seibert, J. A., Leidholdt, E. M., and Boone, J. M. *"The essential physics of medical imaging"*. Baltimore: Williams & Wilkins; **1994**.
- 27) Cadet, E. R., Gafni, R. I., McCarthy, E. F., McCray, D. R., Bacher, J. D., Barnes, K. M., and Baron, J. *"Mechanisms responsible for longitudinal growth of the cortex: coalescence of trabecular bone into cortical bone"* J Bone Joint Surg Am **2003; 85-A (9):1739-48**
- 28) Canny, J. *"A computational approach to edge detection."* IEEE TRANS on Pattern Analysis and Machine Intelligence **1986; PAMI-8 (6):679-698**
- 29) Carter, D. R. *"Mechanical loading histories and cortical bone remodeling"* Calcif Tissue Int **1984; 36 Suppl 1 S19-24**
- 30) Carter, D. R., and Orr, T. E. *"Skeletal development and bone functional adaptation"* J Bone Miner Res **1992; 7 Suppl 2 S389-95**
- 31) Cendre, E., Kaftandjian, V., Peix, G., Jourlin, M., Mitton, D., and Babot, D. *"An investigation of segmentation methods and texture analysis applied to tomographic images of human vertebral cancellous bone"* J Microsc **2000; 197 (Pt 3) 305-16**
- 32) Chen, M. M., Jee, W. S., Ke, H. Z., Lin, B. Y., Li, Q. N., and Li, X. J. *"Adaptation of cancellous bone to aging and immobilization in growing rats"* Anat Rec **1992; 234 (3):317-34**
- 33) Cheng, M. Z., Zaman, G., and Lanyon, L. E. *"Estrogen enhances the stimulation of bone collagen synthesis by loading and exogenous prostacyclin, but not prostaglandin E2, in organ cultures of rat ulnae"* J Bone Miner Res **1994; 9 (6):805-16**
- 34) Cheng, M. Z., Zaman, G., Rawlinson, S. C., Suswillo, R. F., and Lanyon, L. E. *"Mechanical loading and sex hormone interactions in organ cultures of rat ulna"* J Bone Miner Res **1996; 11 (4):502-11**

- 35) Ciarelli, T. E., Fyhrie, D. P., Schaffler, M. B., and Goldstein, S. A. *"Variations in three-dimensional cancellous bone architecture of the proximal femur in female hip fractures and in controls"* J Bone Miner Res **2000**; **15** (1):32-40
- 36) Clarkson, T. B., Anthony, M. S., Cline, J. M., Lees, C. J., and Ederveen, A. G. *"Multisystem evaluations of the long-term effects of tibolone on postmenopausal monkeys"* Maturitas **2004**; **48 Suppl 1** S24-9
- 37) Compston, J. E., Mellish, R. W., and Garrahan, N. J. *"Age-related changes in iliac crest trabecular microanatomic bone structure in man"* Bone **1987**; **8** (5):289-92
- 38) Cowin, S. C., and Firoozbakhsh, K. *"Bone remodeling of diaphysial surfaces under constant load: theoretical predictions"* J Biomech **1981**; **14** (7):471-84
- 39) Dare, A., Hachisu, R., Yamaguchi, A., Yokose, S., Yoshiki, S., and Okano, T. *"Effects of ionizing radiation on proliferation and differentiation of osteoblast-like cells"* J Dent Res **1997**; **76** (2):658-64
- 40) David, V., Laroche, N., Boudignon, B., Lafage-Proust, M. H., Alexandre, C., Rueggsegger, P., and Vico, L. *"Noninvasive in vivo monitoring of bone architecture alterations in hindlimb-unloaded female rats using novel three-dimensional microcomputed tomography"* J Bone Miner Res **2003**; **18** (9):1622-31
- 41) David, V., Laroche, N., Boudignon, B., Lafage-Proust, M. H., Alexandre, C., Rueggsegger, P., and Vico, L. *"Noninvasive in vivo monitoring of bone architecture alterations in hindlimb-unloaded female rats using novel three-dimensional microcomputed tomography"* Journal of Bone and Mineral Research **2003**; **18** (9):1622-1631
- 42) Day, J. S. *"Bone quality: the mechanical effects of microarchitecture and matrix properties."* Rotterdam, The Netherlands; **2005**.
- 43) Day, J. S., Ding, M., Odgaard, A., Sumner, D. R., Hvid, I., and Weinans, H. *"Parallel plate model for trabecular bone exhibits volume fraction-dependent bias"* Bone **2000**; **27** (5):715-20
- 44) Day, J. S., Ding, M., van der Linden, J. C., Hvid, I., Sumner, D. R., and Weinans, H. *"A decreased subchondral trabecular bone tissue elastic modulus is associated with pre-arthritic cartilage damage"* J Orthop Res **2001**; **19** (5):914-8
- 45) de Gooyer, M. E., Deckers, G. H., Schoonen, W. G., Verheul, H. A., and Kloosterboer, H. J. *"Receptor profiling and endocrine interactions of tibolone"* Steroids **2003**; **68** (1):21-30
- 46) De Souza, R. L., Matsuura, M., Eckstein, F., Rawlinson, S. C., Lanyon, L. E., and Pitsillides, A. A. *"Non-invasive axial loading of mouse tibiae increases cortical bone formation and modifies trabecular organization: a new model to study cortical and cancellous compartments in a single loaded element"* Bone **2005**; **37** (6):810-8
- 47) Dempster, D. W., Birchman, R., Xu, R., Lindsay, R., and Shen, V. *"Temporal changes in cancellous bone structure of rats immediately after ovariectomy"* Bone **1995**; **16** (1):157-61
- 48) Diderich, K. E. M., Waarsing, J. H., Day, J. S., Brandt, R. M. C., Amling, M., Hoeijmakers, J. H. J., Weinans, H., van der Horst, G. T. J., and van Leeuwen, J. P. *"Accelerated bone loss and disturbed periosteal apposition with ageing in DNA repair deficient trichothiodystrophy mice."* Submitted **2006**;
- 49) Ding, M., Dalstra, M., Weinans, H., Ederveen, A. G., and Hvid, I. *"Treatment with tibolone partially protects 3-D microarchitecture of lumbar vertebral bone tissues and prevents ovariectomy-induced reduction in mechanical properties."* Journal of Bone and Mineral Research **2004**; **19** S237-S237
- 50) Ding, M., Odgaard, A., and Hvid, I. *"Accuracy of cancellous bone volume fraction measured by micro-CT scanning"* J Biomech **1999**; **32** (3):323-6
- 51) Dufresne, T. *"Segmentation techniques for analysis of bone by three-dimensional computed tomographic imaging"* Technol Health Care **1998**; **6** (5-6):351-9

- 52) Ederveen, A. G., and Kloosterboer, H. J. *"Tibolone exerts its protective effect on trabecular bone loss through the estrogen receptor"* J Bone Miner Res **2001; 16 (9):1651-7**
- 53) Ederveen, A. G., Spanjers, C. P., Quaijtaal, J. H., and Kloosterboer, H. J. *"Effect of 16 months of treatment with tibolone on bone mass, turnover, and biomechanical quality in mature ovariectomized rats"* J Bone Miner Res **2001; 16 (9):1674-81**
- 54) Ehrlich, P. J., and Lanyon, L. E. *"Mechanical strain and bone cell function: a review"* Osteoporos Int **2002; 13 (9):688-700**
- 55) Elmoutaouakkil, A., Peyrin, F., Elkafi, J., and Laval-Jeantet, A. M. *"Segmentation of cancellous bone from high-resolution computed tomography images: influence on trabecular bone measurements"* IEEE Trans Med Imaging **2002; 21 (4):354-62**
- 56) Fajardo, R. J., Ryan, T. M., and Kappelman, J. *"Assessing the accuracy of high-resolution X-ray computed tomography of primate trabecular bone by comparisons with histological sections"* Am J Phys Anthropol **2002; 118 (1):1-10**
- 57) Feldkamp, L. A., Goldstein, S. A., Parfitt, A. M., Jesion, G., and Kleerekoper, M. *"The direct examination of three-dimensional bone architecture in vitro by computed tomography"* J Bone Miner Res **1989; 4 (1):3-11**
- 58) Finch, C. E. *"Reproductive senescence in rodents: factors in the decline of fertility and loss of regular estrous cycles"*. In: E. L. Schneider (ed.), *The aging reproductive system*, Aging **4**, pp. **193-212**. New York: Raven Press; **1978**.
- 59) Frost, H. M. *"Bone "mass" and the "mechanostat": a proposal"* Anat Rec **1987; 219 (1):1-9**
- 60) Frost, H. M. *"On the estrogen-bone relationship and postmenopausal bone loss: A new model"* J Bone Miner Res **1999; 14 (9):1473-7**
- 61) Fyhrle, D. P., and Carter, D. R. *"A unifying principle relating stress to trabecular bone morphology"* J Orthop Res **1986; 4 (3):304-17**
- 62) Geusens, P., Dequeker, J., Gielen, J., and Schot, L. P. *"Non-linear increase in vertebral density induced by a synthetic steroid (Org OD 14) in women with established osteoporosis"* Maturitas **1991; 13 (2):155-62**
- 63) Gombert, B. R., Saha, P. K., and Wehrli, F. W. *"Topology-based orientation analysis of trabecular bone networks"* Med Phys **2003; 30 (2):158-68**
- 64) Gordon, C. L., Webber, C. E., Adachi, J. D., and Christoforou, N. *"In vivo assessment of trabecular bone structure at the distal radius from high-resolution computed tomography images"* Phys Med Biol **1996; 41 (3):495-508**
- 65) Gordon, C. L., Webber, C. E., Christoforou, N., and Nahmias, C. *"In vivo assessment of trabecular bone structure at the distal radius from high-resolution magnetic resonance images"* Medical Physics **1997; 24 (4):585-593**
- 66) Grynblas, M. D., Tupy, J. H., and Sodek, J. *"The distribution of soluble, mineral-bound, and matrix-bound proteins in osteoporotic and normal bones"* Bone **1994; 15 (5):505-13**
- 67) Gustafsson, B. I., Westbroek, I., Waarsing, J. H., Waldum, H., Solligard, E., Brunsvik, A., Dimmen, S., van Leeuwen, J. P., Weinans, H., and Syversen, U. *"Long-term serotonin administration leads to higher bone mineral density, affects bone architecture, and leads to higher femoral bone stiffness in rats"* J Cell Biochem **2006; 97 (6):1283-91**
- 68) Haapasalo, H., Kontulainen, S., Sievanen, H., Kannus, P., Jarvinen, M., and Vuori, I. *"Exercise-induced bone gain is due to enlargement in bone size without a change in volumetric bone density: a peripheral quantitative computed tomography study of the upper arms of male tennis players"* Bone **2000; 27 (3):351-7**
- 69) Hahn, M., Vogel, M., Pompesius-Kempa, M., and Delling, G. *"Trabecular bone pattern factor--a new parameter for simple quantification of bone microarchitecture"* Bone **1992; 13 (4):327-30**

- 70) Hamilton, S. A., Pecaut, M. J., Gridley, D. S., Travis, N. D., Bandstra, E. R., Willey, J. S., Nelson, G., and Bateman, T. A. *"A Murine Model for Bone Loss from Therapeutic and Space-Relevant Sources of Radiation"* J Appl Physiol **2006**;
- 71) Hara, T., Tanck, E., Homminga, J., and Huiskes, R. *"The influence of microcomputed tomography threshold variations on the assessment of structural and mechanical trabecular bone properties"* Bone **2002**; **31** (1):107-9
- 72) Heikkinen, J., Kyllonen, E., Kurttila-Matero, E., Wilen-Rosenqvist, G., Lankinen, K. S., Rita, H., and Vaananen, H. K. *"HRT and exercise: effects on bone density, muscle strength and lipid metabolism. A placebo controlled 2-year prospective trial on two estrogen-progestin regimens in healthy postmenopausal women"* Maturitas **1997**; **26** (2):139-49
- 73) Heinonen, A., Sievanen, H., Kannus, P., Oja, P., Pasanen, M., and Vuori, I. *"High-impact exercise and bones of growing girls: a 9-month controlled trial"* Osteoporos Int **2000**; **11** (12):1010-7
- 74) Henderson, J. H., and Carter, D. R. *"Mechanical induction in limb morphogenesis: the role of growth-generated strains and pressures"* Bone **2002**; **31** (6):645-53
- 75) Hildebrand, T., and Rueggsegger, P. *"A new method for the model-independent assessment of thickness in three-dimensional images"* Journal of Microscopy-Oxford **1997**; **185** 67-75
- 76) Hildebrand, T., and Rueggsegger, P. *"Quantification of Bone Microarchitecture with the Structure Model Index"* Comput Methods Biomech Biomed Engin **1997**; **1** (1):15-23
- 77) Hoenderop, J. G., van Leeuwen, J. P., van der Eerden, B. C., Kersten, F. F., van der Kemp, A. W., Merillat, A. M., Waarsing, J. H., Rossier, B. C., Vallon, V., Hummler, E., and Bindels, R. J. *"Renal Ca²⁺ wasting, hyperabsorption, and reduced bone thickness in mice lacking TRPV5"* J Clin Invest **2003**; **112** (12):1906-14
- 78) Hohmann, E. L., Elde, R. P., Rysavy, J. A., Einzig, S., and Gebhard, R. L. *"Innervation of periosteum and bone by sympathetic vasoactive intestinal peptide-containing nerve fibers"* Science **1986**; **232** (4752):868-71
- 79) Homminga, J., McCreddie, B. R., Ciarelli, T. E., Weinans, H., Goldstein, S. A., and Huiskes, R. *"Cancellous bone mechanical properties from normals and patients with hip fractures differ on the structure level, not on the bone hard tissue level"* Bone **2002**; **30** (5):759-64
- 80) Homminga, J., Van-Rietbergen, B., Lochmuller, E. M., Weinans, H., Eckstein, F., and Huiskes, R. *"The osteoporotic vertebral structure is well adapted to the loads of daily life, but not to infrequent "error" loads"* Bone **2004**; **34** (3):510-6
- 81) Honda, A., Sogo, N., Nagasawa, S., Shimizu, T., and Umemura, Y. *"High-impact exercise strengthens bone in osteopenic ovariectomized rats with the same outcome as Sham rats"* J Appl Physiol **2003**; **95** (3):1032-7
- 82) Hsieh, Y. F., Robling, A. G., Ambrosius, W. T., Burr, D. B., and Turner, C. H. *"Mechanical loading of diaphyseal bone in vivo: the strain threshold for an osteogenic response varies with location"* J Bone Miner Res **2001**; **16** (12):2291-7
- 83) Huddleston, A. L., Rockwell, D., Kulund, D. N., and Harrison, R. B. *"Bone mass in lifetime tennis athletes"* Jama **1980**; **244** (10):1107-9
- 84) Huiskes, R., Ruimerman, R., van Lenthe, G. H., and Janssen, J. D. *"Effects of mechanical forces on maintenance and adaptation of form in trabecular bone"* Nature **2000**; **405** (6787):704-6
- 85) Iida, H., and Fukuda, S. *"Age-related changes in bone mineral density, cross-sectional area and strength at different skeletal sites in male rats"* J Vet Med Sci **2002**; **64** (1):29-34
- 86) Issever, A. S., Walsh, A., Lu, Y., Burghardt, A., Lotz, J. C., and Majumdar, S. *"Micro-computed tomography evaluation of trabecular bone structure on loaded mice tail vertebrae"* Spine **2003**; **28** (2):123-8

- 87) Ito, M., Nakamura, T., Matsumoto, T., Tsurusaki, K., and Hayashi, K. "Analysis of trabecular microarchitecture of human iliac bone using microcomputed tomography in patients with hip arthrosis with or without vertebral fracture" *Bone* **1998; 23 (2):163-9**
- 88) Jacobsson, M., Jonsson, A., Albrektsson, T., and Turesson, I. "Alterations in bone regenerative capacity after low level gamma irradiation. A quantitative study" *Scand J Plast Reconstr Surg* **1985; 19 (3):231-6**
- 89) Jagger, C. J., Chambers, T. J., and Chow, J. W. "Stimulation of bone formation by dynamic mechanical loading of rat caudal vertebrae is not suppressed by 3-amino-1-hydroxypropylidene-1-bisphosphonate (AHPBP)" *Bone* **1995; 16 (3):309-13**
- 90) Jagger, C. J., Chow, J. W., and Chambers, T. J. "Estrogen suppresses activation but enhances formation phase of osteogenic response to mechanical stimulation in rat bone" *J Clin Invest* **1996; 98 (10):2351-7**
- 91) Jansen, J. H., Jahr, H., Verhaar, J. A., Pols, H. A., Chiba, H., Weinans, H., and van Leeuwen, J. P. "Stretch-induced modulation of matrix metalloproteinases in mineralizing osteoblasts via extracellular signal-regulated kinase-1/2" *J Orthop Res* **2006;**
- 92) Jarvinen, T. L., Kannus, P., Pajamaki, I., Vuohelainen, T., Tuukkanen, J., Jarvinen, M., and Sievanen, H. "Estrogen deposits extra mineral into bones of female rats in puberty, but simultaneously seems to suppress the responsiveness of female skeleton to mechanical loading" *Bone* **2003; 32 (6):642-51**
- 93) Jarvinen, T. L., Kannus, P., and Sievanen, H. "Estrogen and bone--a reproductive and locomotive perspective" *J Bone Miner Res* **2003; 18 (11):1921-31**
- 94) Jarvinen, T. L., Sievanen, H., Jokihaara, J., and Einhorn, T. A. "Revival of bone strength: the bottom line" *J Bone Miner Res* **2005; 20 (5):717-20**
- 95) Jessop, H. L., Sjoberg, M., Cheng, M. Z., Zaman, G., Wheeler-Jones, C. P., and Lanyon, L. E. "Mechanical strain and estrogen activate estrogen receptor alpha in bone cells" *J Bone Miner Res* **2001; 16 (6):1045-55**
- 96) Jinnai, H., Watashiba, H., Kajihara, T., Nishikawa, Y., Takahashi, M., and Ito, M. "Surface curvatures of trabecular bone microarchitecture" *Bone* **2002; 30 (1):191-4**
- 97) Judex, S., Chung, H., Torab, A., Xie, L., Rubin, C., Donahue, L., and Xu, S. "Micro-CT induced radiation does not exacerbate disuse related bone loss". 51st Annual Meeting of the Orthopaedic Research Society. Washington, USA; **2005**.
- 98) Kalu, D. N. "The ovariectomized rat model of postmenopausal bone loss" *Bone Miner* **1991; 15 (3):175-91**
- 99) Kimmel, D. B. "A paradigm for skeletal strength homeostasis" *J Bone Miner Res* **1993; 8 Suppl 2 S515-22**
- 100) Kinney, J. H., Haupt, D. L., Balooch, M., Ladd, A. J., Ryaby, J. T., and Lane, N. E. "Three-dimensional morphometry of the L6 vertebra in the ovariectomized rat model of osteoporosis: biomechanical implications" *J Bone Miner Res* **2000; 15 (10):1981-91**
- 101) Kinney, J. H., Lane, N. E., and Haupt, D. L. "In vivo, three-dimensional microscopy of trabecular bone" *J Bone Miner Res* **1995; 10 (2):264-70**.
- 102) Klinck, R., and Boyd, S. "The effect of radiation on bone architecture for in vivo microcomputed tomography". 52nd Annual Meeting of the Orthopaedic Research Society. Chicago, IL, USA; **2006**.
- 103) Kloosterboer, H. J. "Tissue-selectivity: the mechanism of action of tibolone" *Maturitas* **2004; 48 Suppl 1 S30-40**
- 104) Kneissel, M., Boyde, A., and Gasser, J. A. "Bone tissue and its mineralization in aged estrogen-depleted rats after long-term intermittent treatment with parathyroid hormone (PTH) analog SDZ PTS 893 or human PTH(1-34)" *Bone* **2001; 28 (3):237-50**
- 105) Kohrt, W. M., Ehsani, A. A., and Birge, S. J., Jr. "HRT preserves increases in bone mineral density and reductions in body fat after a supervised exercise program" *J Appl Physiol* **1998; 84 (5):1506-12**

- 106) Kohrt, W. M., Snead, D. B., Slatopolsky, E., and Birge, S. J., Jr. *"Additive effects of weight-bearing exercise and estrogen on bone mineral density in older women"* J Bone Miner Res **1995; 10 (9):1303-11**
- 107) Kuhn, J. L., Goldstein, S. A., Feldkamp, L. A., Goulet, R. W., and Jesion, G. *"Evaluation of a microcomputed tomography system to study trabecular bone structure"* J Orthop Res **1990; 8 (6):833-42**
- 108) Laib, A., Hildebrand, T., Hauselmann, H. J., and Rueggsegger, P. *"Ridge number density: a new parameter for in vivo bone structure analysis"* Bone **1997; 21 (6):541-6**
- 109) Laib, A., Kumer, J. L., Majumdar, S., and Lane, N. E. *"The temporal changes of trabecular architecture in ovariectomized rats assessed by MicroCT"* Osteoporos Int **2001; 12 (11):936-41**
- 110) Laib, A., Newitt, D. C., Lu, Y., and Majumdar, S. *"New model-independent measures of trabecular bone structure applied to in vivo high-resolution MR images"* Osteoporosis International **2002; 13 (2):130-136**
- 111) Laib, A., and Rueggsegger, P. *"Comparison of structure extraction methods for in vivo trabecular bone measurements"* Comput Med Imaging Graph **1999; 23 (2):69-74**
- 112) Lane, N. E., Thompson, J. M., Haupt, D., Kimmel, D. B., Modin, G., and Kinney, J. H. *"Acute changes in trabecular bone connectivity and osteoclast activity in the ovariectomized rat in vivo"* J Bone Miner Res **1998; 13 (2):229-36**
- 113) Lane, N. E., Thompson, J. M., Haupt, D., Kimmel, D. B., Modin, G., and Kinney, J. H. *"Acute changes in trabecular bone connectivity and osteoclast activity in the ovariectomized rat in vivo"* J Bone Miner Res **1998; 13 (2):229-36**
- 114) Lanyon, L., and Skerry, T. *"Postmenopausal osteoporosis as a failure of bone's adaptation to functional loading: a hypothesis"* J Bone Miner Res **2001; 16 (11):1937-47**
- 115) Lanyon, L. E. *"Using functional loading to influence bone mass and architecture: objectives, mechanisms, and relationship with estrogen of the mechanically adaptive process in bone"* Bone **1996; 18 (1 Suppl):37S-43S**
- 116) Leblanc, A. D., Schneider, V. S., Evans, H. J., Engelbretson, D. A., and Krebs, J. M. *"Bone mineral loss and recovery after 17 weeks of bed rest"* J Bone Miner Res **1990; 5 (8):843-50**
- 117) Lee, K. C., Jessop, H., Suswillo, R., Zaman, G., and Lanyon, L. E. *"The adaptive response of bone to mechanical loading in female transgenic mice is deficient in the absence of oestrogen receptor-alpha and -beta"* J Endocrinol **2004; 182 (2):193-201**
- 118) LeFevre, J., and McClintock, M. K. *"Reproductive senescence in female rats: a longitudinal study of individual differences in estrous cycles and behavior"* Biol Reprod **1988; 38 (4):780-9**
- 119) Li, C. Y., Jee, W. S., Chen, J. L., Mo, A., Setterberg, R. B., Su, M., Tian, X. Y., Ling, Y. F., and Yao, W. *"Estrogen and "exercise" have a synergistic effect in preventing bone loss in the lumbar vertebra and femoral neck of the ovariectomized rat"* Calcif Tissue Int **2003; 72 (1):42-9**
- 120) Lindberg, M. K., Moverare, S., Skrtic, S., Gao, H., Dahlman-Wright, K., Gustafsson, J. A., and Ohlsson, C. *"Estrogen receptor (ER)-beta reduces ERalpha-regulated gene transcription, supporting a "ying yang" relationship between ERalpha and ERbeta in mice"* Mol Endocrinol **2003; 17 (2):203-8**
- 121) Mach, D. B., Rogers, S. D., Sabino, M. C., Luger, N. M., Schwei, M. J., Pomonis, J. D., Keyser, C. P., Clohisy, D. R., Adams, D. J., O'Leary, P., and Mantyh, P. W. *"Origins of skeletal pain: sensory and sympathetic innervation of the mouse femur"* Neuroscience **2002; 113 (1):155-66**

- 122) Maes, F., Collignon, A., Vandermeulen, D., Marchal, G., and Suetens, P. *"Multimodality image registration by maximization of mutual information"* Ieee Transactions on Medical Imaging **1997; 16 (2):187-198**
- 123) Majumdar, S., Genant, H. K., Grampp, S., Newitt, D. C., Truong, V. H., Lin, J. C., and Mathur, A. *"Correlation of trabecular bone structure with age, bone mineral density, and osteoporotic status: In vivo studies in the distal radius using high resolution magnetic resonance imaging"* Journal of Bone and Mineral Research **1997; 12 (1):111-118**
- 124) Martin, E. A., Ritman, E. L., and Turner, R. T. *"Time course of epiphyseal growth plate fusion in rat tibiae"* Bone **2003; 32 (3):261-7**
- 125) Matsumoto, T., Nakayama, K., Kodama, Y., Fuse, H., Nakamura, T., and Fukumoto, S. *"Effect of mechanical unloading and reloading on periosteal bone formation and gene expression in tail-suspended rapidly growing rats"* Bone **1998; 22 (5 Suppl):89S-93S**
- 126) Mawatari, T., Miura, H., Higaki, H., Kurata, K., Moro-oka, T., Murakami, T., and Iwamoto, Y. *"Quantitative analysis of three-dimensional complexity and connectivity changes in trabecular microarchitecture in relation to aging, menopause, and inflammation"* J Orthop Sci **1999; 4 (6):431-8**
- 127) McNitt-Gray, M. F. *"AAPM/RSNA Physics Tutorial for Residents: Topics in CT. Radiation dose in CT"* Radiographics **2002; 22 (6):1541-53**
- 128) Meazzini, M. C., Toma, C. D., Schaffer, J. L., Gray, M. L., and Gerstenfeld, L. C. *"Osteoblast cytoskeletal modulation in response to mechanical strain in vitro"* J Orthop Res **1998; 16 (2):170-80**
- 129) Mekkaldi, S., Lafage-Proust, M. H., Bloomfield, S., Alexandre, C., and Vico, L. *"Changes in vasoactive factors associated with altered vessel morphology in the tibial metaphysis during ovariectomy-induced bone loss in rats"* Bone **2003; 32 (6):630-41**
- 130) Mellish, R. W., Garrahan, N. J., and Compston, J. E. *"Age-related changes in trabecular width and spacing in human iliac crest biopsies"* Bone Miner **1989; 6 (3):331-8**
- 131) Mitton, D., Cendre, E., Roux, J. P., Arlot, M. E., Peix, G., Rumelhart, C., Babot, D., and Meunier, P. J. *"Mechanical properties of ewe vertebral cancellous bone compared with histomorphometry and high-resolution computed tomography parameters"* Bone **1998; 22 (6):651-8**
- 132) Mosekilde, L. *"Sex differences in age-related loss of vertebral trabecular bone mass and structure--biomechanical consequences"* Bone **1989; 10 (6):425-32**
- 133) Mullender, M., El Haj, A. J., Yang, Y., van Duin, M. A., Burger, E. H., and Klein-Nulend, J. *"Mechanotransduction of bone cells in vitro: mechanobiology of bone tissue"* Med Biol Eng Comput **2004; 42 (1):14-21**
- 134) Mullender, M., van Rietbergen, B., Ruegsegger, P., and Huiskes, R. *"Effect of mechanical set point of bone cells on mechanical control of trabecular bone architecture"* Bone **1998; 22 (2):125-31**
- 135) Mullender, M. G., and Huiskes, R. *"Osteocytes and bone lining cells: which are the best candidates for mechano-sensors in cancellous bone?"* Bone **1997; 20 (6):527-32**
- 136) Mullender, M. G., Huiskes, R., and Weinans, H. *"A physiological approach to the simulation of bone remodeling as a self-organizational control process"* J Biomech **1994; 27 (11):1389-94**
- 137) Muller, R., Hildebrand, T., Hauselmann, H. J., and Ruegsegger, P. *"In vivo reproducibility of three-dimensional structural properties of noninvasive bone biopsies using 3D-pQCT"* J Bone Miner Res **1996; 11 (11):1745-50**
- 138) Muller, R., Hildebrand, T., and Ruegsegger, P. *"Non-invasive bone biopsy: a new method to analyse and display the three-dimensional structure of trabecular bone"* Phys Med Biol **1994; 39 (1):145-64**

- 139) Muller, R., Koller, B., Hildebrand, T., Laib, A., Gianolini, S., and Ruegsegger, P. *"Resolution dependency of microstructural properties of cancellous bone based on three-dimensional mu-tomography"* Technol Health Care **1996; 4 (1):113-9**
- 140) Muller, R., Van Campenhout, H., Van Damme, B., Van Der Perre, G., Dequeker, J., Hildebrand, T., and Ruegsegger, P. *"Morphometric analysis of human bone biopsies: a quantitative structural comparison of histological sections and micro-computed tomography"* Bone **1998; 23 (1):59-66**
- 141) Newitt, D. C., van Rietbergen, B., and Majumdar, S. *"Processing and analysis of in vivo high-resolution MR images of trabecular bone for longitudinal studies: Reproducibility of structural measures and micro-finite element analysis derived mechanical properties"* Osteoporosis International **2002; 13 (4):278-287**
- 142) Niebur, G. L., Feldstein, M. J., and Keaveny, T. M. *"Biaxial failure behavior of bovine tibial trabecular bone"* J Biomech Eng **2002; 124 (6):699-705**
- 143) Notomi, T., Okimoto, N., Okazaki, Y., Nakamura, T., and Suzuki, M. *"Tower climbing exercise started 3 months after ovariectomy recovers bone strength of the femur and lumbar vertebrae in aged osteopenic rats"* J Bone Miner Res **2003; 18 (1):140-9**
- 144) Ochoa, J. A., Sanders, A. P., Heck, D. A., and Hillberry, B. M. *"Stiffening of the femoral head due to inter-trabecular fluid and intraosseous pressure"* J Biomech Eng **1991; 113 (3):259-62**
- 145) Ochoa, J. A., Sanders, A. P., Kiesler, T. W., Heck, D. A., Toombs, J. P., Brandt, K. D., and Hillberry, B. M. *"In vivo observations of hydraulic stiffening in the canine femoral head"* J Biomech Eng **1997; 119 (1):103-8**
- 146) Odgaard, A. *"Three-dimensional methods for quantification of cancellous bone architecture"* Bone **1997; 20 (4):315-28.**
- 147) Odgaard, A. *"Three-dimensional methods for quantification of cancellous bone architecture"* Bone **1997; 20 (4):315-28**
- 148) Odgaard, A., Andersen, K., Ullerup, R., Frich, L. H., and Melsen, F. *"Three-dimensional reconstruction of entire vertebral bodies"* Bone **1994; 15 (3):335-42**
- 149) Odgaard, A., and Gundersen, H. J. *"Quantification of connectivity in cancellous bone, with special emphasis on 3-D reconstructions"* Bone **1993; 14 (2):173-82**
- 150) Otomo, H., Sakai, A., Ikeda, S., Tanaka, S., Ito, M., Phipps, R. J., and Nakamura, T. *"Regulation of mineral-to-matrix ratio of lumbar trabecular bone in ovariectomized rats treated with risedronate in combination with or without vitamin K2"* J Bone Miner Metab **2004; 22 (5):404-14**
- 151) Parfitt, A. M., Drezner, M. K., Glorieux, F. H., Kanis, J. A., Malluche, H., Meunier, P. J., Ott, S. M., and Recker, R. R. *"Bone histomorphometry: standardization of nomenclature, symbols, and units. Report of the ASBMR Histomorphometry Nomenclature Committee"* J Bone Miner Res **1987; 2 (6):595-610**
- 152) Parfitt, A. M., Mathews, C. H., Villanueva, A. R., Kleerekoper, M., Frame, B., and Rao, D. S. *"Relationships between surface, volume, and thickness of iliac trabecular bone in aging and in osteoporosis. Implications for the microanatomic and cellular mechanisms of bone loss"* J Clin Invest **1983; 72 (4):1396-409**
- 153) Pavlov, P. W., Ginsburg, J., Kicovic, P. M., van der Schaaf, D. B., Prelevic, G., and Bennink, H. J. *"Double-blind, placebo-controlled study of the effects of tibolone on bone mineral density in postmenopausal osteoporotic women with and without previous fractures"* Gynecol Endocrinol **1999; 13 (4):230-7**
- 154) Prelevic, G. M., Markou, A., Arnold, A., Bartram, C., Puzigaca, Z., and Ginsburg, J. *"The effect of tibolone on bone mineral density in postmenopausal women with osteopenia or osteoporosis--8 years follow-up"* Maturitas **2004; 47 (3):229-34**
- 155) Pytlík, M. *"Effects of tibolone on the development of osteopenia induced by ovariectomy in rats"* Pol J Pharmacol **2002; 54 (1):35-43**

- 156) Rho, J. Y., Ashman, R. B., and Turner, C. H. *"Young's modulus of trabecular and cortical bone material: ultrasonic and microtensile measurements"* J Biomech **1993; 26 (2):111-9**
- 157) Riera-Espinoza, G., Ramos, J., Carvajal, R., Belzares, E., Stanbury, G., Farias, R., Valderrama, I., Alvarez, K., and Riera-Gonzalez, G. *"Changes in bone turnover during tibolone treatment"* Maturitas **2004; 47 (2):83-90**
- 158) Riggs, B. L., Khosla, S., and Melton, L. J., 3rd *"A unitary model for involutional osteoporosis: estrogen deficiency causes both type I and type II osteoporosis in postmenopausal women and contributes to bone loss in aging men"* J Bone Miner Res **1998; 13 (5):763-73**
- 159) Riggs, B. L., Khosla, S., and Melton, L. J., 3rd *"Sex steroids and the construction and conservation of the adult skeleton"* Endocr Rev **2002; 23 (3):279-302**
- 160) Robling, A. G., and Turner, C. H. *"Mechanotransduction in bone: genetic effects on mechanosensitivity in mice"* Bone **2002; 31 (5):562-9**
- 161) Rodan, G. A. *"Mechanical loading, estrogen deficiency, and the coupling of bone formation to bone resorption"* J Bone Miner Res **1991; 6 (6):527-30**
- 162) Roschger, P., Gupta, H. S., Berzlanovich, A., Ittner, G., Dempster, D. W., Fratzl, P., Cosman, F., Parisien, M., Lindsay, R., Nieves, J. W., and Klaushofer, K. *"Constant mineralization density distribution in cancellous human bone"* Bone **2003; 32 (3):316-23**
- 163) Roux, W. *"Der Kampf der Theile im Organismus"*. Leipzig: W. Engelmann; **1881**.
- 164) Rubin, C. T., Bain, S. D., and McLeod, K. J. *"Suppression of the osteogenic response in the aging skeleton"* Calcif Tissue Int **1992; 50 (4):306-13**
- 165) Ruimerman, R., Van Rietbergen, B., Hilbers, P., and Huiskes, R. *"The effects of trabecular-bone loading variables on the surface signaling potential for bone remodeling and adaptation"* Ann Biomed Eng **2005; 33 (1):71-8**
- 166) Russ, J. *"The image processing handbook"*. CRC Press, Springer, IEEE Press; **1999**.
- 167) Rymer, J., Robinson, J., and Fogelman, I. *"Ten years of treatment with tibolone 2.5 mg daily: effects on bone loss in postmenopausal women"* Climacteric **2002; 5 (4):390-8**
- 168) Saxon, L. K., and Turner, C. H. *"Estrogen receptor beta: the antimechanostat?"* Bone **2005; 36 (2):185-92**
- 169) Schuit, S. C., van der Klift, M., Weel, A. E., de Laet, C. E., Burger, H., Seeman, E., Hofman, A., Uitterlinden, A. G., van Leeuwen, J. P., and Pols, H. A. *"Fracture incidence and association with bone mineral density in elderly men and women: the Rotterdam Study"* Bone **2004; 34 (1):195-202**
- 170) Seeman, E. *"Pathogenesis of bone fragility in women and men"* Lancet **2002; 359 (9320):1841-50**
- 171) Shen, V., Liang, X. G., Birchman, R., Wu, D. D., Healy, D., Lindsay, R., and Dempster, D. W. *"Short-term immobilization-induced cancellous bone loss is limited to regions undergoing high turnover and/or modeling in mature rats"* Bone **1997; 21 (1):71-8**
- 172) Sims, N. A., Dupont, S., Krust, A., Clement-Lacroix, P., Minet, D., Resche-Rigon, M., Gaillard-Kelly, M., and Baron, R. *"Deletion of estrogen receptors reveals a regulatory role for estrogen receptors-beta in bone remodeling in females but not in males"* Bone **2002; 30 (1):18-25**
- 173) Sims, N. A., Morris, H. A., Moore, R. J., and Durbridge, T. C. *"Increased bone resorption precedes increased bone formation in the ovariectomized rat"* Calcif Tissue Int **1996; 59 (2):121-7**
- 174) Snyder, B. D., Piazza, S., Edwards, W. T., and Hayes, W. C. *"Role of trabecular morphology in the etiology of age-related vertebral fractures"* Calcif Tissue Int **1993; 53 Suppl 1 S14-22**

- 175) Srinivasan, S., and Gross, T. S. *"Canalicular fluid flow induced by bending of a long bone"* Med Eng Phys **2000**; **22** (2):127-33
- 176) Studd, J., Arnala, I., Kicovic, P. M., Zamblera, D., Kroger, H., and Holland, N. *"A randomized study of tibolone on bone mineral density in osteoporotic postmenopausal women with previous fractures"* Obstet Gynecol **1998**; **92** (4 Pt 1):574-9
- 177) Takeda, S., Eleftheriou, F., Levasseur, R., Liu, X., Zhao, L., Parker, K. L., Armstrong, D., Ducey, P., and Karsenty, G. *"Leptin regulates bone formation via the sympathetic nervous system"* Cell **2002**; **111** (3):305-17
- 178) Tanck, E., Hannink, G., Ruimerman, R., Buma, P., Burger, E. H., and Huiskes, R. *"Cortical bone development under the growth plate is regulated by mechanical load transfer"* J Anat **2006**; **208** (1):73-9
- 179) Tanck, E., Homminga, J., van Lenthe, G. H., and Huiskes, R. *"Increase in bone volume fraction precedes architectural adaptation in growing bone"* Bone **2001**; **28** (6):650-4
- 180) Thomsen, J. S., Ebbesen, E. N., and Mosekilde, L. *"Static histomorphometry of human iliac crest and vertebral trabecular bone: a comparative study"* Bone **2002**; **30** (1):267-74
- 181) Thornton, J. W., Need, E., and Crews, D. *"Resurrecting the ancestral steroid receptor: ancient origin of estrogen signaling"* Science **2003**; **301** (5640):1714-7
- 182) Tomkinson, A., Reeve, J., Shaw, R. W., and Noble, B. S. *"The death of osteocytes via apoptosis accompanies estrogen withdrawal in human bone"* J Clin Endocrinol Metab **1997**; **82** (9):3128-35
- 183) Turner, C. H. *"Toward a mathematical description of bone biology: the principle of cellular accommodation"* Calcif Tissue Int **1999**; **65** (6):466-71
- 184) Turner, R. T. *"Mechanical signaling in the development of postmenopausal osteoporosis"* Lupus **1999**; **8** (5):388-92
- 185) van Bezooijen, R. L., ten Dijke, P., Papapoulos, S. E., and Lowik, C. W. *"SOST/sclerostin, an osteocyte-derived negative regulator of bone formation"* Cytokine Growth Factor Rev **2005**; **16** (3):319-27
- 186) van der Eerden, B. C., Emons, J., Ahmed, S., van Essen, H. W., Lowik, C. W., Wit, J. M., and Karperien, M. *"Evidence for genomic and nongenomic actions of estrogen in growth plate regulation in female and male rats at the onset of sexual maturation"* J Endocrinol **2002**; **175** (2):277-88
- 187) van der Linden, J. C., Day, J. S., Verhaar, J. A., and Weinans, H. *"Altered tissue properties induce changes in cancellous bone architecture in aging and diseases"* J Biomech **2004**; **37** (3):367-74
- 188) van der Linden, J. C., Homminga, J., Verhaar, J. A., and Weinans, H. *"Mechanical consequences of bone loss in cancellous bone"* J Bone Miner Res **2001**; **16** (3):457-65.
- 189) Van Der Linden, J. C., Verhaar, J. A., and Weinans, H. *"A three-dimensional simulation of age-related remodeling in trabecular bone"* J Bone Miner Res **2001**; **16** (4):688-96
- 190) van der Linden, Y. M., and Leer, J. W. *"Impact of randomized trial-outcome in the treatment of painful bone metastases; patterns of practice among radiation oncologists. A matter of believers vs. non-believers?"* Radiother Oncol **2000**; **56** (3):279-81
- 191) Van Rietbergen, B., Huiskes, R., Eckstein, F., and Rueggsegger, P. *"Trabecular bone tissue strains in the healthy and osteoporotic human femur"* J Bone Miner Res **2003**; **18** (10):1781-8
- 192) Van Rietbergen, B., Odgaard, A., Kabel, J., and Huiskes, R. *"Direct mechanics assessment of elastic symmetries and properties of trabecular bone architecture"* J Biomech **1996**; **29** (12):1653-7
- 193) Verhaeghe, J., Van Herck, E., Van Bree, R., Van Assche, F. A., and Bouillon, R. *"Osteocalcin during the reproductive cycle in normal and diabetic rats"* J Endocrinol **1989**; **120** (1):143-51

- 194) Waarsing, J. H., Day, J. S., van der Linden, J. C., Ederveen, A. G., Spanjers, C., De Clerck, N., Sasov, A., Verhaar, J. A., and Weinans, H. *"Detecting and tracking local changes in the tibiae of individual rats: a novel method to analyse longitudinal in vivo micro-CT data"* Bone **2004; 34 (1):163-9**
- 195) Waarsing, J. H., Day, J. S., Verhaar, J. A., Ederveen, A. G., and Weinans, H. *"Bone loss dynamics result in trabecular alignment in aging and ovariectomized rats"* J Orthop Res **2006; 24 (5):926-35**
- 196) Waarsing, J. H., Day, J. S., and Weinans, H. *"An automatic algorithm to segment 3D microCT scans of bone"*. The IXth congress of the international society of bone morphometry. Edinburgh, UK; **2002**.
- 197) Waarsing, J. H., Day, J. S., and Weinans, H. *"An Improved Segmentation Method for In Vivo microCT Imaging"* J Bone Miner Res **2004; 19 (10):1640-50**
- 198) Wainwright, S. A., Marshall, L. M., Ensrud, K. E., Cauley, J. A., Black, D. M., Hillier, T. A., Hochberg, M. C., Vogt, M. T., and Orwoll, E. S. *"Hip fracture in women without osteoporosis"* J Clin Endocrinol Metab **2005; 90 (5):2787-93**
- 199) Wakley, G. K., Evans, G. L., and Turner, R. T. *"Short-term effects of high dose estrogen on tibiae of growing male rats"* Calcif Tissue Int **1997; 60 (1):37-42**
- 200) Wang, L., Banu, J., McMahan, C. A., and Kalu, D. N. *"Male rodent model of age-related bone loss in men"* Bone **2001; 29 (2):141-8**
- 201) Warden, S. J., Robling, A. G., Sanders, M. S., Bliziotes, M. M., and Turner, C. H. *"Inhibition of the serotonin (5-hydroxytryptamine) transporter reduces bone accrual during growth"* Endocrinology **2005; 146 (2):685-93**
- 202) Weber, M. H., Sharp, J. C., Latta, P., Sramek, M., Hassard, H. T., and Orr, F. W. *"Magnetic resonance imaging of trabecular and cortical bone in mice: comparison of high resolution in vivo and ex vivo MR images with corresponding histology"* Eur J Radiol **2005; 53 (1):96-102**
- 203) Weinans, H. *"Is osteoporosis a matter of over-adaptation?"* Technol Health Care **1998; 6 (5-6):299-306**
- 204) Weinans, H., Huiskes, R., and Grootenboer, H. J. *"The behavior of adaptive bone-remodeling simulation models"* J Biomech **1992; 25 (12):1425-41**
- 205) Weinans, H., and Prendergast, P. J. *"Tissue adaptation as a dynamical process far from equilibrium"* Bone **1996; 19 (2):143-9**
- 206) Westbroek, I., van der Plas, A., de Rooij, K. E., Klein-Nulend, J., and Nijweide, P. J. *"Expression of serotonin receptors in bone"* J Biol Chem **2001; 276 (31):28961-8**
- 207) Westerlind, K. C., Wronski, T. J., Ritman, E. L., Luo, Z. P., An, K. N., Bell, N. H., and Turner, R. T. *"Estrogen regulates the rate of bone turnover but bone balance in ovariectomized rats is modulated by prevailing mechanical strain"* Proc Natl Acad Sci U S A **1997; 94 (8):4199-204**
- 208) Wolff, J. *"Das Gesetz der Transformation der Knochen"*. Berlin: Hirschwald; **1892**.
- 209) Wolpert, L. *"Positional information revisited"* Development **1989; 107 Suppl 3-12**
- 210) Wronski, T. J., Dann, L. M., Scott, K. S., and Cintron, M. *"Long-term effects of ovariectomy and aging on the rat skeleton"* Calcif Tissue Int **1989; 45 (6):360-6**
- 211) Yamazaki, I., and Yamaguchi, H. *"Characteristics of an ovariectomized osteopenic rat model"* J Bone Miner Res **1989; 4 (1):13-22**
- 212) Yoshitake, K., Yokota, K., Kasugai, Y., Kagawa, M., Sukamoto, T., and Nakamura, T. *"Effects of 16 weeks of treatment with tibolone on bone mass and bone mechanical and histomorphometric indices in mature ovariectomized rats with established osteopenia on a low-calcium diet"* Bone **1999; 25 (3):311-9**

Dankwoord

Op deze laatste paar pagina's van dit proefschrift had ik graag iedereen willen bedanken die ook maar op de één of andere manier bijgedragen heeft aan dit boekje. Maar ja, hoe zelfstandig je ook probeert te werken, er zijn meer mensen belangrijk geweest voor je werk dan je hier mogelijk zou kunnen opnoemen. Dus wat volgt kan niet anders dan een wat beperkt dankwoord zijn.

In de jaren dat ik aan mijn promotie heb gewerkt, is het lab flink veranderd. Zes jaar geleden waren we een klein groepje van zo'n 7 à 8 man, terwijl we nu een flinke groep met meer dan 25 mensen zijn. Met al die mensen die zijn gekomen en gegaan is ook de sfeer in het lab voortdurend veranderd. En zo ook mijn leeftijd. Op de één of andere manier ben ik van één van de jongsten, één van de oudsten geworden.

Van de verdwenen mensen uit het oude lab wil ik vooral Franci en Teun bedanken. Franci voor haar inspanningen mij in te wijden in de geheimen van de botbiologie en de afkortingen-geheimtaal die daar bijhoort. En natuurlijk voor het introduceren van de Cake van de Week! Al moet ik eerlijk bekennen dat soms, als ik voor de vierde keer in dezelfde week weer een stuk taart naar binnen moet werken dit wel eens een klein beetje betreurt. Teun wil ik bedanken voor alle programmeerhulp, de liefde voor film en muziek, de filosofische gesprekken en alle keren in het Westerpaviljoen, of waar dan ook, als de nacht maar voortschreed...

To one of the most prominent among the disappeared, mr. Judd Day, I owe a lot of thanks. You've spiced up our existence in the lab and helped me a lot to understand and enjoy science. You were never short of new ideas and thoughts on how to do things better. Thanks for all the delicious side dishes. Thanks for all the hours we spent talking about love, life, science, politics, music and cool little gadgets. Of course all while enjoying some wine/beer, whiskey or tequila. I hope your life in the States is working out, I wish you all the best and I hope we will still meet now and again...(say hi to Liza!)

Terug naar het Nederlands. Nu ben jij aan de beurt Jacqueline. Je was er als eerste en hebt het hele lab helpen vormen, waarvan ik een onderdeelje was. Bedankt voor alle samenwerking en ik weet zeker dat er daar nog veel van zal volgen.

In de afgelopen jaren was het een komen en gaan van aankomende orthopeden. De één bleef wat langer dan de andere, met de één heb ik wat meer contact gehad dan met de andere, maar allemaal hebben jullie bijgedragen aan mijn 'lab-beleving'. Dus: Koen, Erik, Jarno, Justus en Elian, mijn eeuwige dank.

Het nieuwe lab bruist van de jonge AIO's, afgestudeerden en analisten. En zoals dat hoort heeft dat een flinke opleving van sociale activiteit tot gevolg. Er wordt weer flink getaart, geborreld, gefeest enz (en ook gewerkt natuurlijk). Echt veel kon ik niet van de partij zijn, de laatste tijd, maar dat gaat vast veranderen. Hoe dan ook, het lab is vrolijker dan ooit! Bedankt voor de samenwerking en de sfeer: Wendy, Nicole, Predrag, Olaf, Yvonne, Yvonne, Ruud, Marieke, Katja, William, Sander, Tom, Anne en Paul.

Holger, veel samengewerkt hebben we niet, daarvoor is jouw werkterrein wel heel anders dan de mijne. Maar met een beetje fantasie moet het ons toch lukken wel een project te bedenken waarin we beide actief kunnen zijn. Al kom je niet echt werk te kort geloof ik. In ieder geval, samen paranimf zijn was ook niet niks, dus een band is er wel! Dank je wel!

Aleko, je bent bij ons gekomen als vrijwilliger, en ook al vond je het micro-ct scannen maar niks, je bent wel gebleven. Dank je wel voor je wilde ideeën, je verhalen en de lekkere hapjes van je vrouw. Ik hoop dat Nederland snel veranderd, zodat jij en je familie eindelijk het leven kunnen leiden dat jullie verdienen.

Beste Harrie, vooral jij bedankt. Zonder jouw bezielende en bezielde leiding was dit nooit wat geworden. Als ik weer eens ontgoocheld naar niet zulke hele geweldige resultaten zat te staren, kon ik altijd bij jou terecht. Wat ongebreideld enthousiasme eroverheen en de meest magere resultaten leken voorboden voor een kast vol nobelprijzen! Enthousiasme, een warme persoonlijkheid, menselijkheid, openheid, flexibiliteit en nieuwsgierigheid. Dit alles met een chaos-sausje. Kortom, een betere begeleider en baas had ik me niet kunnen wensen.

Ik ben bang dat ik in het bovenstaande stukje niet iedereen genoemd heb met wie ik samengewerkt heb of wie een rol heeft gespeeld in mijn lab-leven. Maar ook aan hen die hun naam niet terug hebben kunnen vinden, heb ik warme herinneringen. Geloof me maar...

Oh, voor ik het vergeet, vinden jullie dit boekje er ook niet mooi uitzien? Allemaal dankzij de tips van Lydia, dank je wel lieve Lydia! Je bijdrage was klein, maar fijn. Mochten de lezertjes thuis toch nog wat aanmerkingen hebben op de layout hier en daar: Ik ben erg eigenwijs en sommige tips heb ik gewoon in de wind geslagen. Alle lelijke details zijn dus mijn eigen schuld.

Straks, tijdens de verdediging van het werk in dit boekje heb ik weer hulp nodig, dit keer van mijn twee paranimfen: René, mijn broertje, en Maurice. Alvast bedankt jongens! René, vroeger als kind liep je altijd achter mij aan en deed je alles na wat ik deed. Maar nu zijn de rollen omgedraaid en jij bent als eerste gepromoveerd. Daar blijft het voorlopig wel bij qua voorbeeld volgen, vader worden ben ik nog steeds niet van plan.

De afgelopen jaren hebben mijn vrienden zich over heel Nederland (en daarbuiten) verspreid. Het kan bijna niet anders dan dat de banden wat verwateren. Maar jij hebt er altijd voor gezorgd dat dat bij ons niet gebeurde,

Maurice! En daarom heb je het dus aan jezelf te danken dat je op moet draven als paranimf, dat begrijp je natuurlijk wel.

En dan nu het thuis-front. Lieve papa en mama, jullie hebben altijd in mij geloofd, meer dan ik ooit waar zal maken ben ik bang. Hoe lang dit alles ook heeft mogen duren, jullie hebben steeds meegeleefd, met alle ups en downs. En uiteindelijk heeft dit dus een boekje opgeleverd, voor in de boekenkast.

Als laatste ben jij aan de beurt lieve Arelly. Jouw warmte en liefde hebben me steeds op de been gehouden. Dit klinkt als een oud cliché, maar het is de puurste waarheid. Je hebt het niet makkelijk gehad in dit koude (letterlijk en figuurlijk) landje. Jouw tranen die af en toe vloeiden brandden gaten in mijn ziel. Bedankt dat jij mijn leven bent blijven delen. Ik hou van jou...

Curriculum Vitae

Jan Hendrik Waarsing is geboren op 6 december 1971 te Stadskanaal en werd Erwin genoemd. Om alle vragen voor te zijn: hij werd benoemd naar zijn opa's Jan en Hendrik en er is absoluut geen relatie tussen zijn doopnamen en zijn roepnaam 'Erwin', maar hij heet dus wel zo. Tegen de tijd dat hij naar de lagere school ging was de familie verhuisd naar Nunspeet. De eerste vier klassen heeft hij doorlopen op de 'Petraschool'. Daarna verhuisden ze naar Renswoude, waar hij de laatste twee lagereschooljaren doorbracht op de 'Borgwal'. De middelbare school werd doorlopen in Veenendaal op het 'Christelijk Lyceum'. Toen dat allemaal achter de rug was, pakte hij zijn boeltje en ging studeren in de 'grote' stad. Op kamers in Enschede studeerde hij electrotechniek aan de Universiteit Twente, alwaar hij afstudeerde, met een biomedische aantekening, in 1996. In die biomedische hoek zou hij blijven zitten. Hij begon zijn loopbaan aan diezelfde universiteit bij het Europese Unie project CREST (Clinical Rehabilitation using Electro Stimulation via Telematics). Na een jaar verkasde hij naar Roessingh R&D, alwaar hij nog twee jaar op dit project bleef werken. De werkzaamheden waren voornamelijk ontwikkelingsgericht en er viel niet zo veel te onderzoeken. Maar ja, dat onderzoeken vond hij wel het leukste. Dus na afloop van het project werd de knoop doorgehakt en Erwin ging op zoek naar een AIO plek, ondanks de financiële consequenties. Uiteindelijk vond hij die plek in Rotterdam bij de vakgroep orthopedie van de medische faculteit van de Erasmus Universiteit (tegenwoordig Erasmus Medische Centrum), onder leiding van Prof. Dr. Jan Verhaar en Dr Ir. (inmiddels Prof) Harrie Weinans. Dit alles heeft geleid, na 6 korte jaartjes, tot het tot stand komen van dit proefschrift.

Voorlopig blijft Erwin werkzaam bij de vakgroep. Hij zal zich de komende tijd bezighouden met beeldverwerking ten behoeve van artrose onderzoek.

Erwin Waarsing woont samen met Arely Sánchez Pineda.

Lijst met publicaties

- 1) Waarsing JH, Day JS, Verhaar JA, Ederveen AG, Weinans H. "*Bone loss dynamics result in trabecular alignment in aging and ovariectomized rats.*" **J Orthop Res.** **2006 May;24(5):926-35.**
- 2) Waarsing JH, Day JS, Weinans H. "*Longitudinal micro-CT scans to evaluate bone architecture.*" **J Musculoskelet Neuronal Interact.** **2005 Oct-Dec;5(4):310-2**
- 3) Waarsing JH, Day JS, Weinans H. "*An improved segmentation method for in vivo microCT imaging.*" **J Bone Miner Res.** **2004 Oct;19(10):1640-50**
- 4) Waarsing JH, Day JS, van der Linden JC, Ederveen AG, Spanjers C, De Clerck N, Sasov A, Verhaar JA, Weinans H. "*Detecting and tracking local changes in the tibiae of individual rats: a novel method to analyse longitudinal in vivo micro-CT data.*" **Bone.** **2004 Jan;34(1):163-9**
- 5) Waarsing JH, Day JS, Verhaar JAN, Sumner DR, Ederveen AGH, Weinans H. "*Effects of tibolone treatment on trabecular architecture in the tibia of mature rats: an in-vivo microCT study.*" **Submitted**
- 6) Waarsing JH, van der Linden JC, Weinans H. "*Local but not global strains are associated with bone formation and resorption.*" **in preparation**
- 7) Gustafsson BI, Westbroek I, Waarsing JH, Waldum H, Solligard E, Brunsvik A, Dimmen S, van Leeuwen JP, Weinans H, Syversen U. "*Long-term serotonin administration leads to higher bone mineral density, affects bone architecture, and leads to higher femoral bone stiffness in rats.*" **J Cell Biochem.** **2006 Apr 15;97(6):1283-91**
- 8) Kranenbarg S, Waarsing JH, Muller M, Weinans H, van Leeuwen JL. "*Lordotic vertebrae in sea bass (*Dicentrarchus labrax* L.) are adapted to increased loads.*" **J Biomech.** **2005 Jun;38(6):1239-46.**
- 9) Hoenderop JG, van Leeuwen JP, van der Eerden BC, Kersten FF, van der Kemp AW, Merillat AM, Waarsing JH, Rossier BC, Vallon V, Hummler E, Bindels RJ. "*Renal Ca²⁺ wasting, hyperabsorption,*

- and reduced bone thickness in mice lacking TRPV5."* **J Clin Invest. 2003 Dec;112(12):1906-14.**
- 10) Botter, SM, van Osch, GJVM, Waarsing, JH, Day, JS, Verhaar, JAN, Pols, HAP, van Leeuwen, JPTM, Weinans, H "*Quantification of subchondral bone changes in a murine osteoarthritis model using micro-CT.*" **Biorheology 2006, 43(3-4):379-88**
- 11) Van der Linden JC, Waarsing JH, Weinans H "*The use of micro-CT to study bone architecture dynamics non-invasively*" Drug Discovery Today, **2006, in press**
- 12) Gregory JS, Waarsing JH, Day J, Pols HA, Reijman M, Weinans H, Aspden RM "*Early identification of osteoarthritis of the hip from radiographs using an active shape model to quantify changes in bone morphometry: a prospective study.*" **submitted**
- 13) Day JS, Waarsing JH, van Lenthe GH, Stauber M, Mulder PG, Sumner DR, Weinans H. "*Inter-individual and Inter-site Variation in Human Trabecular Bone Morphometry*", **submitted**
- 14) Diderich KEM, Waarsing JH, Day JS, Brandt RMC, Amling M, Hoeijmakers JHJ, Weinans H, van der Horst GTJ, van Leeuwen JPTM. "*Accelerated bone loss and disturbed periosteal apposition with ageing in DNA repair deficient trichothiodystrophy mice.*" **submitted**
- 15) Weber TB, Kranenburg S, Hedenström A, Waarsing JH, Weinans H "*Inter- and intraspecific comparison of flight feather shaft morphology of two warbler species with different moult schedules: a quantitative study using μ CT imaging*" **submitted**
- 16) Westbroek I, Waarsing JH, van Leeuwen JPTM, Waldum H, Reseland JE, Zahlsen K, Solligård E, Weinans H, Syversen U, Gustafsson BI "*Long-term fluoxetine effects on bone metabolism in growing rats*" **submitted**